

Master's Thesis

---

Flow characterization by indentation  
methods of unidirectional  
thermoplastic composites

---

T. H. Koopman

University of Twente  
Mechanical Engineering  
Faculty of Engineering Technology  
Chair of Production Technology

*Examination Committee*

Prof. Dr. Ir. R. Akkerman

Dr. Ir. E. R. Pierik

Ir. G. Bieleman

Dr. T. Mishra

April 2025

## Acknowledgements

I would like to thank Remko for his guidance and insights, and helping me with conducting my graduation research. I would also like to thank Martin for his guidance at the beginning of the graduation period and Rens for his guidance at the end of the graduation period. In addition I would like to thank TPRC for supplying me with the material needed to do my research and the University of Twente, in particular Nick and Bert, for allowing me to use their lab facility for my research. Finally I would like to thank my friends, family and especially Yasmin for supporting me during my final moments as a student.

## **Abstract**

The application of thermoplastic composite materials are of great interest for automotive and aerospace industries for their high stiffness relative to their weight. Furthermore, they can be easily molded, shaped, formed, re-heated and reformed during manufacturing and therefore have potential for faster production rates and recyclability. To realize this potential the deformation and flow behavior needs to be investigated. Experimental research was conducted to develop a new method to characterize the transverse flow behavior of unidirectional (UD) thermoplastic composites. In this research, the materials LMPAEK and carbon fiber LMPAEK composite (C/LMPAEK) were brought to above melting temperature in a rheometer and were subjected to indentation tests at different constant indentation velocities. The LMPAEK material was indented with an axisymmetric spherical indenter and the measured normal forces over indentation depth were compared to conventional viscosity test methods, a closed form solution, and finite element method simulations. The C/LMPAEK material was indented with a cylindrical indenter in the fiber direction to isolate the transverse flow behavior from the longitudinal flow behavior. A plane strain Kelvin model simulation was fitted to the measured indentation force over indentation depth to see if it was possible to characterize the flow behavior of the transverse viscosity of C/LMPAEK in melt. It was found that the LMPAEK indentation tests could not accurately describe material behavior, due to rheometer not being as accurate in its measurements as needed. The C/LMPAEK indentation tests showed rate dependent behavior and together with the simulations flow behavior was described.

# Nomenclature

$\alpha$	angular rotation	rad
$\alpha_d$	damping coefficient	Ns/m
$\beta$	slip coefficient	m <sup>3</sup> /Ns
$\Delta x$	distance between Winkler elements	m
$\delta$	loss angle	°
$\dot{\epsilon}$	strain rate	s <sup>-1</sup>
$\dot{\gamma}$	shear rate	s <sup>-1</sup>
$\dot{\sigma}$	stress rate	Pa/s
$\dot{\tau}$	shear stress rate	Pa/s
$\dot{d}$	indentation velocity	m/s
$\epsilon$	strain	—
$\eta$	viscosity	Pa s
$\eta'$	dynamic viscosity or the real part of the complex viscosity	Pa s
$\eta''$	imaginary part of the complex viscosity	Pa s
$\eta^*$	complex viscosity	Pa s
$\eta_0$	zero shear viscosity	Pa s
$\frac{du}{dy}$	velocity gradient	—
$\gamma$	shear strain	—
$\lambda$	shear thinning transition time constant	s
$\omega$	angular frequency	rad/s
$\sigma$	normal stress	Pa
$\tau$	shear stress	Pa
$\tau^*$	critical shear stress	Pa
$\tau_f$	friction stress	Pa

---

$\tau_R$	shear stress at the total radius	Pa
$A$	fit parameter	$\text{N/m}^{1/2}$
$a$	contact radius	m
$B$	fit parameter	$\text{N/m}$
$C$	fit parameter	$\text{N/m}^2$
$C_b$	bulk modulus	Pa
$d$	indentation depth	m
$E$	elasticity modulus	MPa
$F_N$	normal force	N
$G$	shear modulus	MPa
$G'$	storage modulus	Pa
$G''$	loss modulus	Pa
$G^*$	complex shear modulus	Pa
$k$	stiffness coefficient	$\text{N/m}$
$M$	torque	$\text{Nm}$
$m$	flow consistency index	$\text{Pa} * \text{s}^n$
$n$	flow behavior index	—
$R$	total radius	m
$r$	variable radius	m
$t$	specimen thickness	m
$v_{rel}$	relative velocity between two bodies	$\text{m/s}$

# Contents

Acknowledgment . . . . .	i
Abstract . . . . .	i
Nomenclature . . . . .	ii
<b>1 Introduction</b>	<b>1</b>
1.1 Motivation . . . . .	1
1.1.1 Research objectives . . . . .	2
1.2 Outline of the report . . . . .	3
<b>2 Background</b>	<b>4</b>
2.1 Material behavior . . . . .	4
2.2 Viscosity test methods . . . . .	7
2.3 Transverse behavior of UD thermoplastic composites . . . . .	11
2.4 Characterization with indentation experiments . . . . .	12
2.4.1 Indentation experiments . . . . .	12
2.4.2 Indentation viscosity of isotropic materials . . . . .	15
2.4.3 Indentation viscosity of UD composite materials . . . . .	17
<b>3 Methodology</b>	<b>18</b>
3.1 Materials and equipment . . . . .	18
3.2 Specimen preparation . . . . .	19
3.3 Rheometry . . . . .	20
3.4 Indentation viscosity tests . . . . .	20
3.5 Microscopy . . . . .	21
3.6 Finite element model simulations . . . . .	22
3.7 Data analysis . . . . .	24
<b>4 Results</b>	<b>26</b>
4.1 Influence of different parameters on the simulations . . . . .	26
4.1.1 Axisymmetric case . . . . .	26
4.1.2 Plane strain case . . . . .	30
4.2 Indentation test . . . . .	32
4.2.1 Matrix material indentation tests . . . . .	32
4.2.2 UD composite material indentation tests . . . . .	34
4.3 Specimen deformation . . . . .	36
4.3.1 Specimen deformation during indentation . . . . .	37
4.3.2 Microscopy imaging of deformed specimen . . . . .	38

---

<b>5 Discussion</b>	<b>41</b>
5.1 Influence of specimen dimensions . . . . .	41
5.2 Matrix material indentation tests . . . . .	41
5.3 UD composite indentation tests . . . . .	42
5.4 Specimen deformation . . . . .	45
<b>6 Conclusion</b>	<b>46</b>
<b>7 Recommendations</b>	<b>47</b>
<b>A Indentation viscosity measurements protocol</b>	<b>51</b>
<b>B Differential Scanning Calorimetry</b>	<b>65</b>
<b>C Simulation files</b>	<b>69</b>
C.1 Construction of the simulated specimen . . . . .	69
C.2 Property parameters . . . . .	69
C.3 Input files . . . . .	70
<b>D Error assessment of the rheometer</b>	<b>76</b>
<b>E Test results</b>	<b>78</b>
E.1 Matrix indentation test results . . . . .	78
E.2 UD composite indentation test results . . . . .	80

# Chapter 1

## Introduction

Fiber composite materials have developed significantly to accommodate for the increasing demand for high-performance materials in industries such as aerospace and automotive. Such composites consist of two constituents (see Figure 1.0.1): a reinforcement material which in this case are fibers that have a high stiffness modulus relative to their weight, and a matrix that keeps the reinforcement material in place, distributes the load over the fibers, and can be molded in various shapes. This makes composites useful for realizing complex shapes and structures. The matrix material is often a thermoset or thermoplastic polymer and while, currently, thermosets are applied in most cases, thermoplastics are of great interest. Thermoplastics are easily molded, shaped, and formed during manufacturing processes and can be re-melted and reshaped. Due to this property thermoplastic composites have a potential for faster production rates and straightforward recyclability. The deformation and flow behavior need to be investigated to realize this potential. One key parameter to explore is the viscosity of the composite and its thermoplastic matrix in melt.

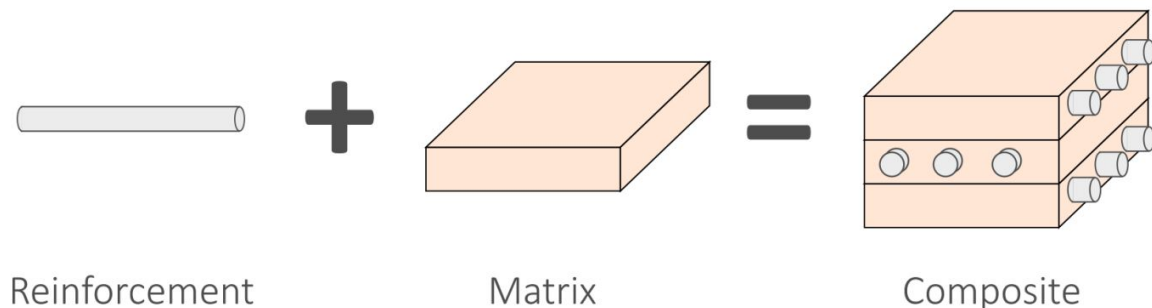


Figure 1.0.1: Schematic overview of the build-up of a composite

### 1.1 Motivation

During the forming process of thermoplastic composites, different plies of which the fibers run in one direction are molded together at a temperature above the matrix melting temperature. These plies are called unidirectional (UD) composite plies. Different deformation mechanisms can occur during this forming process of composites. These mechanisms are summarized from previous research by Haanappel [1]. Here, among other mechanisms, it can be seen that the longitudinal and transverse shear, which are illustrated in Figure 1.1.1, in UD composite plies are of importance. Furthermore, the transverse flow behavior can be seen as rather important as claimed by Brands [2]. One can imagine that the composite material flows differently in a transverse direction than a longitudinal one. Longitudinal shear can be characterized by torsion bar experiments, as proposed by Haanappel

[3]. For transverse shear, however, less methods are steadily available.

Methods to determine the viscous behavior of composites have been researched in the past but each has its drawbacks, as can be seen in Table 1.1.1. In this research, an alternative test is proposed and investigated to characterize the mechanical behavior transverse to the fibers in UD thermoplastic composites such as carbon LMPAEEK with a high fiber volume. The alternative concerns an indentation testing method that utilizes a standard rheometer and small test specimens. This method might be faster and simpler than other test methods researched in the past, while not needing large set-ups or laborious preparation.

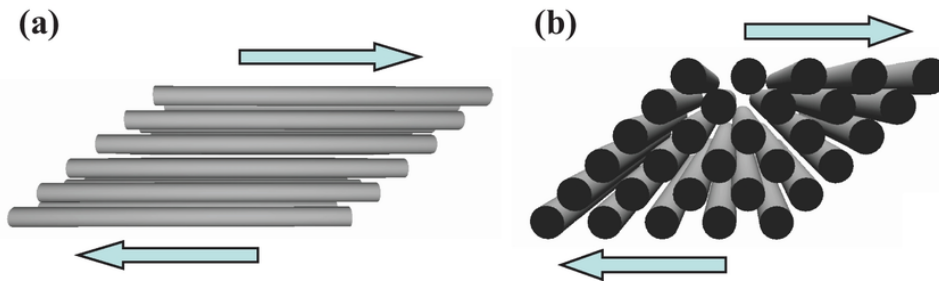


Figure 1.1.1: schematic representation of (a) longitudinal shear going parallel to the fibers, and (b) transverse shear going across the fibers [4]

Table 1.1.1: Advantages and disadvantages of different composite viscosity experiments.

Method	Advantages	Disadvantages
Squeeze flow experiment [5, 6]	-Reasonably accurate results -Works for transverse and longitudinal viscosity	-Self-made non-conventional set-up
Picture frame experiment [7]	-Works for cross-ply fabric reinforced materials	-Does not work for UD materials
Linear oscillation experiment [8, 9]	-Works for transverse and longitudinal viscosity	-Only attempted with viscous fluids at room temperature -Self-made non-conventional set-up
Pull-out experiment [10]	-Works for transverse and longitudinal viscosity	-Only attempted with viscous fluids at room temperature -Self-made non-conventional set-up

### 1.1.1 Research objectives

Based on the motivation, this research is shaped by the following research question:

*How can the deformation behavior in transverse direction of uni-directional thermoplastic composites be characterized using indentation methods?*

This broad question can not be answered with one simple solution, as many aspects must be considered. One such aspect are the contact mechanics of indentation problems. These differ per the shape of the indenter and possibly in relation to the type of material that is indented. Ideally, the

method should be validated by comparing the results to the outcome of a reference test on a reference material with known properties and supported by deformation and stress analysis by means of analytical or numerical modeling. This means that the viscosity of the matrix material will first be measured with a conventional method and then with the indentation method before the flow behavior of the composite is tested with the indentation method. A secondary goal of this thesis is to see if a rheometer is suitable equipment for this test method. Taking this into consideration, a set of sub-questions can be formulated:

- What type of indentation tool is needed?
- How do specimen dimensions influence the end results?
- How does this method compare to conventional methods to characterize flow behavior?
- Which methods can be used to accurately model the material behavior during indentation testing?
- Is a rheometer suitable equipment for indentation tests?

## 1.2 Outline of the report

The contents of the report and its structure are presented in Figure 1.2.1. The list of references, and appendices follow the conclusion and recommendation.

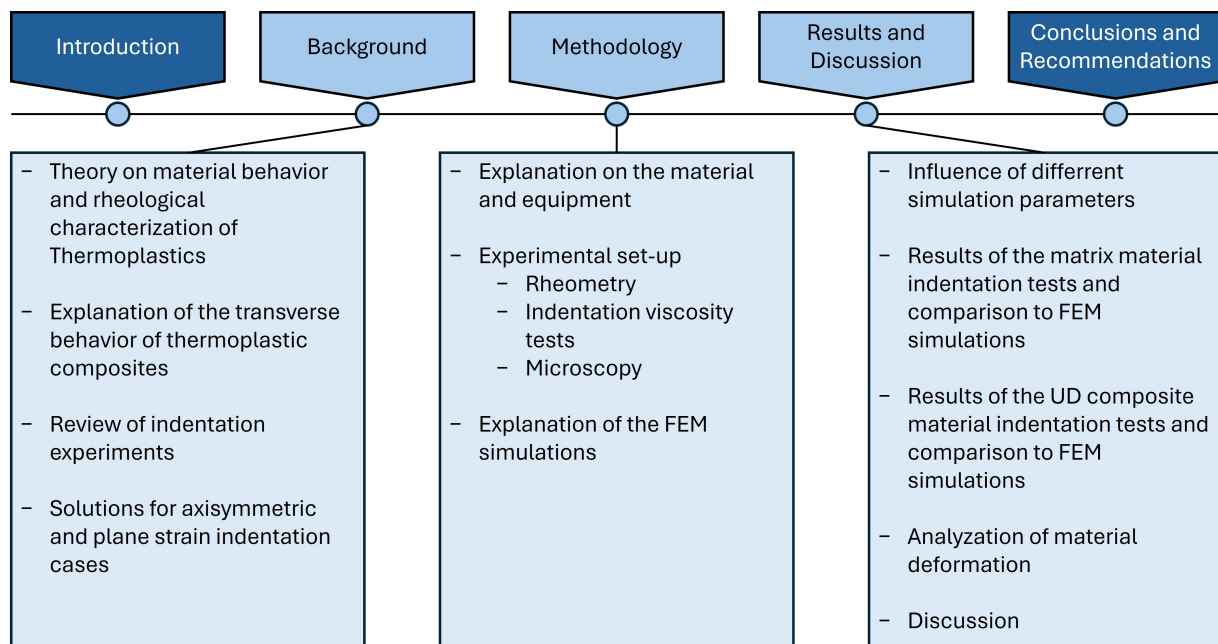


Figure 1.2.1: Outline and corresponding topics of the report

# Chapter 2

## Background

### 2.1 Material behavior

Before elaborating on indentation testing, the fundamental background on elementary material behavior is briefly recapitulated. To this end, viscous, elastic, and visco-elastic behavior will be considered.

#### Viscosity

Viscosity refers to the resistance to a change of shape or movement of a fluid by a neighboring portion relative to one another. This means that fluids with high viscosity have difficulty flowing from one point to another, while fluids with low viscosity can easily flow. Different types of fluids react differently to the amount of shear rate applied. In Figure 2.1.1 it can be seen how different types of fluids behave. An in depth explanation of viscous materials can be found in [11, 12, 13].

A few numerical models can be used to describe different types of fluids. These models could eventually be used to validate the analytical results gained from the viscosity testing methods. The simplest way to describe viscosity is with a model that describes Newtonian fluids:

$$\tau = \eta \cdot \frac{du}{dy} = \eta \cdot \dot{\gamma} \quad (2.1.1)$$

where  $\tau$  [Pa] is the shear stress,  $\eta$  [Pa \* s] is the viscosity,  $\frac{du}{dy}$  is the velocity gradient, and  $\dot{\gamma}$  [ $s^{-1}$ ] is the shear rate. In this model, the viscosity does not change when the shear rate changes making this model linear, as can be seen in Figure 2.1.2. This model is unsuitable for describing polymers, as they are shear-thinning fluids when molten. Therefore, other models are needed. One such model is the power law [12]:

$$\eta(\dot{\gamma}) = m \cdot \dot{\gamma}^{n-1} \quad (2.1.2)$$

Where  $m$  [Pa \*  $s^n$ ] is the flow consistency index and  $n$  [–] is the flow behavior index. The power law describes Newtonian and non-Newtonian fluids where  $n$  determines the fluid type. If  $n < 1$  the model describes shear thinning behavior, if  $n > 1$  the model describes shear thickening behavior, and if  $n = 1$  the model describes Newtonian behavior. The shear rate influences the viscosity of the material due to the behavior when  $n$  is either smaller or larger than 1, unlike Newtonian fluids where viscosity remains constant.  $m$  is used to fit non-Newtonian data across shear rates. This model describes shear-thinning/thickening behavior but omits the Newtonian plateau in polymer melts. The Cross model describes non-Newtonian behavior and the Newtonian plateau [15]:

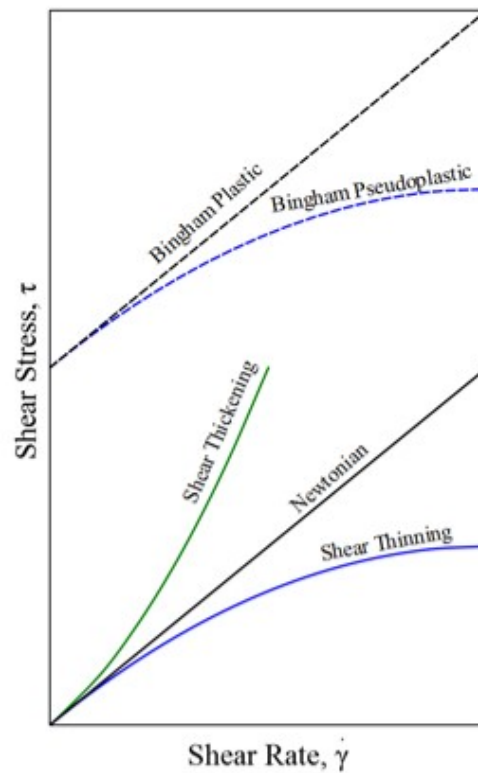


Figure 2.1.1: Shear stress as a function of shear rate for several kinds of fluids [14]

$$\eta(\dot{\gamma}) = \frac{\eta_0}{1 + \left(\frac{\eta_0 \dot{\gamma}}{\tau^*}\right)^{(1-n)}} \quad (2.1.3)$$

where  $\eta_0$  [ $Pa \cdot s$ ] is the zero shear viscosity, a constant value that the viscosity function approaches as  $\dot{\gamma}$  gets small and nearly equal to the value of the Newtonian plateau,  $\tau^*$  [ $Pa$ ] is the critical shear stress which is determined by the moment where the shear forces overcome the restrictive forces and can move the fluids more freely.  $\tau^*$  can also be described as  $\eta_0/\lambda$ , where  $\lambda$  [s] is a time constant for the fluid that determines the shear rate at which the transition occurs from the Newtonian plateau to the power-law portion. Now Equation 2.1.3 can be rewritten as:

$$\eta(\dot{\gamma}) = \frac{\eta_0}{1 + (\lambda \cdot \dot{\gamma})^{(1-n)}} \quad (2.1.4)$$

This model can fit most viscosity versus shear-rate data but does not consider the constant  $\eta_\infty$  that is present in the Carreau-Yasuda model [12]. This constant denotes a second Newtonian plateau that appears in molten thermoplastics as  $\dot{\gamma}$  gets large. However, this is not of importance for this research as the shear rates needed for this to happen are unlikely to be reached. In Figure 2.1.2 the Cross model model is compared to a power-law model and a Newtonian fluid model.

## Elasticity

Elasticity refers to the ability of a material to resist deformation by a force or influence, and the ability of said material to return to its original shape when the force or influence is removed. This means that the elastic deformation of perfect elastic materials is nonpermanent. Furthermore, the elasticity was described by Hooke as a linear relation between the strain and stress placed upon a material [11].

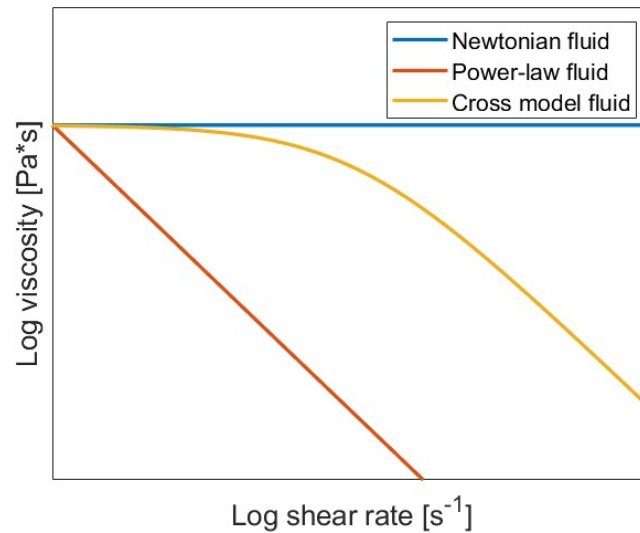


Figure 2.1.2: Comparison between Newtonian, power law, and Cross model fluids.

In Figure 2.1.3 [16] it can be seen how different types of elastic materials behave, and what happens after the elastic region ends. Brittle materials generally break, while ductile and elastomer materials enter a non-linear plastic region where some permanent deformation takes place.

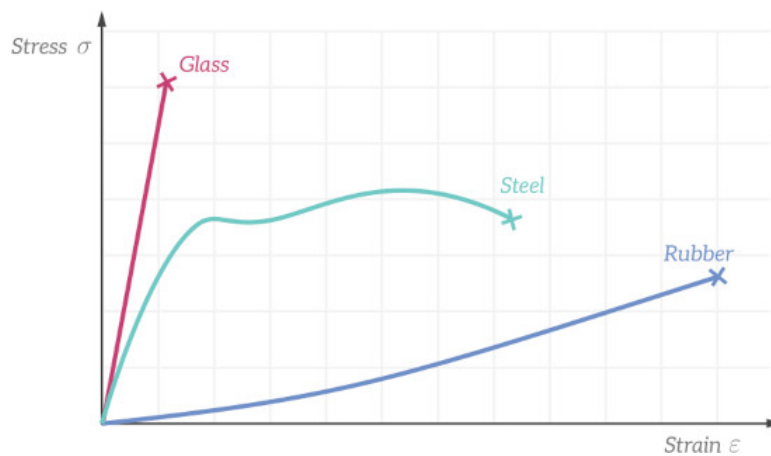


Figure 2.1.3: Examples of stress-strain curves for glass (brittle material), steel (ductile material), and rubber (elastomer).

## Viscoelasticity

Macosko [11] provided a detailed description of viscoelasticity. Viscoelastic materials exhibit both viscous and elastic behavior under deformation. They are also time dependent, meaning that when stress is applied, they show an immediate elastic response and a delayed flow or relaxation. At smaller strains the material has a linear relation between stress relaxation and strain. This region is called the linear viscoelastic region (LVER). At larger strains this relation does not hold anymore and this is called the non-linear viscoelastic region (NLVER). In the NLVER material behavior like shear thinning or thickening is apparent.

In rheology viscoelastic behavior is often characterized with the complex shear modulus  $G^*$ , and the storage and loss moduli  $G'$  and  $G''$  respectively:

$$G^*(\omega) = G'(\omega) + iG''(\omega) \quad (2.1.5)$$

$$\tan(\delta) = \frac{G''}{G'} \quad (2.1.6)$$

where  $\omega$  [rad/s] is the angular frequency, and  $\delta$  [°] is the loss angle. The storage modulus represents the elastic behavior of the material and when it is larger than the loss modulus the material behaves more elastic. The loss modulus represents the viscous behavior of the material and when it is larger than the storage modulus the material behaves more viscous like. The loss angle represents the ratio between the elastic and viscous component of a material and has a value between 0°, where the material displays purely elastic behavior, and 90°, where the material displays purely viscous behavior.

Viscoelastic materials can be modeled in various ways, one possible model is the Maxwell model [13]. In the Maxwell model a spring and dashpot are placed in series where the spring provides a strain contribution and the dashpot provides a strain rate contribution, which gives a total strain rate for the Maxwell model as:

$$\dot{\epsilon} = \frac{\dot{\sigma}}{E} + \frac{\sigma}{\eta} \quad (2.1.7)$$

where  $\dot{\epsilon}$  [ $s^{-1}$ ] is the strain rate,  $\sigma$  [Pa] is the normal stress,  $E$  [Pa] is the elasticity modulus, and  $\dot{\sigma}$  [Pa/s] is the stress rate. The shear strain rate according to a Maxwell model can be described in a similar way:

$$\dot{\gamma} = \frac{\dot{\tau}}{G} + \frac{\tau}{\eta} \quad (2.1.8)$$

where,  $\dot{\tau}$  [Pa/s] is the shear stress rate and  $G$  [Pa] is the shear modulus. Another model to describe viscoelastic behavior is a Kelvin-Voigt (Kelvin) model. In a Kelvin the spring and dashpot are placed in parallel and the normal stress can be described with:

$$\sigma = E \cdot \epsilon + \eta \cdot \dot{\epsilon} \quad (2.1.9)$$

The shear stress can be described in a similar way:

$$\tau = G \cdot \gamma + \eta \cdot \dot{\gamma} \quad (2.1.10)$$

where  $\gamma$  [–] is the shear strain. A schematic overview of both models can be seen in Figure 2.1.4[17]. In the same figure the models respective response to stress relaxation and creep tests is shown. Here it is seen that a Maxwell model gives a better qualitative description of the relaxation behavior of viscoelastic material, while a Kelvin model gives a better qualitative description of the creep behavior of viscoelastic material.

## 2.2 Viscosity test methods

Measuring the viscosity of fluids can be done in many ways with different devices based on distinct methods. Examples are capillary, falling sphere, dip cup, and rotational viscometers [18, 19]. Although these methods use different techniques, they all apply the same principle of determining a

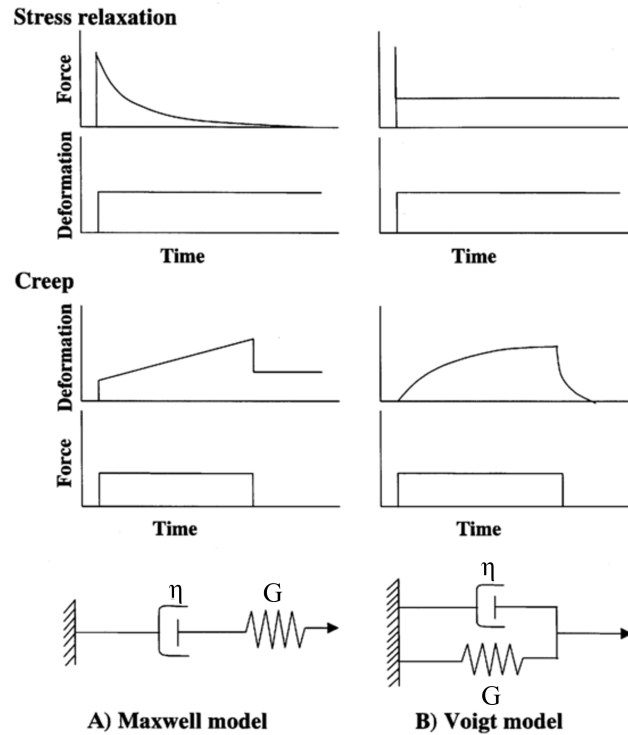


Figure 2.1.4: schematic overview of a A) Maxwell model and B) Kelvin-Voigt model, together with their corresponding stress relaxation and creep response [17].

fluid's resistance in one way or another.

For thermoplastics, however, the viscosity is usually measured using a rheometer [11, 20]. A rheometer is a device where a molten specimen is placed between two fixtures. One of the fixtures will either rotate or oscillate at different angular speeds or frequencies to determine the specimen's viscosity. The Couette rheometer (Figure 2.2.1a) has a rotor inside a vat with a molten sample in between, a cone-plate configuration (Figure 2.2.1b) has a conical fixture rotating parallel to a bottom plate fixture, and a plate-plate configuration (Figure 2.2.1c) has a top plate fixture rotating parallel to a bottom plate fixture. Macosko [11] has summarized the errors that need to be corrected and the utility for each rheometer configuration, which can be seen in Table 2.2.1.

Rheometers can do either rotational or oscillatory measurements. With rotational measurements the moving fixture can rotate with either controlled shear rate which results in a measured torque or shear stress, or with controlled shear stress which results in a measured angular velocity or shear rate. One example of an oscillatory measurement is a shear strain rate sweep. With oscillatory measurements the moving fixture rotates back and forth at either a constant angular frequency and increasing shear strain which is called an amplitude sweep, or at a constant amplitude of the shear strain, that lays within the LVER, with an increasing angular frequency, which is called a frequency sweep. Oscillatory tests are performed for evaluating time-dependent viscoelastic behavior, like shear thinning behavior of polymers [21].

As the plate-plate configuration was used in this research, an overview on how shear stress, shear strain, shear rate, Torque, angular rotation, angular velocity, angular frequency, and viscosity are related to each other, given by Macosko [11]. The upcoming equations are under the assumptions of:

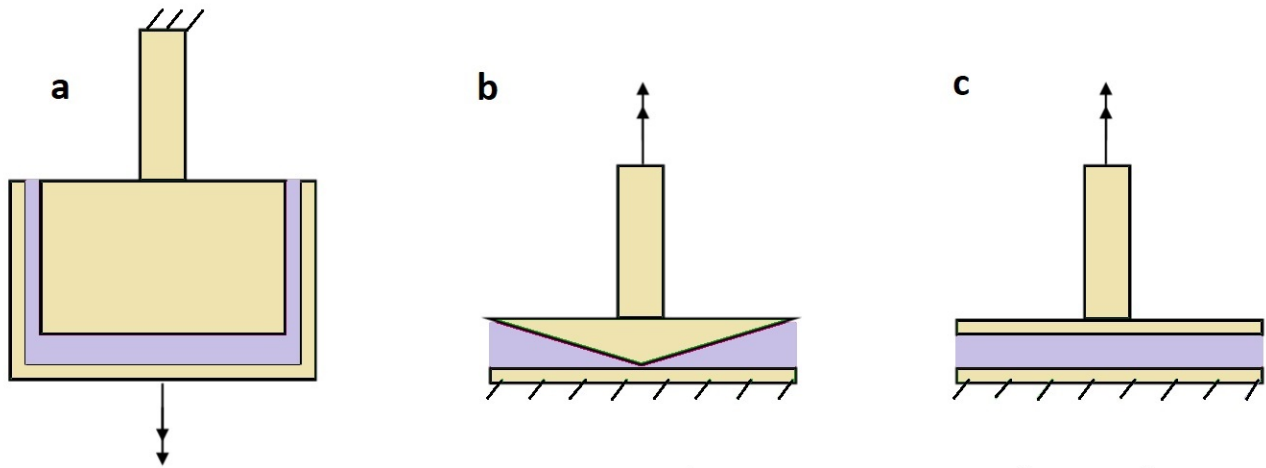


Figure 2.2.1: Schematic overview of different configurations of rheometers with (a) a Couette configuration (b) a cone-plate configuration (c) a plate-plate configuration, where blue indicates the material being measured

- Steady, non-oscillatory, laminar, isothermal flow
- Only angular velocity unequal to zero
- Negligible body forces
- Cylindrical edge

The shear strain and shear rate are defined as:

$$\gamma = \frac{\alpha \cdot r}{t} \quad (2.2.1)$$

$$\dot{\gamma} = \frac{\omega \cdot r}{t} \quad (2.2.2)$$

with the shear strain and shear rate at the edge of the specimen being:

$$\gamma_R = \frac{\alpha \cdot R}{t} \quad (2.2.3)$$

$$\dot{\gamma}_R = \frac{\omega \cdot R}{t} \quad (2.2.4)$$

where  $\alpha$  [rad] is the angular rotation,  $r$  [m] is the variable radius,  $R$  [m] is the total specimen radius, and  $t$  [m] is the specimen thickness. As  $r$  is variable a shear strain/rate gradient forms over the sample. Thus, an integral is used to relate shear stress to total torque:

$$M = \int_0^R \tau(r) \cdot 2\pi \cdot r^2 dr \quad (2.2.5)$$

where  $M$  [N · m] is the torque. Rearranging and differentiating this using Leibniz's rule gives:

Table 2.2.1: Rheometer configuration listed with their errors that need to be corrected and their utility

Configuration	Errors	Utility
Couette	<ul style="list-style-type: none"> <li>-End effects</li> <li>-Wall slip</li> <li>-Inertia and secondary flows</li> <li>-Eccentricities</li> <li>-Viscous heating</li> </ul>	<ul style="list-style-type: none"> <li>-Best for lower viscosity systems (<math>\eta_0 &lt; 100 \text{ Pa}\cdot\text{s}</math>)</li> <li>-Good for high shear rates</li> <li>-Gravity settling of suspensions has less effect than in cone-plate</li> <li>-Normal stresses hard to measure because of curvature and need to transmit signal through a rotating shaft</li> <li>-Rod climbing</li> </ul>
Cone-plate	<ul style="list-style-type: none"> <li>-Inertia and secondary flow</li> <li>-Torque correction</li> <li>-Gap opening</li> <li>-Shear heating</li> </ul>	<ul style="list-style-type: none"> <li>-Most common instrument for normal stress measurements</li> <li>-Simple working equations: homogeneous deformation</li> <li>-Nonlinear viscoelasticity</li> <li>-Useful for low and high viscosity materials</li> <li>-High viscosity limited by elastic edge materials</li> <li>-Low viscosity limited by inertia corrections, secondary flow, and loss of sample at edges</li> </ul>
Plate-plate	<ul style="list-style-type: none"> <li>-Inertia and secondary flow</li> <li>-Edge failure (same as cone-plate)</li> <li>-Shear heating</li> <li>-Nonhomogeneous strain field (correctable)</li> </ul>	<ul style="list-style-type: none"> <li>-Sample preparation and loading is simpler for very viscous materials and soft solids</li> <li>-Can vary shear rate (and shear strain) independently by rotation rate or by changing the gap; permits increased range with a given experimental set-up</li> <li>-Determine wall slip by taking measurements at two gaps</li> <li>-Delay edge failure to higher shear rate by decreasing gap during an experiments (requires change of cone angle in cone-plate)</li> <li>-Measure <math>N_2</math> when used with cone and plate thrust data</li> <li>-Preferred geometry for viscous melts for small strain material functions</li> </ul>

$$\tau_R = \frac{M}{2\pi \cdot R^3} \left[ 3 + \frac{d(\ln M)}{d(\ln \dot{\gamma}_R)} \right] \quad (2.2.6)$$

which can be simplified to the apparent shear stress, which is the shear stress for Newtonian viscosities:

$$\tau(r) = \frac{2M \cdot r}{\pi \cdot R^4} \quad (2.2.7)$$

The apparent shear stress is used to calculate the viscosity which is given by rewriting Equation 2.1.1. This viscosity applies to Newtonian liquids or non-Newtonian liquids at small shear rates

before shear thinning or thickening takes place. For polymers, a shear strain rate sweep is used at low shear rates to determine  $\eta_0$ , but does not provide much more information about the polymer. To relate frequency to viscosity the complex viscosity needs to be defined [13, 22]:

$$\eta^* = \frac{G^*}{i\omega} = \eta' - i\eta'' \quad (2.2.8)$$

where  $\eta^*$  [Pa s] is the complex viscosity,  $\eta'$  [Pa · s] is the dynamic viscosity/real part of the complex viscosity, and  $\eta''$  [Pa · s] is the imaginary part of the complex viscosity. The real part of the complex viscosity versus the angular frequency gives an idea of the shear thinning behavior of materials. To only consider the real part of the complex viscosity, Equation 2.2 can be rewritten as:

$$|\eta^*|(\omega) = \frac{|G^*|}{\omega} = \eta' \quad (2.2.9)$$

A frequency sweep can be used to find the real part of the complex viscosity, as well as the storage and loss moduli. It can do so for a wider range than possible for shear strain rate sweeps. Cox and Merz found that viscosity was nearly identical to complex viscosity in the low frequency and shear rate limits [22], and from this the formulated the Cox-Merz rule:

$$\eta(\dot{\gamma})|_{\dot{\gamma} \rightarrow 0} = |\eta^*(\omega)|_{\omega \rightarrow 0}, \quad \dot{\gamma} = \omega \quad (2.2.10)$$

Shear strain rate sweeps can not be done at high shear rates due to specimen fracture and secondary flow behavior. The Cox-Merz rule aims to predict viscous behavior from oscillatory measurement by comparing viscosity measured with a shear strain rate sweep and complex viscosity measured with a frequency sweep at low ranges, to then predict the viscous behavior at higher ranges with a frequency sweep. If the data of both sweeps at the low shear rates and frequencies coincide, the complex viscosity from the frequency sweep at high frequencies can be seen as the viscosity of the material at high shear rates.

As the reasons for doing a shear strain rate and frequency sweep are reviewed, the amplitude sweep needs to be discussed as well. An amplitude sweep is done to find the LVER. It measures storage and loss moduli versus strain, which stay constant in the LVER. When the strain gets too high the storage and loss moduli drop and the NLVER is reached. In general, an amplitude sweep is done before frequency sweeps to make sure the imposed strain is within the LVER.

## 2.3 Transverse behavior of UD thermoplastic composites

Although plate-plate rheometry is useful for finding the viscous behavior of neat polymer, it can not be used for UD thermoplastic composites. When UD composites in melt are subjected to any rotational motion, the fibers would go out of alignment and lose its UD properties. Therefore, transverse behavior of UD composite should be described differently. In Section 1.1 the deformation mechanisms and flow behavior of UD composites have been briefly mentioned, but a more in depth explanation will be given in this section, with a focus on the transverse behavior.

The main deformation mechanisms in composites can be categorized in inter-ply mechanisms, where one ply interacts with another ply or a forming tool, or the intra-ply mechanisms, where deformation takes place in one UD ply of a composite. One intra-ply mechanism of interest is the transverse shearing of the ply as seen in Figure 1.1.1. It is related to the transverse sliding of the fibers inside the

ply, which can be caused, among others, by matrix percolation [23]. Matrix percolation is the flow of matrix material either through the fiber bed or along the fiber lengths. It allows the matrix material to be locally redistributed and it is the main mechanism for allowing the bonding of adjacent plies. However, percolation flow is usually limited due to the density of the fiber bundles in combination with the high viscosity of the matrix material. It is even analytically and experimentally shown that this is more the case in transverse directions than in longitudinal directions [24]. To help the flow through the fibers it is possible to apply pressure to the composite. However, this can cause the squeeze flow mechanism to happen.

When a normal pressure is applied to a continuous fiber composite laminate, the composite can deform in such a way that it behaves like an anisotropic suspension. This means that not only the matrix material flows, but the fibers flow and displace as well. The high extensional viscosity in the fiber direction ensures that this deformation is mostly perpendicular to the fiber direction, although longitudinal percolation may still occur at low deformation rates [6, 25]. Furthermore, it is shown that a higher fiber volume fraction results in a higher transverse viscosity [5]. However, this experiment was done by modeling a transversely isotropic composite out of clay and nylon bristles. Transverse isotropy can not be assumed in commercially available thermoplastic composites as is shown with the torsion bar method [2, 3].

The torsion bar method was introduced by Haanappel and Akkerman [3] to identify shear characteristics in UD composites as well. This method was executed by placing a UD composite bar inside a rheometer with the fibers aligned in the length direction and oscillating it above melting temperature. This would introduce intra-ply longitudinal shear deformation in the bar. However, this could only be done under the assumption that the bar was transversely isotropic. Brands [2] found that this was not the case by repeating the experiments (albeit with two minor alterations), measuring the deformation on the surface, and finding that in all cases one transverse direction was deformed significantly more than the other.

It can be concluded that the transverse behavior of UD composites is different than the longitudinal behavior. However, it is difficult to characterize separately and a new characterization method can be helpful to further understand it.

## 2.4 Characterization with indentation experiments

Characterizing through indentation methods will be researched as a new method to better understand the transverse behavior of UD composites. First, existing indentation experiments will be reviewed. Then, viscosity measurements for polymer in melts, and UD composites are presented. Finally, numerical simulations will be introduced to help understand observed trends and for use of estimating experimental parameters.

### 2.4.1 Indentation experiments

The most commonly used indentation tests are hardness tests, which exist for many types of materials. In Table 2.4.1 different hardness tests and their indenter geometries are summarized. The tests all use different geometries and/or protocols where either the indentation depth, or the indentation force is measured.

For example, the Janka hardness test measures the hardness of wood with a standardized metal ball with a diameter of 11.3 mm. The force needed to press the ball halfway into the material at 5.6

mm/minute as an indicator for the hardness [26].

Two standardized tests exist for rubbers: The International Rubber Hardness Degree (IRHD) and the Shore hardness scale. IRHD has 4 different tests of which three depend on the hardness of the material and the fourth one is used for micro samples. All tests use a spherically tipped indenter. The diameter of the sphere varies between tests and the force used for all tests is the same at 5.7 N, except for the micro tests where a smaller force of 153.3 mN is used. During testing, a sample is clamped in the testing machine and a weight is placed on the sample with a calibrating force of 0.3 N or 8.3 mN for micro tests for 5 seconds, after which the force is increased to 5.7 N or 153.3 mN for micro tests and held for 30 seconds. The displacement is measured and converted to an IRHD value.

The Shore hardness scale uses different tests for higher or lower hardnesses in rubbers as well. It can also be used for some plastics. In total, eight test types exist, all with a different combination of indenter type, diameter, and load. The indenter types used are a cone, a truncated cone, a sphere, and a disk. The indenter is placed on the sample and attached to the indenter is a spring which load needs to be overcome for a presser foot to contact the sample. The indentation that is made is recorded after a dwell time of around 1 to 3 seconds and converted to the Shore scale. Morgans et al. summarized and explained the difference between IRHD scale and the Shore hardness scale [27]. In Figure 2.4.1 a comparison between the most used Shore hardness scales with example materials is given [28].

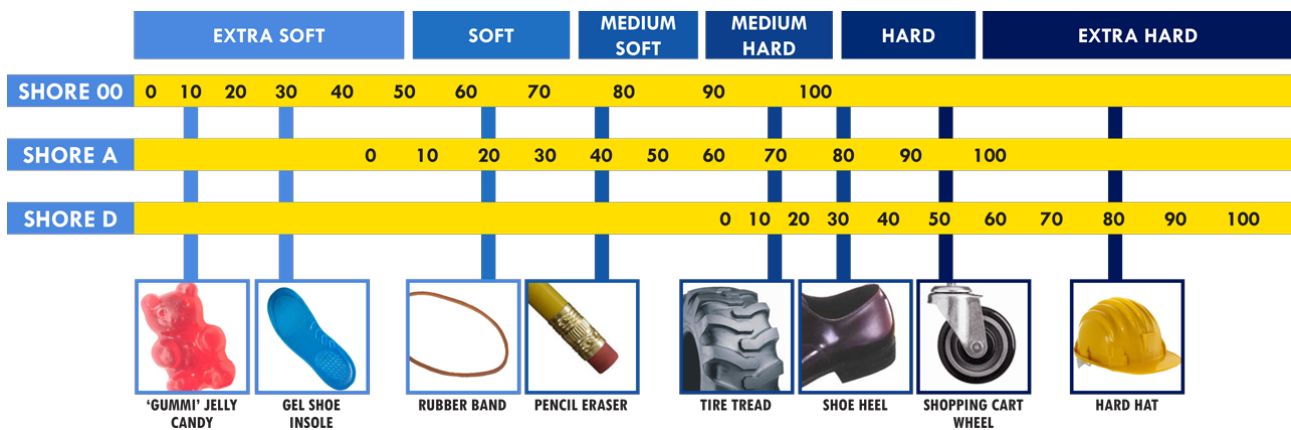


Figure 2.4.1: Shore hardness scales

The Barcol hardness test is used for plastics, polyesters, and soft metals, but it can be used for composite materials as well. A mobile apparatus is used to do the tests by applying pressure on the apparatus, which causes the cone-shaped needle to penetrate the test sample, which gives a hardness on the Barcol scale [29].

The Knoop hardness test is a micro-hardness test, where an elongated pyramidal-shaped indenter is pressed into a test sample, and light microscopy is used to measure the projected area, together with the force, the hardness is calculated in MPa. This test is mainly used for thin or brittle materials as the indentation is small and can not completely damage the sample [30]. Another micro-hardness test is the nanoindentation test. This test is mainly used for measuring the hardness of thermoplastics. It is nearly identical in use to the Knoop hardness test, however, the difference is that most often a triangular pyramid-shaped Berkovich indenter is used [31].

The first widely used standardized hardness test for metals is the Brinell hardness test. In this test, a standardized indenter sphere made from steel or tungsten carbide with a diameter of 10 mm is

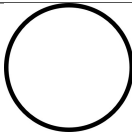
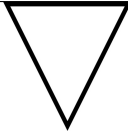
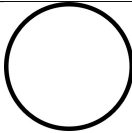
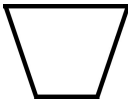
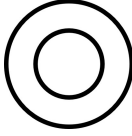
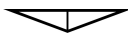
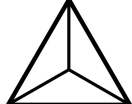
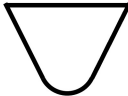
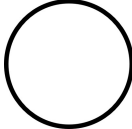
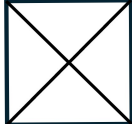
pressed down with a 3000 kgf (29.42 kN) force. The diameter of the indentation is measured and used to determine the Brinell hardness in MPa. Although this test is not used much due to its large indentation, the hardness number gained from this test can be correlated to the tensile strength, although this depends on the material[32].

The Rockwell hardness test is one of the most used for metals and other materials. Much like the IRHD and Shore hardness, the Rockwell test uses different scales to assess the hardness of materials, using a spheroconical diamond or a tungsten carbide sphere with diameters ranging from 1.59 to 12.70 mm to indent the material. These different scales are used for materials ranging from cemented carbides to cast iron to thermoplastics. The test is done by first placing an initial load of 98 N on the material and then indent the material with the main load ranging from 147 to 1470 N depending on the scale used, until the indentation has stopped. The machine measures the indentation depth by displacement of the tip and a dimensionless number representing the hardness is calculated and given by the machine [32].

The Vickers hardness test is another widely used test for metals. The principle is that regardless of size, a square pyramid-shaped indenter would make a similar impression with well-defined measurement points which can be used to find out the hardness in MPa. The hardness is calculated by dividing the indentation force with the remaining indentation area. When this test is performed correctly on isotropic materials, the indentation shape is symmetrical. This means that if the test is not performed correctly, it is easily seen as the indentation is not symmetrical [32].

Reviewing the overview in Table 2.4.1, it can be concluded that spherical indenters are used most often in indentation tests. For cases of isotropic materials, like the polymer matrix in composite materials, a spherical indenter will be considered from now on. However, UD composite is anisotropic. Therefore, a plane strain solution will be considered caused by indentation of a cylindrical indenter with, ideally, negligible deformation in the fiber direction. For all indentation tests mentioned in this section the maximum force is related to the plastic deformation of the material to find a hardness value. The indentation test method that will be done during this research is different, as the force development during indentation will be measured, and force-displacement data will be used to further characterize the indented material.

Table 2.4.1: Types of hardness tests and their indenter profiles

Indenter shape	Test	Shape of indentation	
		Side view	Top view
Sphere	Janka IRHD Shore Brinell Rockwell		
			
			
			
			
spheroconical	Rockwell		
Pyramid	Vickers		

### 2.4.2 Indentation viscosity of isotropic materials

With the explored geometries of existing indentation test a closed form solution for measuring viscosity of isotropic viscoelastic materials through indentation can be found. However, before that can be done the mathematical background of the closed form solution needs to be explained. The in depth explanation is given by Popov et al. [33], but the important aspects will be given in the upcoming section.

In classical elastic contact problems as considered by Hertz [34], the substrate material used is a linear-elastic, homogeneous, isotropic half-space. While viscoelastic materials behave differently than the materials Hertz modeled with, half-spaces are to be assumed either way. A half-space is a semi-infinite body bounded by a plane, which, in this context, is the contact plane between the half-space and indenter. Because a half-space is impossible in the real world, a few assumptions need to be made to make the analytical solution work [35]:

- The radii of curvature of the contacting bodies are large compared to the radius of the circle of contact.
- The dimensions of each body are large compared to the radius of the circle of contact.

- The contacting bodies are in frictionless contact.

While assuming half-spaces reduces the effort needed to calculate the exact solution, multi-dimensional reduction (MDR) is needed to reduce three-dimensional contacts to an array of one-dimensional independent contacts using a Winkler foundation. A Winkler foundation in elastic contact problems is a linear arrangement of linear-elastic spring elements with independent degrees of freedom and a sufficiently small distance  $\Delta x$  between them. For viscous bodies, the springs get replaced by dashpots, which represent a viscous component, and in the case of viscoelastic bodies, the springs get replaced by individual Kelvin models. The given Winkler foundations are illustrated in Figure 2.4.2.

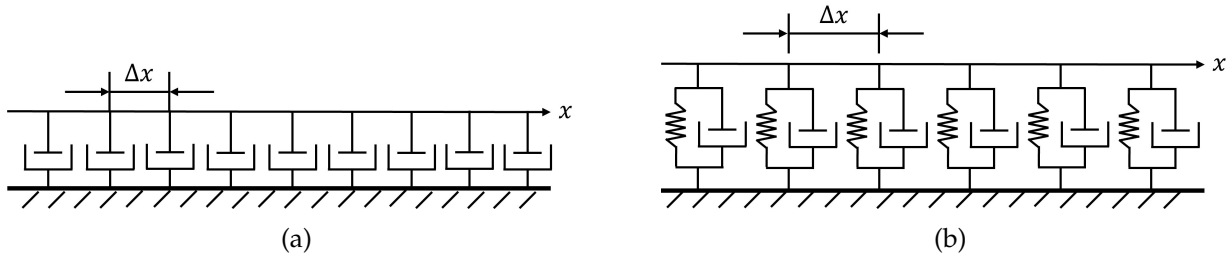


Figure 2.4.2: One-dimensional Winkler foundations for (a) viscous materials made of dashpots and (b) viscoelastic materials made of Kelvin models.

From this a closed form solution for viscous and viscoelastic materials can be derived.

### Viscous closed form solution

The dashpots have a damping coefficient that can be expressed with:

$$\Delta\alpha_d = 4\eta \cdot \Delta x \quad (2.4.1)$$

where  $\alpha$  [ $Ns/m$ ] is the damping coefficient and  $\Delta x$  [ $m$ ] is the distance between Winkler elements. The normal force of one dashpot element is determined by multiplying the damping coefficient from Equation 2.4.1 with the indentation speed:

$$\Delta F_N = 4\eta \cdot \dot{d} \cdot \Delta x \quad (2.4.2)$$

where  $\dot{d}$  [ $m/s$ ] is the indentation velocity. To convert the individual element force to a total normal force, the individual element force needs to be multiplied by the number of elements in contact with the indenter, which is  $2a/\Delta x$ . This results in a total normal force for viscous bodies of:

$$F_N = 8\eta \cdot a \cdot \dot{d} \quad (2.4.3)$$

Where  $a$  [ $m$ ] is the contact radius between the indentation tool and material. The 3 dimensional indenter profile  $\tilde{z}$  is a function of the radius  $f(r)$ . This profile needs to be transformed to a plane profile function of  $x$   $g(x)$ . This can be done with:

$$g(x) = |x| \int_0^{|x|} \frac{f'(r)}{\sqrt{x^2 - r^2}} dr \quad (2.4.4)$$

According to Herz [34], the indentation profile shape of a spherical indenter is characterized as a parabola, which makes the 3 dimensional indenter profile  $f(r) = r^2/2R$ . When this 3 dimensional profile is used in Equation 2.4.4, it will be transformed to the plane profile  $g(x) = x^2/R$ . With this plane profile an equation for the contact radius can be formulated. The indentation depth  $d$  [ $m$ ] is

equal to the plane profile at the width of the contact radius,  $d(t) = g(a(t))$ . Rewriting this gives the contact radius:

$$a = \sqrt{R \cdot d} \quad (2.4.5)$$

Substituting this in Equation 2.4.3 gives the closed form solution for viscous materials.

$$F_N(d) = 8\eta \cdot \sqrt{R \cdot d} \cdot \dot{d} \quad (2.4.6)$$

### Viscoelastic closed form solution

The closed form solution for viscoelastic material is derived much the same. However, the spring parallel to the dashpot requires that an extra term is added to the total normal force. The stiffness coefficient of the spring is defined as:

$$\Delta k = 4G \cdot \Delta x \quad (2.4.7)$$

where  $k$  [N/m] is the stiffness coefficient. The normal force of one spring element is determined by multiplying the stiffness coefficient with the indentation depth:

$$\Delta F_N = 4G \cdot d \cdot \Delta x \quad (2.4.8)$$

Adding Equation 2.4.1 and Equation 2.4.8 gives the normal force for one Kelvin element:

$$\Delta F_N = 4G \cdot d \cdot \Delta x + 4\eta \cdot \dot{d} \cdot \Delta x \quad (2.4.9)$$

From here the normal force for one Kelvin element is multiplied with the contact radius of Equation 2.4.5 to get the closed form solution for a viscoelastic material:

$$F_N(d) = 8G \cdot \sqrt{R \cdot d} \cdot d + 8\eta \cdot \sqrt{R \cdot d} \cdot \dot{d} \quad (2.4.10)$$

Using these equations, a closed form analysis can be done to further understand the viscous or viscoelastic behavior of matrix material using a spherical indenter moving at a constant velocity. This can be compared to numerical analysis done by finite element simulations to get two theoretical solutions to compare to the experimental data. The difference between the half-space solution of the analytical analysis and the numerical analysis with finite dimensions will be apparent. It is expected that the force-depth diagrams will be in the same order of magnitude, albeit with slightly different values.

### 2.4.3 Indentation viscosity of UD composite materials

UD composite materials are not isotropic and therefore it is difficult to find a closed form solution for indentation problems. Furthermore, because the transverse viscosity behavior is the one characteristic to characterize, an axisymmetric indenter like a sphere is unfavorable. For that reason a plane strain set-up is needed. Experimental data can be acquired by pressing a cylindrical indenter parallel to the fibers onto a specimen. With this a line and subsequently cylindrical contact between indenter and specimen is created, pushing the material away in transverse direction. Numerical simulations of this load case can be done to help understand and explain experimental data and possibly for parameter estimation as well.

# Chapter 3

## Methodology

In this chapter, the methodology used to describe the behavior of the material is discussed. Initially, the materials and equipment is introduced. Subsequently, the sample preparation is described. Finally, the different tests to characterize the material and the quality of the material are described.

### 3.1 Materials and equipment

The polymer used for the first set of experiments was a Low-Melt PolyArylEtherKetone (LMPAEK) in powder form from Victrex [36]. This material was used as PAEKs in general have excellent mechanical properties, but they are difficult to use in manufacturing due to the high processing temperatures. LMPAEK however has a lower melting point than other standard PAEKs while still retaining its normal glass transition temperature, and thus it provides excellent material properties at high temperatures [37]. Given its favorable properties, LMPAEK is frequently subject to current research. The properties of the material are given in Table 3.1.1[38].

Table 3.1.1: Properties of LMPAEK [38]

Property	Unit	Parameter
Density (specific gravity)	$[g/cm^3]$	1.30
Tg (glass transition temperature)	$[^{\circ}C]$	147
Tm (melt temperature)	$[^{\circ}C]$	305
Tc (crystallinity temperature)	$[^{\circ}C]$	263
Tp (processing temperature)	$[^{\circ}C]$	340-385

The composite material used for the second set of experiments was the UD Carbon LMPAEK (C/LMPAEK) 0.14 mm thick preimpregnated fibers (pre-preg) tape [38]. The matrix of the composite is of the same LMPAEK used in the first set of experiments, making it easier to compare the two sets, with carbon fiber inserted in the material in one direction. The relevant properties are given in Table 3.1.2 [38]

Table 3.1.2: Properties of C/LMPAEK [38]

Property	Unit	Parameter
Areal weight per ply (PAW)	$[g/m^2]$	221
Consolidated ply thickness (CPT)	$[mm]$	0.14
Density	$[g/cm^3]$	1.59

Four different pieces of equipment were used during the course of this research and all of their uses

will be explained in detail. A hot plate press was used to make samples, a Differential Scanning Calorimeter (DSC) was used to find exact melting points of material and to see if any degradation had taken place during making and testing the specimens, a rheometer was used to do the bulk of the experiments, and a microscope was used to investigate the specimens after the rheometer experiments.

### 3.2 Specimen preparation

Before creating the specimens the LMPAEK granules and the C/LMPAEK tape was dried in an oven overnight at 125 °C. Then, a Fontijne platen press LabPro 200 was used to mold LMPAEK disks with a diameter of 25 mm for plate-plate rheometry, a 6 mm thick LMPAEK plate of 150 mm by 150 mm, and a 7.5 mm thick UD C/LMPAEK plate of 150 mm by 150 mm. For each respective shape, a frame was taped down with kapton tape to a metal plate with Polyimide foil between the frame and metal plate. The frame was filled with 1.5 times the needed volume of material to compensate for any leaking between the frame and metal plate and to avoid voids in the final product. Another layer of polyimide foil was placed over the frame and a second metal plate was used to cover the whole part. The mold set-up is displayed in Figure 3.2.1.

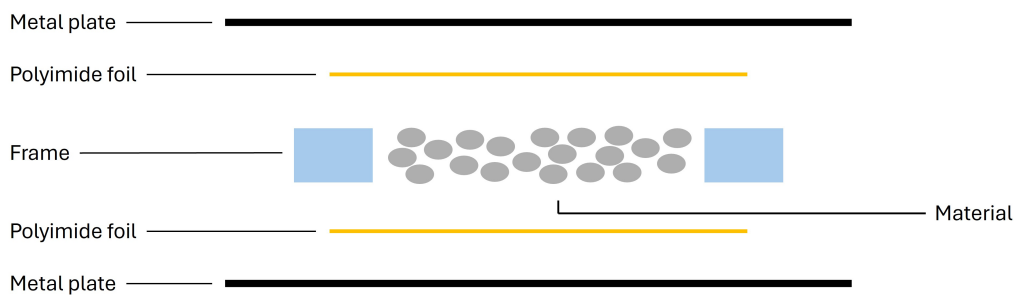


Figure 3.2.1: Schematic cross section of the general mold lay-up used for pressing the specimens. The material that was to be pressed placed between the polyimide foils and within the frame in the middle. The material represents either the LMPAEK granules or the C/LMPAEK tape

The two metal plates and the frame were coated with a release agent. The press was heated to 350 °C and when that temperature was reached, the press was closed with a force of 10 kN or a laminate pressure of 0.44 MPa at 20% of the maximum closing speed of the press to ensure that all material would gradually melt and simultaneously be pressed into the mold while giving it time to release any trapped air in the material. When the press was closed it stayed at 10kN for 10 minutes. Then, the pressure was increased by 10 kN every 30 seconds until a force of 90 kN or a laminate pressure of 4 MPa was reached. The press was then cooled to room temperature before opening to ensure a fully solidified end product. A temperature and force profile of the molding process can be found in Figure 3.2.2 of the press After the press opened up and the end product was taken out, possible pieces of foil that stuck to the end product were removed. The LMPAEK disks were finished products. The LMPAEK plate was cut in 16 by 16 mm squares and C/LMPAEK plate was cut in 10 by 16 mm rectangles with a diamond saw. These squares and rectangles were used as specimens. The length and width of the specimens were restricted to the dimensions of the environmental chamber, the bottom plate of the rheometer, and for the C/LMPAEK specimen the length of the cylindrical indenter as well. A specimen with this volume could still be contained on the bottom plate if it were to melt and flow away from the center. The thickness of the specimens was restricted by the availability of the material and the height of the frame used to form the square. The night before testing took place, the specimen were again dried overnight in a 125 °C oven to ensure no moisture

was present.

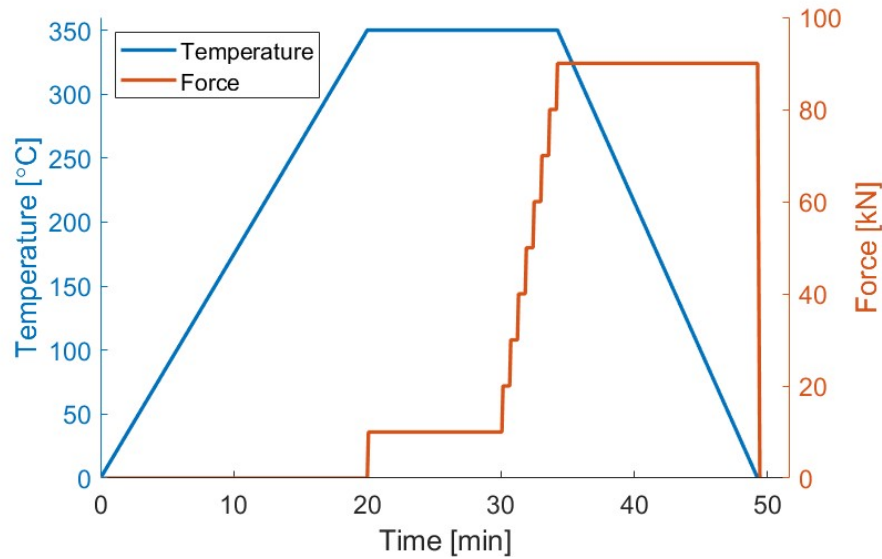


Figure 3.2.2: A profile of the temperature and force over time for the molding process.

### 3.3 Rheometry

The LMPAEEK disks were used in rheometer experiments to find the viscosity of LMPAEEK by means of means of oscillatory and rotational plate-plate experiments. The test is done on the TA Instruments Rheometer HR20 [39], with  $N_2$  shielding gas flowing at 10 L/min. A test temperature of 365 °C was chosen as this temperatures is somewhat in the middle of the processing temperature of LMPAEEK, as seen in Table 3.1.1. First, an oscillatory amplitude sweep with a strain range from 0.01 to 100% at a frequency of 10  $rad/s$  was done to determine the linear viscoelastic region (LVER), which took 2 minutes. The LVER is material-dependent, therefore it does not have to be repeated per new specimen or at different temperatures.

Due to the large deformations placed upon the specimen during the amplitude sweep, the contact between the specimen and plates could deteriorate. Hence a new specimen was loaded for the frequency sweep, which was again heated to 365 °C. Then, a oscillatory frequency sweep was done to determine the complex viscosity over a frequency range from 0.1 to 200  $rad/s$ . The frequency sweep was done at 1% strain, which is found to be well within the LVER. This took 4 minutes.

After the frequency sweep, a rotational shear strain rate sweep at 365 °C was done to validate the frequency sweep at small strains. The shear strain rate sweep was done with a shear strain rate range from 0.01 to 10  $s^{-1}$ , which took 9 minutes. The frequency sweep was done before the shear strain rate sweep because the shear strain rate sweep could irreversibly deform the specimen and deteriorate the contact between the specimen and the disks. The types of sweeps and their ranges can be found in Table 3.3.1.

### 3.4 Indentation viscosity tests

The indentation viscosity tests were conducted on the rheometer as well. Specialized tools based of a standard 25 mm diameter rheometer top fixture were made for the purpose of conducting this tests. These tools were made by milling a top fixture from a block of aluminum with either a semi-sphere

Table 3.3.1: The types of sweeps and their ranges done with the rheometer.

Type of sweep	Range of sweep
Amplitude	0.01% to 100%
Frequency	1 rad/s to 100 rad/s
shear strain rate	$0.01 \text{ s}^{-1}$ to $10 \text{ s}^{-1}$

with a radius of 3 mm, or a semi-cylinder with a radius of 3 mm and a length of 10 mm milled on top. A render can be seen in Figure 3.4.1. The indentation tools were installed as the top fixture of the rheometer. A specimen of LMPAEEK, covered on all sides except the top with aluminum foil to prevent the material from flowing while molten, was placed on top of a piece of polyimide foil inside the environmental chamber of the rheometer. The specimens were heated up to  $365 \text{ }^\circ\text{C}$  and during the whole test an  $\text{N}_2$  flow of 10 L/min was supplied as shielding gas. The specimens stayed at  $365 \text{ }^\circ\text{C}$  for at least 2 minutes before continuing the tests to ensure a homogeneous temperature throughout the specimen. Then, the indenter was lowered with a constant indentation velocity or rate of either  $400 \text{ } \mu\text{m/s}$ ,  $800 \text{ } \mu\text{m/s}$ , or  $1600 \text{ } \mu\text{m/s}$  until an indentation depth of 1 mm was reached. For the matrix material, a linear sampling rate of 4 points per second was chosen. However, the sampling frequency of axial tests is limited to around 2 points per second. This means that it is possible that data points gathered within a 0.5 second time frame can repeat the measurements from the previous data point to fill the gap in the sampling frequency. For the UD composite the fast sampling rate on the rheometer was chosen. This setting start at a high sampling frequency but logarithmically decreases the sampling frequency per decade. The reasoning behind these sampling settings can be found in Appendix D.

In these tests, the force and indentation depth were measured over time, and with these parameters, viscosity can be calculated according to Equation 2.4.6, in case the solution for a half space is applicable, i.e. for specimen sizes large enough and indenter size small enough. These tests were repeated several times according to Table 3.4.1. One difference between the testing of LMPAEEK and C/LMPAEEK was that the C/LMPAEEK did not need a aluminum foil cover as the material would not flow away when heated. A full test protocol can be found in Appendix A. DSC tests were done to see if any degradation took place during the whole test procedure. These can be found in Appendix B

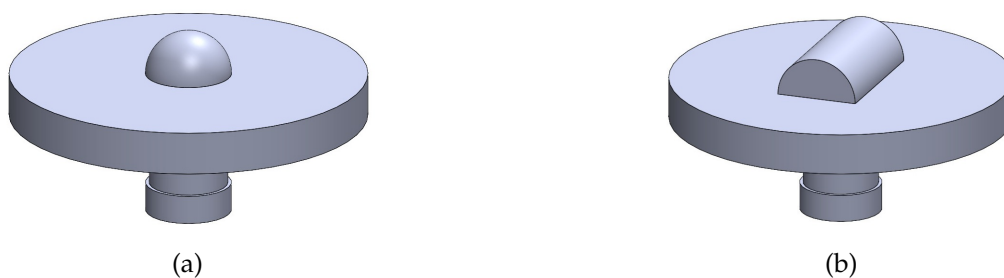


Figure 3.4.1: The indenters used for the indentation viscosity tests. Both with an outer diameter of 25 mm and for (a) a spherical indenter of 3 mm and for (b) cylindrical indenter with a radius and length of 3 and 10 mm respectively.

### 3.5 Microscopy

Microscopy imaging was used to further analyze a select few C/LMPAEEK specimens after indentation. This was done with a Keyence VHX 7000 microscope with the VH-Z20R/W/T lens at 100x

Table 3.4.1: Test matrix for the indentation foil test, where the number of repetitions is given.

Specimen material (indenter type)	Indentation velocity [ $\mu\text{m/s}$ ]		
	400	800	1600
LMPAEK (3 mm spherical indenter)	3	3	3
C/LMPAEK (3 mm cylindrical indenter)	3	3	3

magnification. The specimens were encased in epoxy and their surface was polished. The stitch programming was used to create a high resolution image. These images were then analyzed for defects and other irregularities in the material that could tell something about the material behavior.

### 3.6 Finite element model simulations

In Section 2.4.2 and Section 2.4.3 numerical simulations have been introduced to understand experimental data, and possibly help in determining material property data from the experimental results. Here, the in-house developed finite element solver 'DiekA' (version 8.1) was used for this purpose, in this case using linear quadrilateral elements with selective reduced integration of the pressure terms to prevent so-called volume locking. In addition, an Arbitrary Lagrange Euler formulation was used to keep the elements in good shape despite the locally large deformations. More details on the latter can be found in the PhD theses of e.g. Huétink, Akkerman and Stoker [40, 41, 42]. Axisymmetric simulations were performed to compare to the LMPAEK indentation test results. Plane strain simulations performed to compare to the C/LMPAEK indentation test results. A schematic overview of a simulated model and its boundary conditions is given in Figure 3.6.1. The material for the axisymmetric simulations was modeled as an axisymmetric cross section. A full stick condition on the bottom was assumed, but it is uncertain if this condition applies to the indentation tests as well. Further research needs to be done to see if this boundary condition applies. A horizontal movement constraint at the center line was defined as well. The material for the plane strain simulations was modeled as one half of a rectangular specimen with the same constraints as in the axisymmetric simulations. In this model an element mesh was created with the elements close to the contact point being finer than the elements at the right edge. The indentation tool is modelled as fully rigid on top of the specimen model. The element mesh and indentation tool can be seen in Figure 3.6.2.

The viscosity of polymers subjected to an increased shear strain rate show a rapid decrease in viscosity, much the same as seen in a cross model. For that reason the material model of the axisymmetric simulations was modeled according to the Cross model in Equation 2.1.4, although this does ignore possible elastic effects in the material. The material properties  $\eta_0$ ,  $\lambda$ , and  $n$  will be obtained from fitting the Cross model on the rheometry results. The material behavior of the plane strain simulations was modeled with the shear stress from a Kelvin model seen in Equation 2.1.10, as the C/LMPAEK was expected to have a more pronounced elastic effect. For both models reversible and nearly incompressible behavior is described by means of an elastic response to volume changes with a sufficiently high bulk modulus  $C_b$  [MPa].

Contact between the indenter and the specimen is modeled by means of contact elements employing a penalty formulation. The contact stiffness  $k$  should be high enough to prevent significant penetration between the tool and the material, while low enough to keep convergence of the iterative scheme sufficiently smooth. In the tangential direction, these contact elements can represent different friction

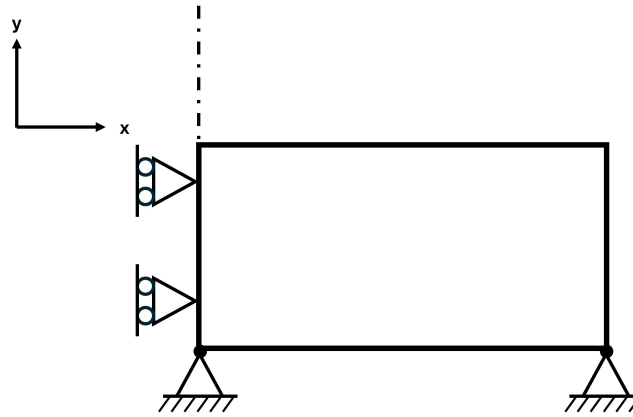


Figure 3.6.1: Schematic overview of the specimen model for the axisymmetric simulation and the boundary conditions it is subjected to. The model for the plane strain simulation is similar, but without the rotational symmetry.

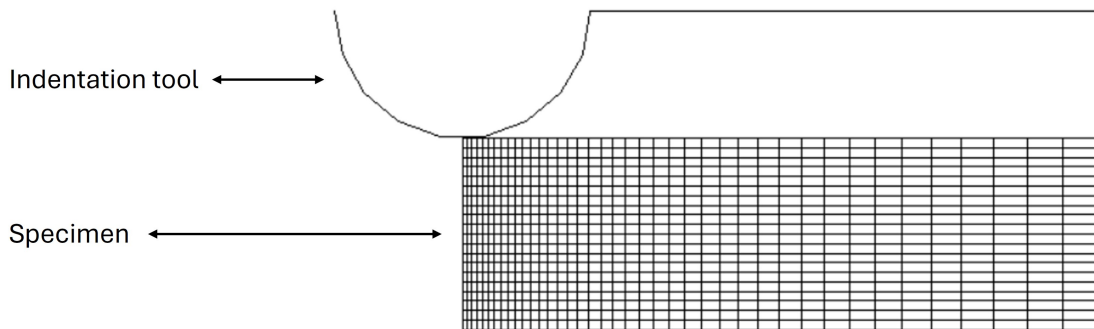


Figure 3.6.2: Overview of the specimen model with mesh and indentation tool

laws. In the current case, a viscous friction law was employed, according to:

$$\tau_f = \frac{1}{\beta} \cdot v_{rel} \quad (3.6.1)$$

with  $\tau_f$  [MPa] as the friction stress,  $\beta$  [ $mm^3/N \cdot s$ ] as a slip coefficient and  $v_{rel}$  as the relative velocity between the two bodies. A high slip coefficient gives a low friction stress.

The parameters used for the simulations can be found in Table 3.6.1, where  $\eta_0$ ,  $\lambda$ , and  $n$  from Table 3.6.1a will be filled in after the rheometry test is done and  $\eta$  from Table 3.6.1b will be changed per indentation velocity to fit indentation test results. In Section 4.1 the influence of the parameters on the simulations will be examined to see if the used parameters were of a sufficient value. A full explanation on how the specimen model is made and how the property parameters are determined can be found in Appendix C.

The user manual [43] provides information on the background and use of the program. The program Dipp (version 10.0) was used for postprocessing the results after the simulations. This program can be used to visualize the FE mesh, the element deformations and to create contour plots of stresses, displacements, forces, and pressure inside the material.

Table 3.6.1: Property parameters used in (a) the axisymmetric simulation and (b) the plane strain simulations

(a)			(b)		
Property	Unit	Parameter	Property	Unit	Parameter
$\eta_0$	[MPa]	-	$\eta$	[MPa · s]	-
$\lambda$	[ms]	-	$G$	[MPa]	$1.67 \cdot 10^{-3}$
$n$	[-]	-	$C_b$	[MPa]	200
$C_b$	[MPa]	200	$k$	$[\frac{N}{mm^3}]$	0.002
$k$	$[\frac{N}{mm^3}]$	0.002	$\beta$	$[\frac{mm^3}{N \cdot s}]$	1000
$\beta$	$[\frac{mm^3}{N \cdot s}]$	1000			

### 3.7 Data analysis

The data obtained from the test was calibrated by manually setting the indentation depth and force to zero at the point of contact between the indenter and the specimen. For the matrix material the point of contact was determined by fitting a line on data points that were clearly before an increase in force and a line on data points that were clearly after an increase in force. The data point closest to the intersection of the two fitted lines was chosen as the data point associated with the point of contact. A clear point where the indentation tool made contact with the specimen could not be found due to the amount of noise the rheometer had when measuring low forces. The noise present in the rheometer can be seen in Appendix D. For the UD composite material, the point where a clear increase in force was measured was used as the point of contact. Test data was deemed unusable when the base plate of the indentation tool reached the indentation limit of 3 mm and would make contact with a specimen. When this happened a massive increase in force was measured and after the test the test data was discarded.

The indentation test data of the matrix material could not be numerically compared with the data obtained from the simulations, due to the nature of the data obtained from the indentation tests. To quantify the matrix material behavior, a linear fit was made on the force-depth diagrams per test. From these fits an average slope per rate was made. The slopes of the average fit of all indentation velocities were compared to each other. Then, axisymmetric simulations were run at the same indentation velocities. A line was plotted between the starting point and the average indentation depth. The slope of this line quantified the simulated force increase over depth and was compared to the slopes of the average test fits. The slopes gave insight in the viscous behavior of the material. Equation 2.4.6 shows that the material behaves like a Newtonian fluid if the slope at a rate of  $800 \mu m/s$  is double that of the slope at a rate of  $400 \mu m/s$ . If the slope is less than double, the material behaves like a shear thinning fluid.

The test results from the UD composite indentation tests were difficult to compare, as the data obtained was not linearly sampled as mentioned in Section 3.4. To describe the measured trends a fit with 3 fitting parameter was made:

$$F(d) = A * \sqrt{d} + B * d + C * d^2 \quad (3.7.1)$$

An average force-depth curve was made from the fits per rate. The average force-depth curves had their own fit parameters as well. The average experimental force-depth curves were compared to the plane strain simulations mentioned in Section 3.6. For each simulation the viscosity parameter was modeled to ensure a good results compared to the experimental force-depth curves, while the shear

modulus remained unchanged.

# Chapter 4

## Results

The results from the various tests to describe the material are presented here. First, the influence of the different simulation parameters are compared and explained. Then the results of the indentation tests are presented together with the results of the rheometry investigations to obtain a better understanding of the test results and to explore the use of the indentation experiments for material characterization purposes. This is then compared to the FEM simulations for further analysis.

### 4.1 Influence of different parameters on the simulations

To explain common contour plots and the influence of the specimen dimensions, mesh density, bulk modulus, contact stiffness, and friction coefficient simple axisymmetric cases with a Newtonian fluid model were simulated. Then, the effects of different viscosities and shear moduli on a plane strain Kelvin model are presented.

#### 4.1.1 Axisymmetric case

The axisymmetric case simulations were done with a disk with similar properties as LMPAEK, a radius of 8 mm, and a thickness of 6 mm. This is equivalent to the dimensions of the LMPAEK specimens and although the LMPAEK specimens are square with a width and length of 16 mm and a thickness of 6 mm, a circle with a radius of 8 mm still fits within the square specimen. The corners of the square could cause a difference in the results between the simulations and the indentation experiments, but this is expected to be negligible. 20 and 40 quadrilateral elements are placed in vertical and horizontal direction respectively for a total of 800 elements in the mesh. Furthermore, the mesh is more refined near the contact point by a factor of 8 and 4 horizontally and vertically respectively. In Figure 4.1.1, mesh plots for different steps in the simulation and their deformations can be seen. In Figure 4.1.2 different types of contour plots which were extrapolated from the mesh plots are depicted. These plots can give some understanding on the typical behavior of LMPAEK at the end of the indentation for small specimens and large specimens. The simulated material with specimen dimensions comparable to the specimens used in the indentation tests was subjected to edge effects, while the material with large dimensions was not.

The last data set gained from the simulations is the force needed to indent the material at a certain depth, depending on the speed of the indentation. With this data set the force-depth curves were made. When the numerical solution of the simulation for Newtonian fluids is compared to the closed form solution given in Equation 2.4.6, it can be seen, in Figure 4.1.3, that the two solutions are

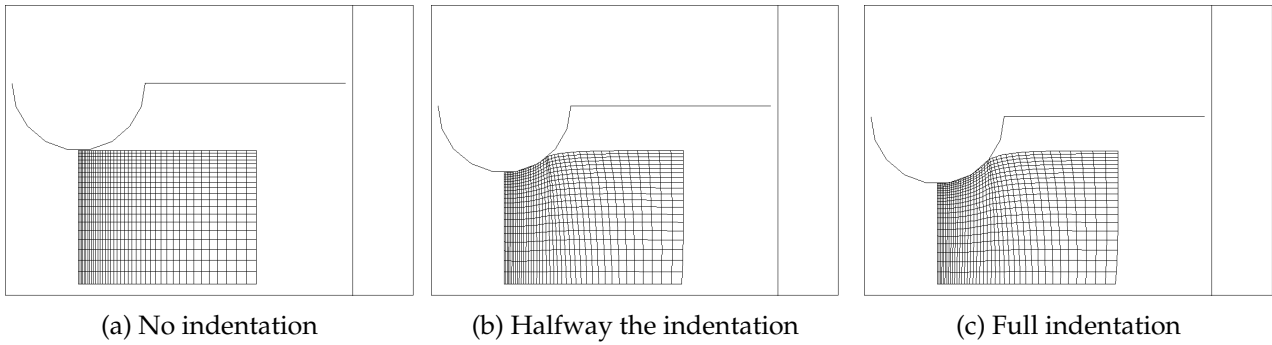


Figure 4.1.1: 3 stages of the indentation simulation, where the indenter is moving with a speed of  $400 \mu\text{m/s}$  and stops when it has reached a depth of  $1.5 \text{ mm}$

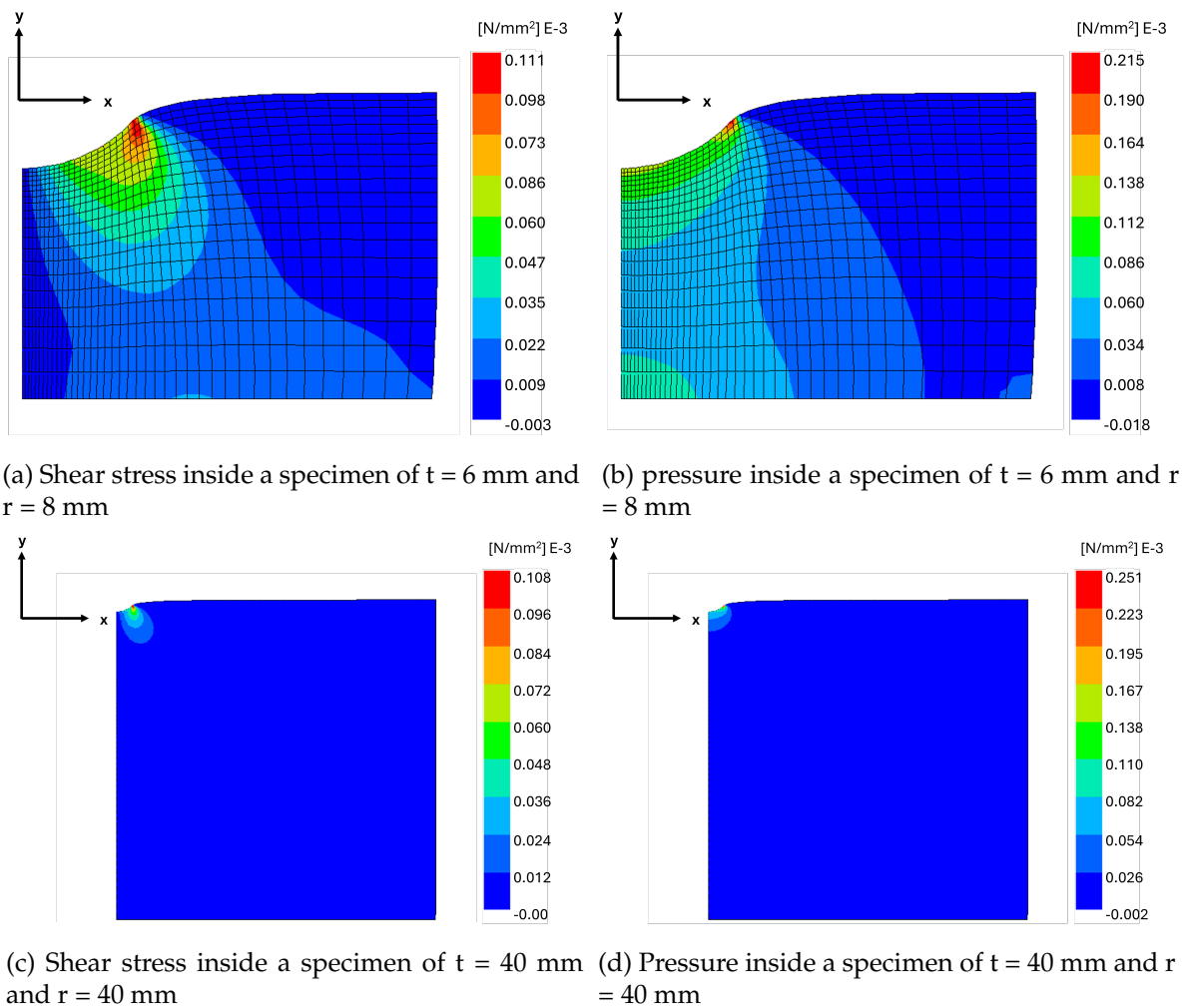


Figure 4.1.2: Typical contour plots of an indented material specimen. The indenter is moving with a speed of  $400 \mu\text{m/s}$  and stops when it has reached a depth of  $1.5 \text{ mm}$ .

comparable, but not equal. This is likely because the closed form solution assumes a half space and the numerical solution assumes finite dimensions, as is mentioned at the end of Section 2.4.2. One more thing to notice with the numerical analysis are the 'steps' in the graph. These steps happen whenever a contact element closes. Upon closing, the stiffness of the model changes instantaneously,

which is reflected in the steps in the force-depth curves.

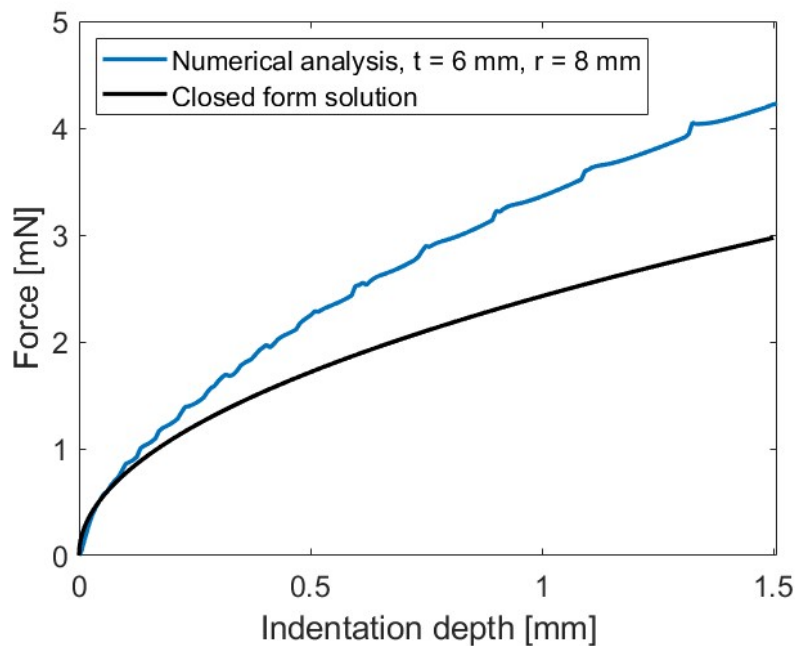


Figure 4.1.3: Comparison between numerical solution of an axisymmetric case with a Newtonian fluid model and the closed form solutions force-depth curve for a rate of  $400 \mu\text{ms/s}$

The influence of dimensions was mentioned before. In Figure 4.1.4 the effect of specimen thickness  $t$  [mm] and specimen radius  $r$  [mm] can be seen. It is clear from the simulations that the resulting force of a thicker specimen is lower than a thinner specimen, while the resulting force of wider specimen is higher than a narrower specimen. Furthermore, it seems that simulations that need to take a larger specimen radius into account are more unstable as they have a more irregular diagram than simulations of a smaller specimen radius. Increasing both the radius and the thickness gives a close approximation to a half-space specimen and approaches the closed form solution.

The mesh density, bulk modulus, contact stiffness, and slip coefficient were mentioned in Section 3.6. Simulations were run to see how each property would affect the outcome. In these simulations one property would change while all other properties remained at their starting value. In Table 4.1.1 the property values used in the simulations are given.

Table 4.1.1: Property parameters used in the axisymmetric case simulations.

Property	Unit	Parameter
Viscosity ( $\eta$ )	[MPa · s]	$438 \cdot 10^{-6}$
Mesh density (-)	[-]	800
Bulk modulus ( $C_b$ )	[MPa]	$2 \cdot 10^2$
Contact stiffness ( $k$ )	$[\frac{N}{\text{mm}^3}]$	0.002
Slip coefficient ( $\beta$ )	$[\frac{\text{mm}^3}{N \cdot s}]$	1000

In Figure 4.1.5a the influence of mesh density is shown. It can be seen that the mesh density does not influence the resulting force, except that more elements cause a more stable simulation. Therefore, mesh density does not greatly impact the simulation results and does not need to be considered in great detail.

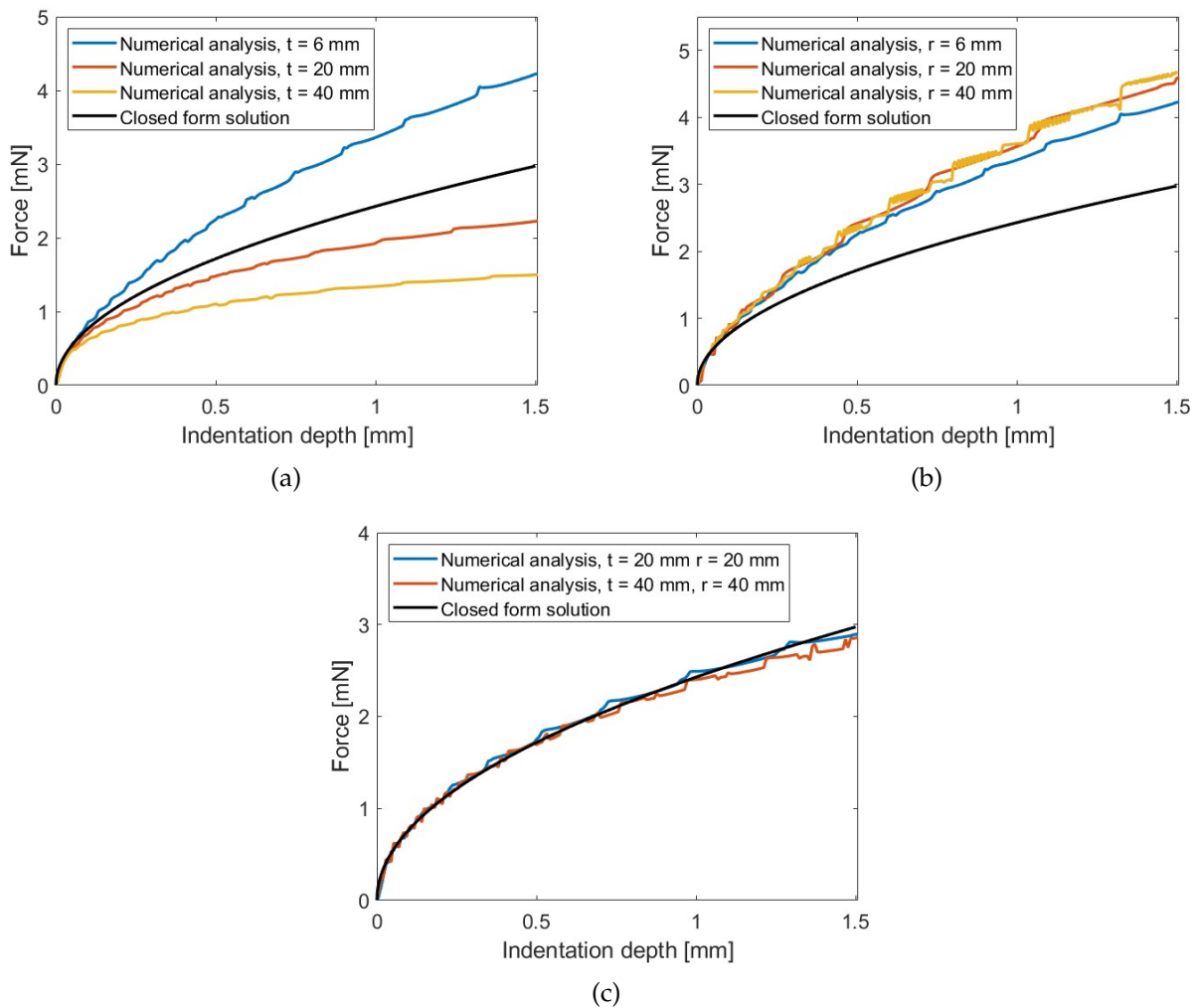


Figure 4.1.4: Force vs. indentation depth where different dimensions show different force responses, where a) shows the difference that the thickness of the specimen gives with a constant radius  $r = 8$  mm and b) shows the difference that the radius of the specimen gives with a constant thickness of  $t = 6$  mm. In c) both the thickness and the radius are increased.

In Figure 4.1.5b the influence of the bulk modulus is shown. Here it can be seen that for a bulk modulus between  $2 \cdot 10^{-2}$  and  $2 \cdot 10^5$  MPa a near identical resulting force is to be expected. For a bulk modulus of  $2 \cdot 10^6$  MPa the approximation is comparable but the simulation is more unstable and for a bulk modulus of  $2 \cdot 10^{-3}$  MPa a different resulting force can be seen. Therefore, the bulk modulus of the simulations should be between  $2 \cdot 10^{-2}$  and  $2 \cdot 10^5$  MPa.

In Figure 4.1.5c the influence of the contact stiffness is shown. It can be seen that all stiffnesses have approximately the same resulting force. However, a contact stiffness above  $2 \cdot 10^{-3}$  N/mm gives a more unstable resulting force. Furthermore, higher stiffnesses result in a longer simulation time. While a contact stiffness of  $2 \cdot 10^{-3}$  N/mm results in a simulation time of approximately 70 seconds, a contact stiffness of 0.2 N/mm results in a simulation time of approximately 60 minutes. When stiffnesses lower than  $2 \cdot 10^{-3}$  N/mm were tried in DiekA the simulations stopped before any indentation happened and thus this was deemed impossible to simulate. It could be that a contact stiffness below  $2 \cdot 10^{-3}$  N/mm causes the contact elements and the mesh elements to overlap, which could give an

error in DiekA. For further simulations, a contact stiffness of  $2 \cdot 10^{-3}$  N/mm was used.

In Figure 4.1.5d the influence of the slip coefficient is shown. It can be seen that with a low slip coefficient and thus a high friction stress between indenter and specimen a higher resulting force occurs. Furthermore, a high friction stress results in a more unbalanced resulting force and a longer simulation time. The slip coefficient does not affect the resulting force by a large amount, but it is not negligible. However, the slip coefficient is unknown and should be further researched before accurate values can be used in the simulations. For now, the slip coefficient is assumed to be large to let the resulting force converge in a nice manner.

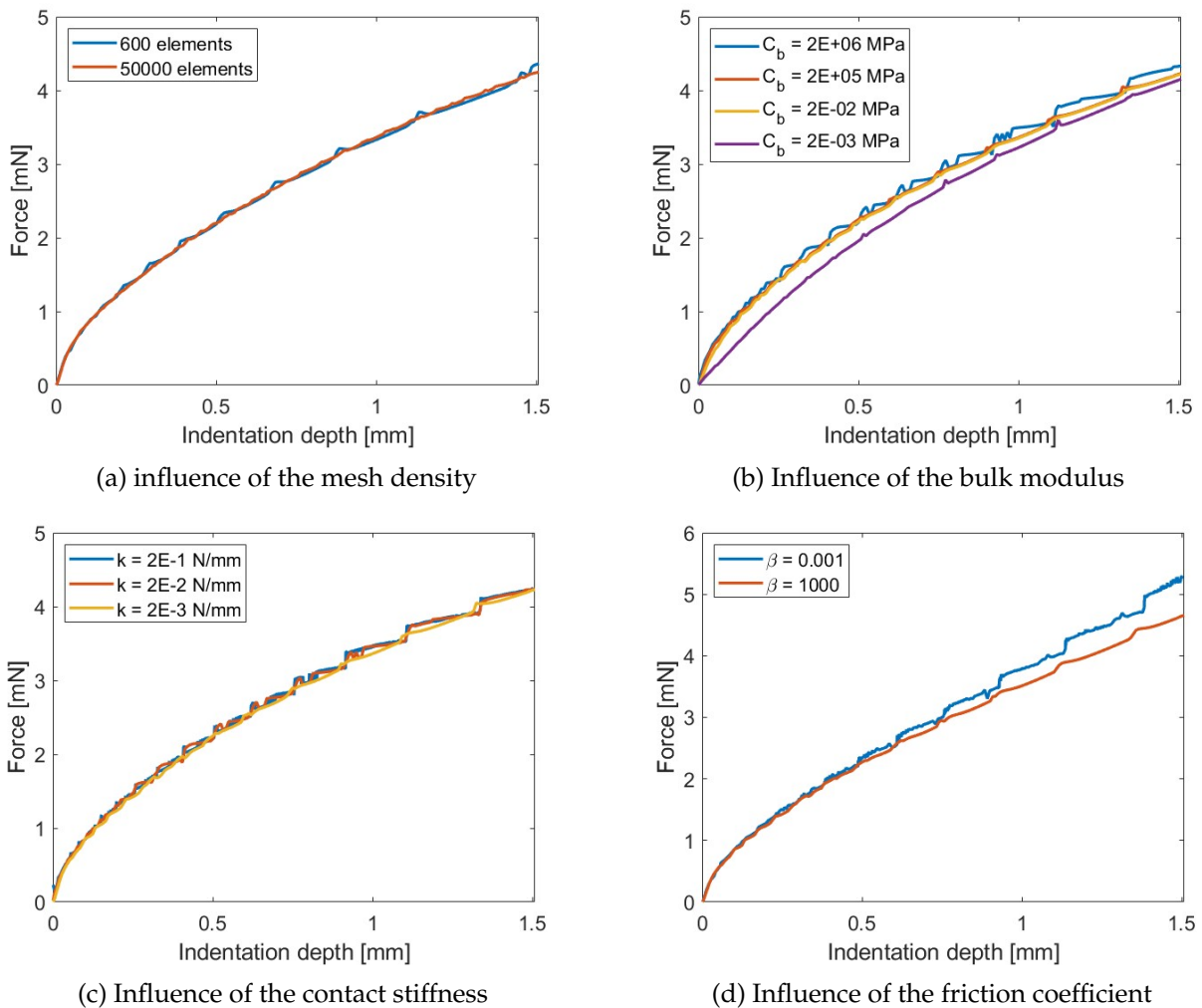


Figure 4.1.5: The influence of different parameters on the outcome of the simulations. In every case all other parameters are kept the same and can be seen in Table 4.1.1.

#### 4.1.2 Plane strain case

The dimensions of the plane strain case simulations were based on the dimensions of the C/LMPAEK tests specimens given in Section 3.2. The simulation specimen have a length of 8 mm, which is half of the length of a test specimen, and a thickness of 7.5 mm. The material is considered to be transversely isotropic in the plane of the analysis. To get the force that is imposed on an actual test specimen, the outcome of the simulation needs to be multiplied by 2 and 10 mm, which is the width of the specimen.

For reference, a material is simulated with  $G = 0.0167$  MPa and  $\eta = 0.05$  MPa\*s that is indented with a cylindrical indenter with a rate of  $400 \mu\text{m/s}$ . The indentation rate and all other parameters were not changed between simulations. In Figure 4.1.6a it can be seen that the forces for all elasticity moduli are nearly equal between 0 and 0.25 mm. At higher indentation depths the forces start to fan out. This implies that in the beginning the response is dominated by the viscous terms and that elastic terms get more dominant at higher indentation depths. This is in agreement with Equation 2.4.10 where the elastic part of the equation is directly influenced by the indentation depth. In the simulation it can be seen that this is the case as well as the force of simulations with more prominent elastic behavior increase faster over the indentation depth. In Figure 4.1.6b it can be seen that the forces between 0 and 0.25 mm increase with higher viscosity. Some fanning out does occur, however the slope for a given indentation direction remains fairly constant. An increase in viscosity primarily causes a shift of the curve in vertical direction.

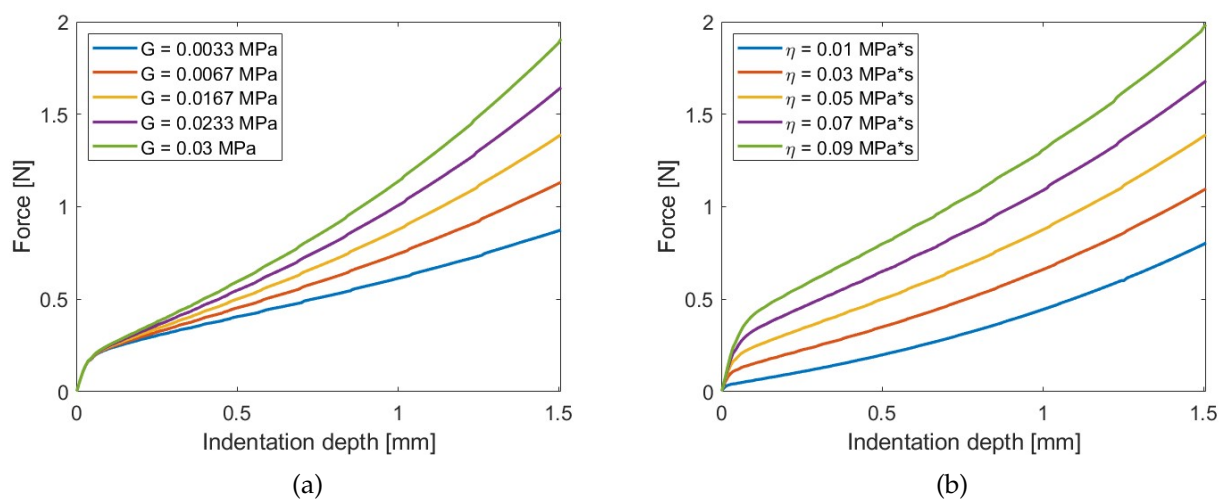


Figure 4.1.6: The influence that a) the shear modulus and b) the viscosity have in the plane strain Kelvin model simulations.

To summarize the effects that the different properties have on the simulations: larger dimensions of the simulated specimen does bring the results closer to the closed form solution and thus approximate the half-space assumption. However, larger specimen tend to be more unstable, as a, compared to the specimen model, small indenter presses on less but larger elements. This is mainly the case when the radius of the specimen is increased. In contrast, increasing the mesh density seems to create a better approximation in the simulation, but the difference between a low density and high density element mesh seems to be negligible. The bulk modulus seems to work as intended between  $2 \cdot 10^5$  and  $2 \cdot 10^{-2}$ . Going higher will create an unstable simulation and going lower will create a wrong approximation of the resulting force. The simulations showed that a contact stiffness of  $2 \cdot 10^{-3}$  N/mm is preferable as higher stiffnesses create an unstable simulation and lower stiffnesses were unable to be simulated. The simulations for the slip coefficient showed that a low coefficient results in a lower resulting force. However, a high slip coefficient creates a more stable approximation. As it is not possible to know what a realistic coefficient of friction is, further simulations were done with a low coefficient of friction to ensure that the resulting force converges in an acceptable manner.

## 4.2 Indentation test

In this section the results of the indentation tests will be examined. First, the matrix indentation tests will be presented and compared with the results from the simulations. Then, the same is done for the UD composite indentation tests.

### 4.2.1 Matrix material indentation tests

The results for the indentation tests of LMPAEK can be found in Figure 4.2.1, the individual test results and their fits can be found in Section E.1.

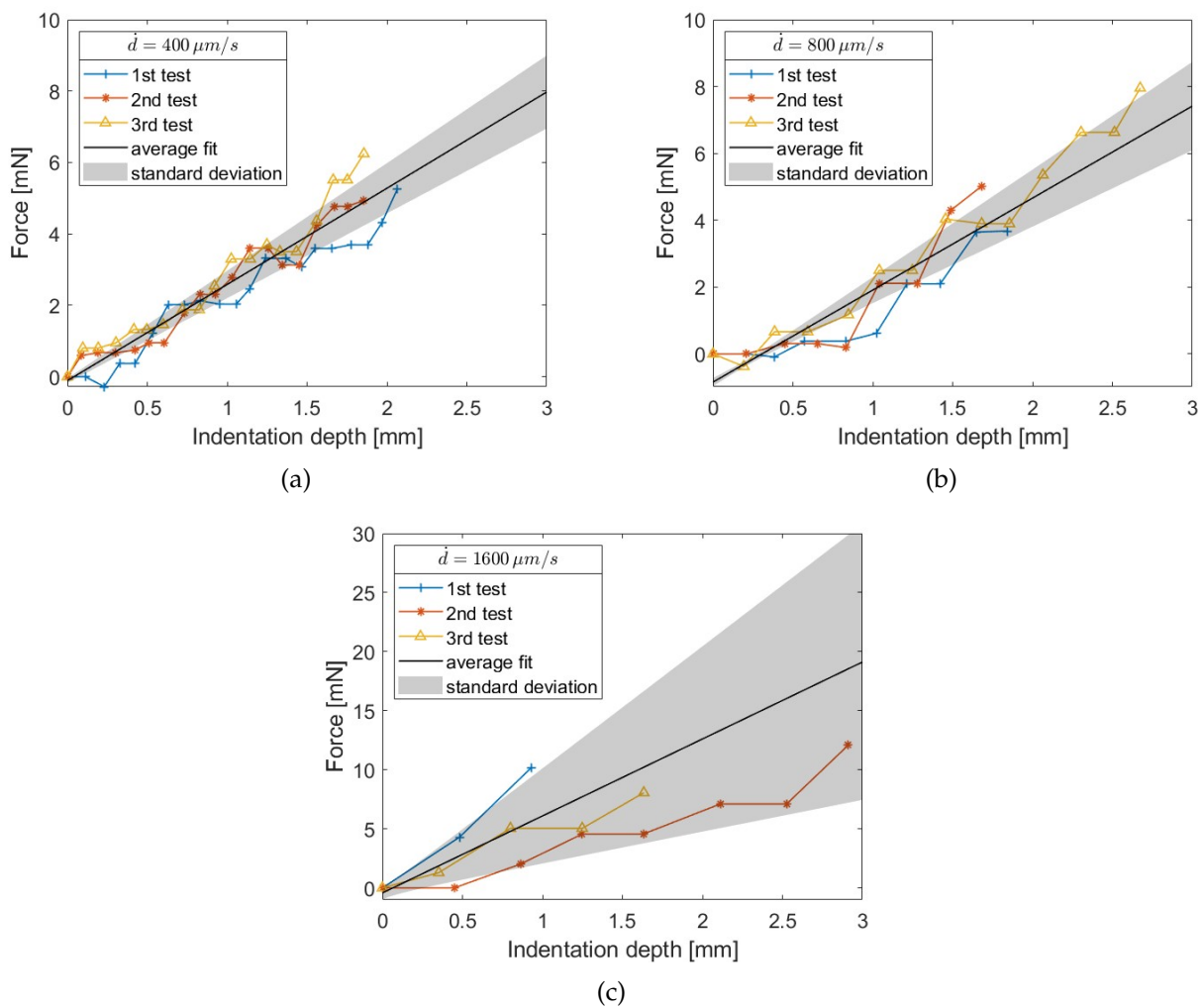


Figure 4.2.1: Test results for all data sets for the matrix material, where the indentation velocity is given in the legend.

At some point during all tests in Figure 4.2.1a and Figure 4.2.1b the measured force arbitrarily decreased from one data point to the other, while an otherwise rising trend was observed. Furthermore, the average indentation depth was 1.94 mm, which exceeded the intended indentation depth of 1 mm.

The results of the rheometry tests can be found in Figure 4.2.2, the property parameters obtained were used with the property parameters from Table 3.6.1a to simulate the force-depth diagrams, which can

be found in Figure 4.2.3. The slopes of the simulations were plotted here as well. The simulations ended at near the average indentation depth at 2 mm. The average slopes and their standard deviations from Figure 4.2.1 were compared with the simulated slopes in Figure 4.2.4. The numerical values of the slopes were compared in Figure 4.2.5.

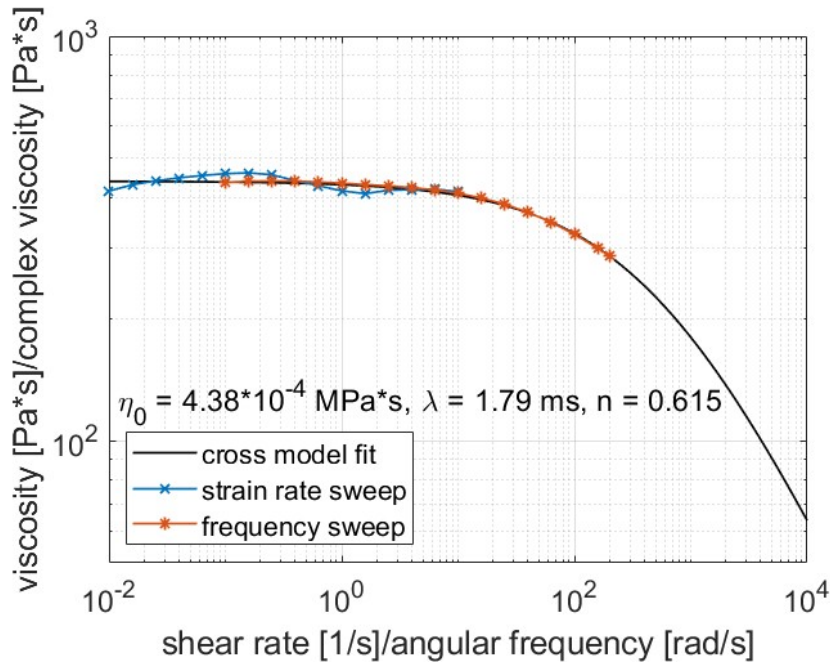


Figure 4.2.2: Results of the rheometry test

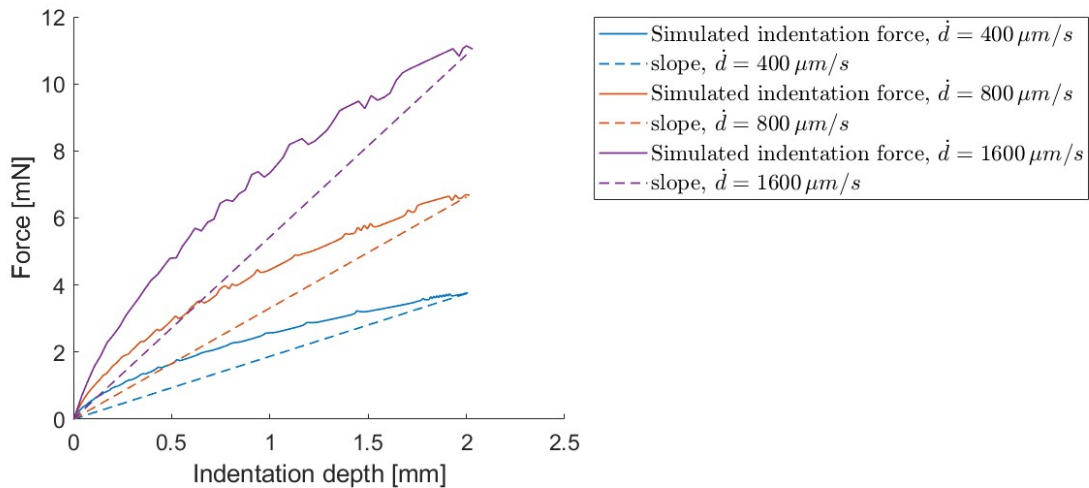


Figure 4.2.3: Results of the axisymmetric simulations with their linear increase in force mentioned as the slope.

Between the rates of 400 and 800  $\mu\text{m/s}$  of the simulations the slope increased with 77% and between the rates of 800 and 1600  $\mu\text{m/s}$  the slope increased with 64%. This indicates that the slope increase of shear thinning materials is not linearly correlated to the indentation velocity and slope increases less at higher indentation velocities. For the test results, the increase in slope between when the material

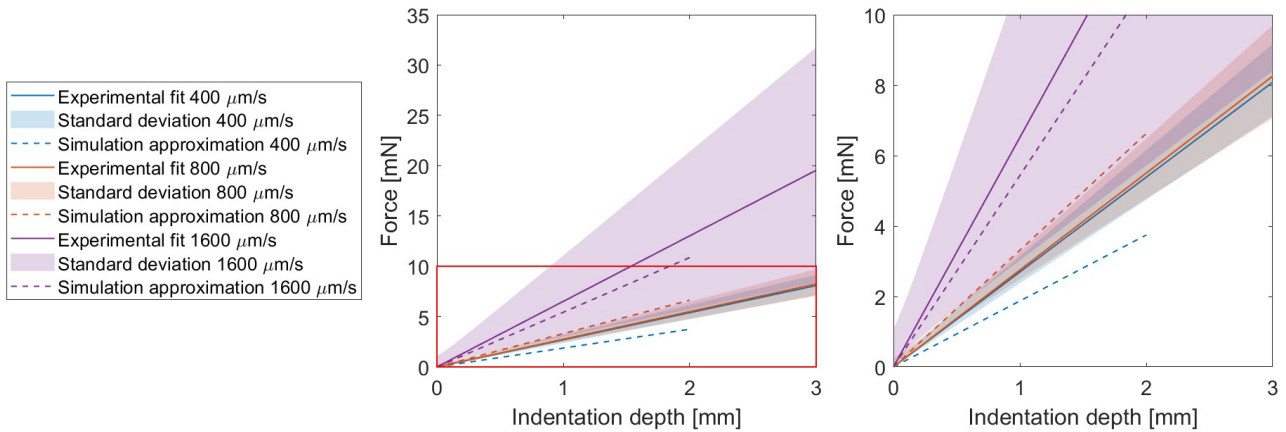
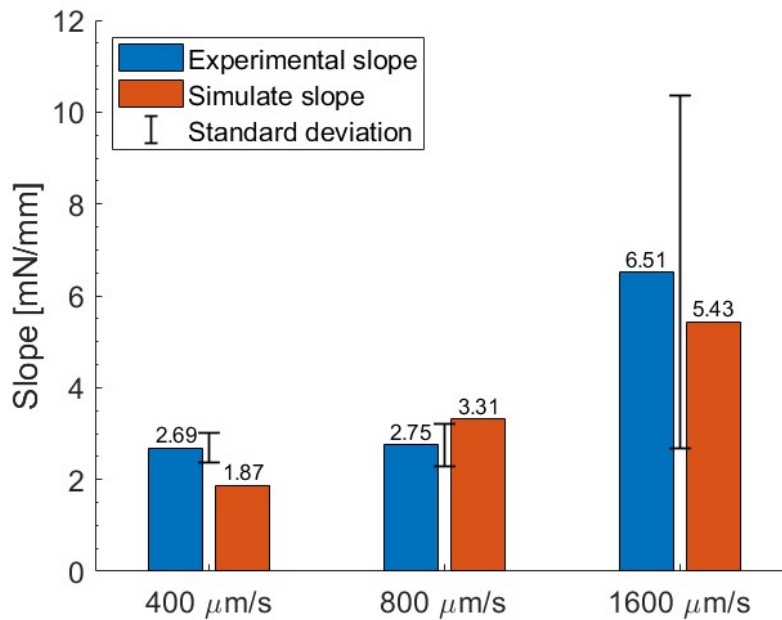


Figure 4.2.4: Comparison between the increase in force of the matrix material data sets and their simulated approximations. The results from indentation speeds 400 and 800  $\mu\text{m}/\text{s}$  were enhanced for better clarity.



ma

Figure 4.2.5: Numerical comparison between the slopes of the average test results and their simulated results.

was indented with a rate of 400 and 800  $\mu\text{m}/\text{s}$  was 2%, and between 800 and 1600  $\mu\text{m}/\text{s}$  was 137%. This does not correspond with the simulated results. Furthermore, the simulated results are not within the standard deviation of test results at 400 and 800  $\mu\text{m}/\text{s}$ . In contrary, the simulated results at an indentation rate of 1600  $\mu\text{m}/\text{s}$  was within the standard deviation of the test results. However, is large compared to the standard deviation of the results at different indentation velocities.

#### 4.2.2 UD composite material indentation tests

The results for the indentation tests of C/LMPAEK can be found in Figure 4.2.6 and the individual test results and their fits can be found Section E.2. All test sets are framed on equal axes for ease of

comparing. The property parameters in Table 3.6.1b were used for the simulations and in Figure 4.2.7 the experimental results and the simulated results are compared. In Figure 4.2.8 the viscosities used in the simulations are compared. A significant drop in viscosity is observed between the simulated fits of rates 800 and 1600  $\mu\text{m}/\text{s}$ . Furthermore, the elastic response of the simulated fit and the experimental fit at a rate of 800  $\mu\text{m}/\text{s}$  behave differently, as the tail end of the simulated fit split off of the experimental fit.

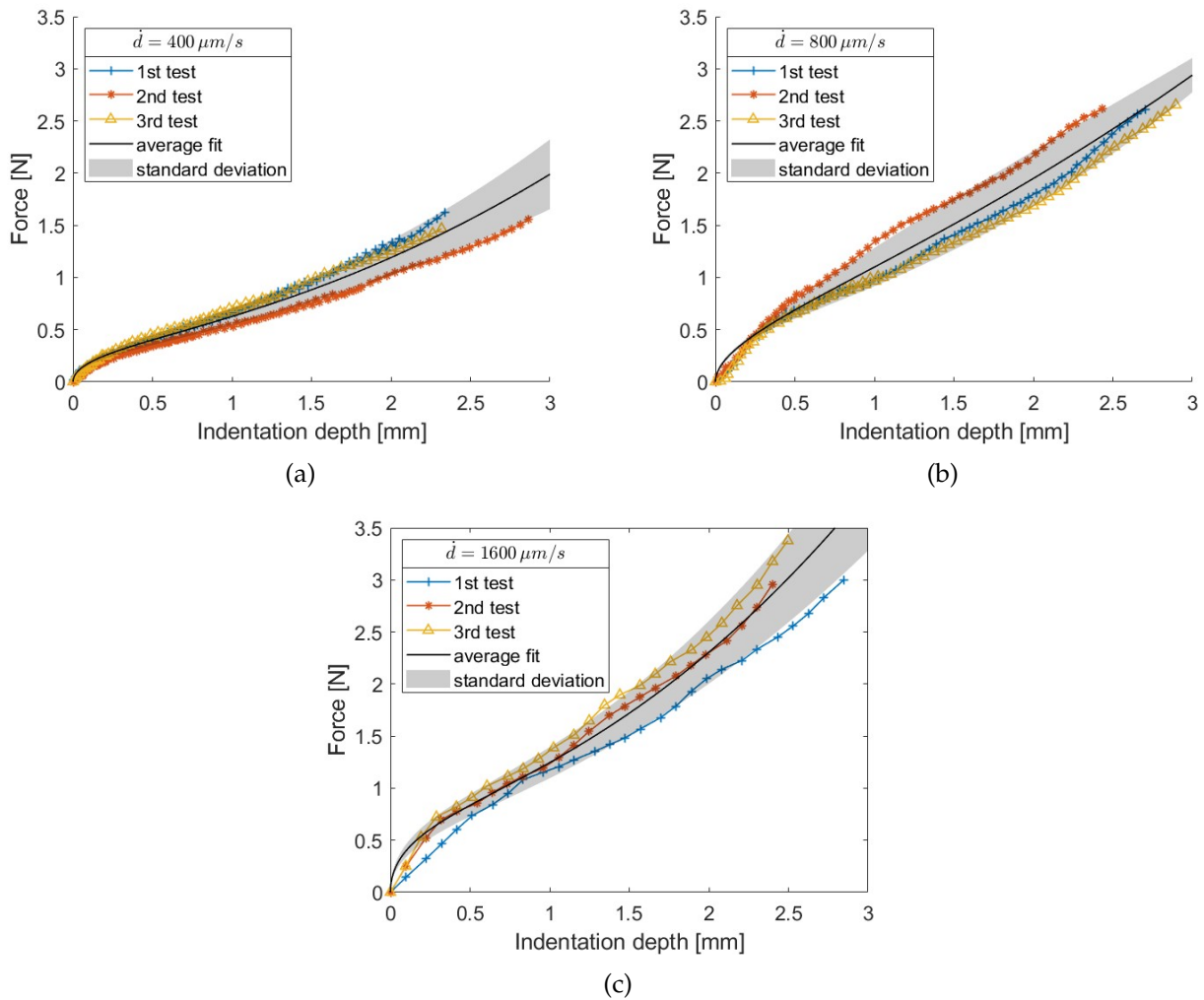


Figure 4.2.6: Test results for all data sets for the UD composite material. In (a) data set 4 is presented, in (b) data set 5 is presented, and in (c) data set 6 is presented.

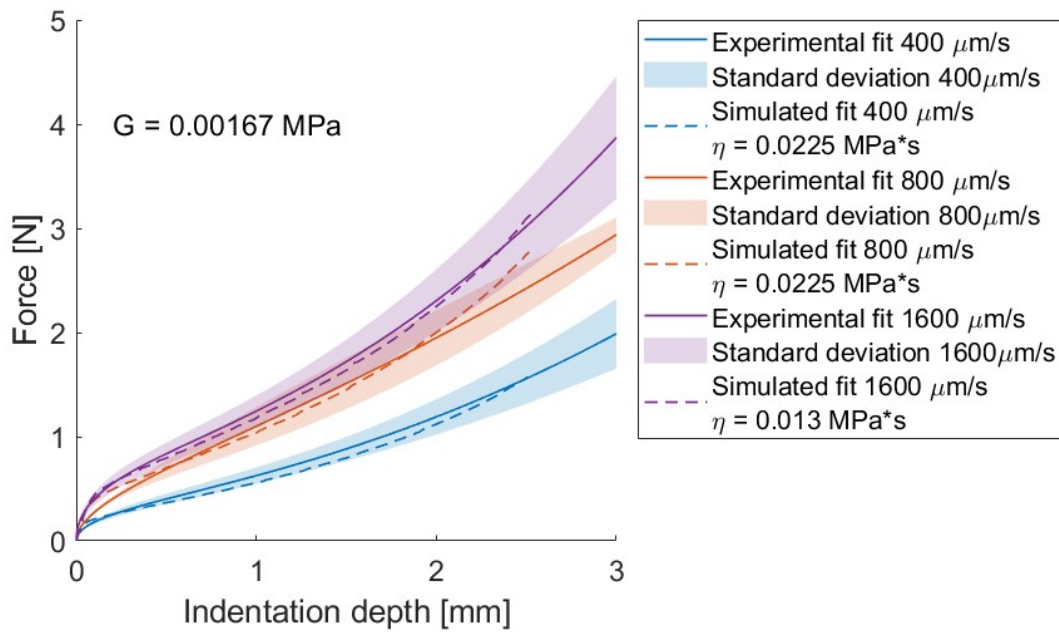


Figure 4.2.7: Comparison between the experimental fits and the simulated fits of the UD composite indentation tests

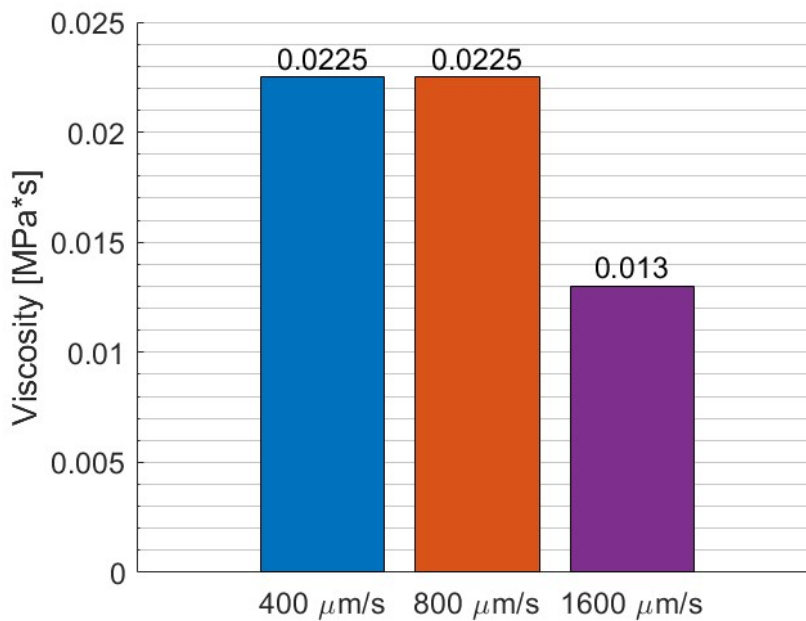


Figure 4.2.8: Comparison between viscosity parameter used in the UD composite indentation simulations.

### 4.3 Specimen deformation

In this section the deformation behavior of different specimens will be examined. First, a C/LMPAEK specimen will be examined during the indentation process to see what kind of deformation takes place during the heating and indentation of the specimen. Then, microscopy images from indented

specimens will be analyzed to see if a difference in indentation velocity caused a noticeable difference.

#### 4.3.1 Specimen deformation during indentation

The deformation of a C/LMPAEK specimen during the heating and indentation process can be seen in Figure 4.3.1. In Figure 4.3.1a line zero is the center of the specimen and will stay at the same place for different stages of the indentation process. Line 1, 2, 3, and 4 are designated to the left side of the middle middle dot, left middle dot, right middle dot, and the top of the middle top dot respectively. During deformation these lines will move with their corresponding dot on the specimen. The undeformed specimen had a height of 7.42 mm and a width of 15.98 mm. The pictures are taken in line with the fibers. Any change in deformation is measured in pixels and converted back to millimeters.

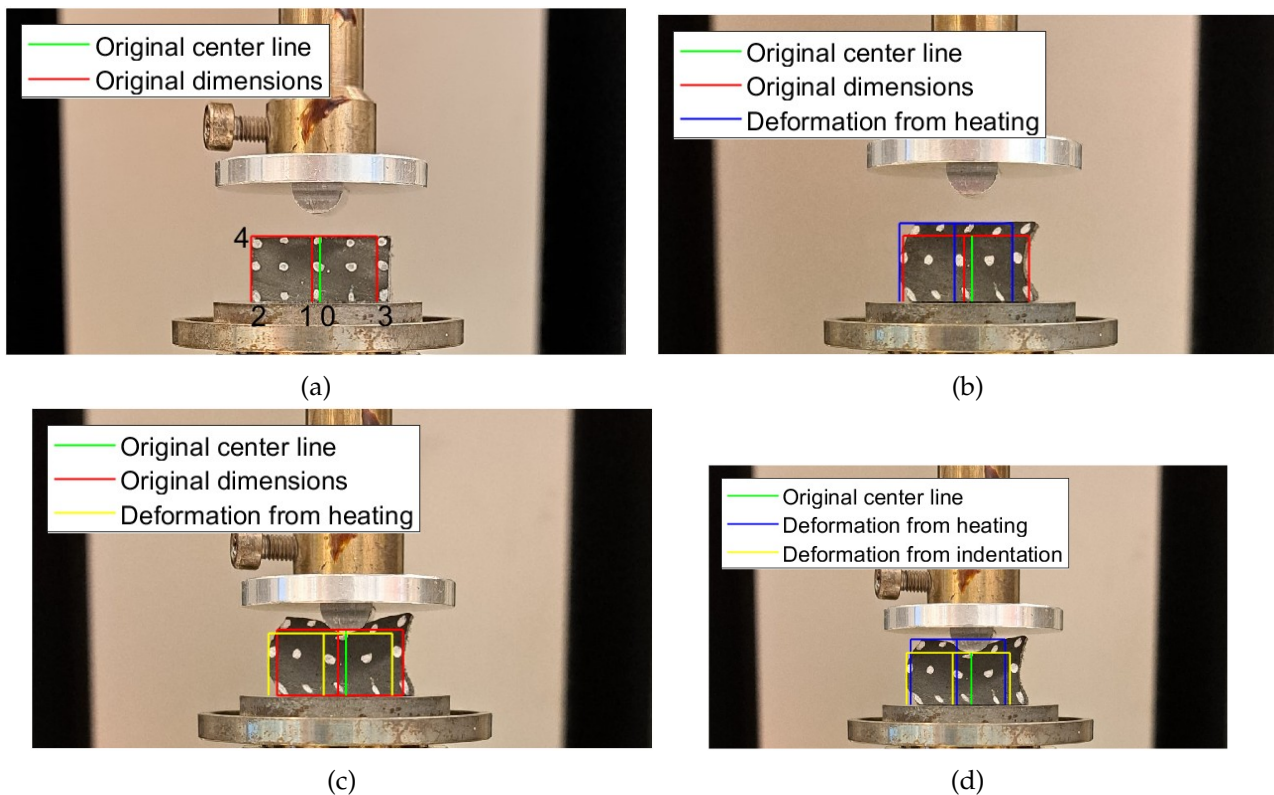


Figure 4.3.1: Deformation of a UD composite specimen at different stages. In (a) the specimen is shown before heating, in (b) the specimen is shown after heating, and in (c) and (d) the specimen is shown after indentation compared to the dimensions of (a) and (b) respectively.

During heating, the height of the specimen increases with 1.40 mm, which is an increase of 18.9%. Another deformation occurs where the center of the specimen shifts to the left. Line 1 moves 1.07 mm, line 2 moves 0.42 mm, and line 3 moves 1.86 mm, resulting in an apparent shift gradient. when indented, line 1 moves an extra 0.56 mm from its original position, while line 2 and 3 respectively move 0.56 mm and 0.65 mm outward from the center.

To see if several boundary conditions were met, other measurements were done as well. The movement of the base before and after indentation is shown in Figure 4.3.2a, where it is seen that during indentation the base moves a total of 0.56 mm outwards. An approximation of the surface area of the front facing surface of the composite is made before and after indentation, which can be seen in

Figure 4.3.2b. Before indentation the area is  $124.06 \text{ mm}^2$  and after indentation the area is  $123.39 \text{ mm}^2$ , meaning that a difference of  $0.67 \text{ mm}^2$  is measured.

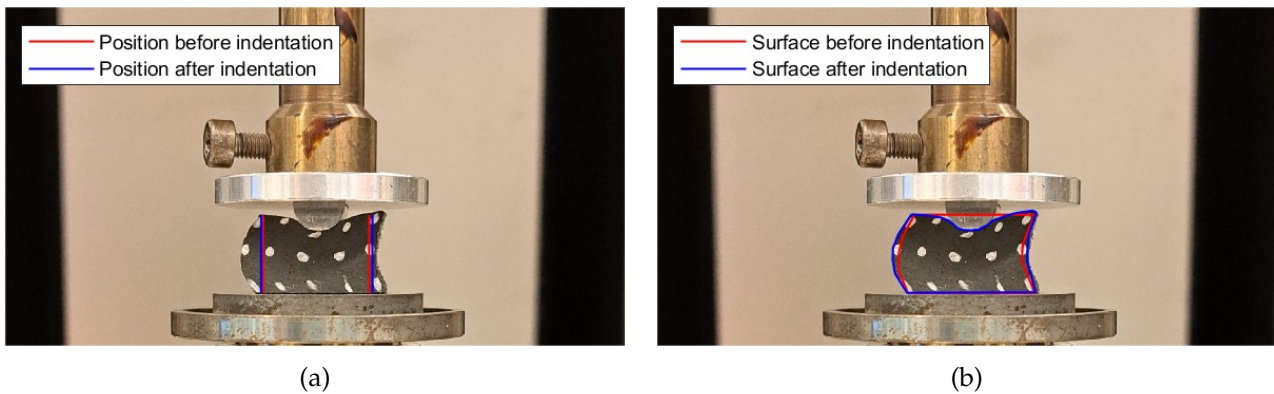


Figure 4.3.2: Deformation comparisons between before indentation and after indentation of (a) the change in bottom width and (b) the change in area of the specimen.

### 4.3.2 Microscopy imaging of deformed specimen

The specimens chosen to be analyzed were the specimens of the third test indented with a rate of  $400 \mu\text{m}/\text{s}$ , the second test indented with a rate of  $800 \mu\text{m}/\text{s}$ , and the first test indented with a rate of  $1600 \mu\text{m}/\text{s}$ . These specimens were the least likely to be damaged during the polishing process. An extra reason to choose the specimen of the second test indented with a rate of  $800 \mu\text{m}/\text{s}$  was that the result from this test seen in Figure 4.2.6b seemed irregular. Full microscopy images can be found in Figure 4.3.3, Figure 4.3.4, and Figure 4.3.5. In these images the black spots are voids, and the dark gray spots are likely voids that were filled with epoxy before the polishing process started. Any other irregularities seen are possible contaminations in or on the epoxy. The composite plies are distinguishable by the 'horizontal' lines. These lines also provide an insight on how the indentation affected the specimens, as the lines are curved at point of indentation but remain relatively straight further down the specimens. No significant differences can be found between the specimens, except that the specimen in Figure 4.3.4 shows significantly more and bigger voids.

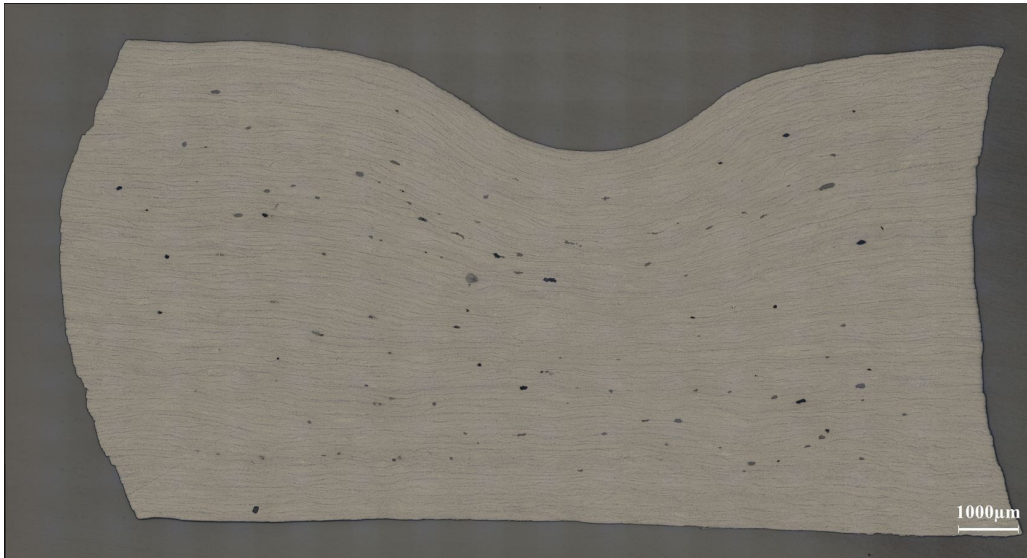


Figure 4.3.3: Microscopy image of the third test specimen at  $400 \mu\text{m}/\text{s}$

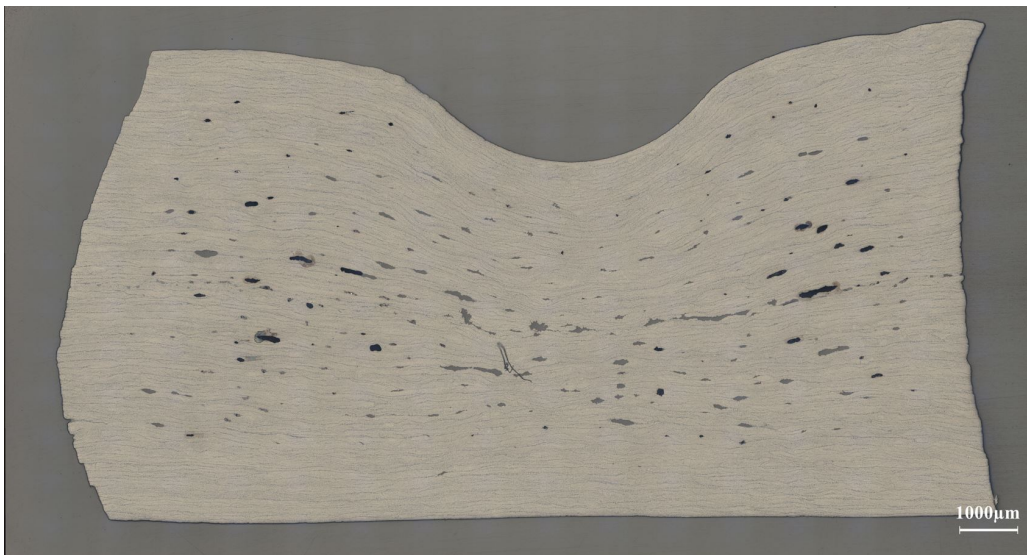


Figure 4.3.4: Microscopy image of the second test specimen at  $800 \mu\text{m}/\text{s}$

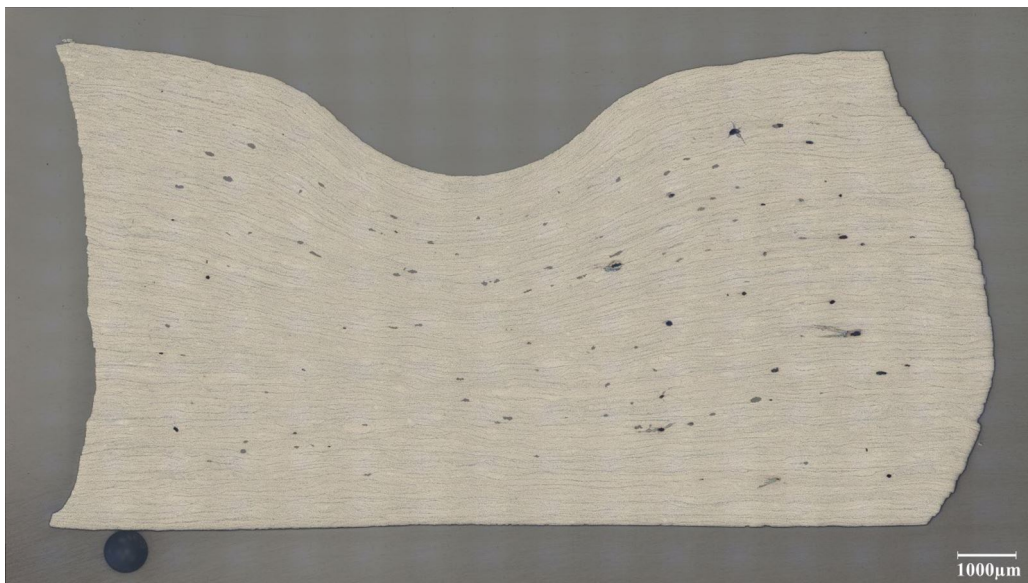


Figure 4.3.5: Microscopy image of the second test specimen at  $1600 \mu\text{m}/\text{s}$

# Chapter 5

## Discussion

In this section the results presented in chapter 4 are discussed with respect to the research question: How can the deformation behavior in transverse direction of uni-directional thermoplastic composites be characterized using indentation methods? To this end, the sub-questions will be discussed one by one. The influence of the specimen dimensions will be considered with respect to simulation results presented in Section 4.1. The comparison between conventional methods and indentation methods will be considered with respect to the results presented in Section 4.2.1. The methods used to describe the material behavior during indentation testing of UD composite will be discussed with respect to the results presented in Section 4.2.2. The last sub-question about the suitability of using the rheometer for indentation tests will be touched upon throughout the discussion section. Furthermore, possible explanations for the material behavior, geometry of the specimen, and boundary conditions, together with limitations found during the research will be examined as well through combining the results of the different observations and literature.

### 5.1 Influence of specimen dimensions

From the contour plots and simulated results in Section 4.1 it can be seen that edge effects affect specimens with the dimensions used in the indentation tests, while the edge effects are less noticeable for larger specimen. The force-depth curve of larger specimen is a better approximation of the closed form solution as well. From this it can be concluded that the results from the indentation test will deviate from a closed form solution that assumes a half space. Using bigger specimens in the indentation tests is advised as edge effects will contribute less to the test results.

### 5.2 Matrix material indentation tests

Conventional methods to characterize the flow behavior of neat polymer materials like plate rheometry gives a great insight on the viscosity and the viscous behavior of neat polymer materials, as can be seen in Figure 4.2.2. The simulated results of the matrix indentation test showed that shear thinning behavior can be seen with indentation tests as well, as the slope does increase with an increase in indentation velocity, but does not linearly correlate with the increase in indentation velocity. It might even be possible that with more simulations at different velocities the shear thinning behavior can be approximated in a slope-indentation velocity curve. The Experimental results however do not show similar behavior. The slope at rates 400 and 800  $\mu\text{m}/\text{s}$  is nearly identical and the slope at rate 1600  $\mu\text{m}/\text{s}$  increases massively. It could be argued that the shear rates acting on the material at the first two indentation velocities are not high enough for the material to show shear thinning behavior and that the material acts as if it is still on the Newtonian plateau mentioned in Section 2.1. However,

this is counter argued by the results from the simulations where shear thinning behavior is apparent.

A possibility for the test results is that the rheometer is not accurate enough. The rheometer is specified to have a normal force sensitivity of 5 mN and a force resolution of 0.5 mN [39], which means that the rheometer can measure a change in force of 5mN and can show a change in force of 0.5 mN per data step. Most tests at rates 400 and 800  $\mu\text{m}/\text{s}$  end with an indentation force of approximately 4 to 6 mN, and show force changes as small as 0.1 mN. The low measured force and force change is below the specified values, meaning that the results can not be completely accurate and should be carefully interpreted. The specified sensitivity could also be the reason why the measured force seems to decline at times. At a rate of 1600  $\mu\text{m}/\text{s}$ , the rheometer seems to be more accurate. The smallest shown change in force is 2.02 mN and the maximum measured forces were higher than 5 mN. However, due to the low sampling frequencies mentioned in Section 3.4, very few data points can be obtained at this velocity, as the indentation tool reaches the intended depth faster and thus the rheometer spends less time acquiring measurements. This was mostly prevalent in the first test at rate 1600  $\mu\text{m}/\text{s}$  (Figure 4.2.1c), where only 3 data points were measured before the test was finished. This test was also the main reason for the large standard deviation, as the results of the other two tests were relatively close to each other. To see if test 1 was an outlier, more test should have been done.

Even though conventional rheometry can describe viscosity and shear thinning behavior, and indentation simulations can at least show shear thinning behavior, this is not yet confirmed to be possible for indentation tests with experimental data. Because of this, finding the viscosity of polymers with indentation methods using a rheometer seems unlikely at the moment. Furthermore, the inaccurate measurements can only be credibly fitted with a linear fit. However, this completely ignores possible nonlinear effects that viscosity or elasticity have on materials. At the moment, the inaccuracy of the rheometer is prevents obtaining usable results. It is possible that the material at lower temperatures and thus at a higher viscosity could produce indentation forces high enough for the rheometer to accurately detect.

### 5.3 UD composite indentation tests

The material behavior of UD composites at different indentation velocities can be approximated with force-depth curves obtained from plane strain simulations using a Kelvin material model. In all simulations a shear modulus of  $G = 1.67 \cdot 10^{-3} \text{ MPa}$  was used and only the viscosity was changed between simulations to fit the simulated results on the experimental results. From this the experimental data revealed that the viscosity at rates 400 and 800  $\mu\text{m}/\text{s}$  was equal while the viscosity at a rate of 1600  $\mu\text{m}/\text{s}$  decreased significantly. However, the elastic response of the test result and simulation results at a rate of 800  $\mu\text{m}/\text{s}$  behaved differently. The indentation forces of the simulated results followed a similar path and would not overlap, while the experimental fits of rates 400 and 800  $\mu\text{m}/\text{s}$  would overlap if the indentation depth would be extended enough. Figure 5.3.1 shows that at a sufficient indentation depth, the indentation force at a rate of 800  $\mu\text{m}/\text{s}$  is lower than that of 400  $\mu\text{m}/\text{s}$ , which should not be possible for specimens with equal elastic material behavior.

The cause of the unexpected material behavior was analyzed and data that was deemed to cause the unexpected behavior was removed. The remaining data was again analyzed to understand the effect the removed data had on the material behavior. The second test in Figure 4.2.1b seemed to show different material behavior, as it did not have a comparable curve with respect to the first and third test. Significantly more and bigger voids were present when microscopy images were made of the test specimen used in the test, compared to the microscopy images made of the other specimens,

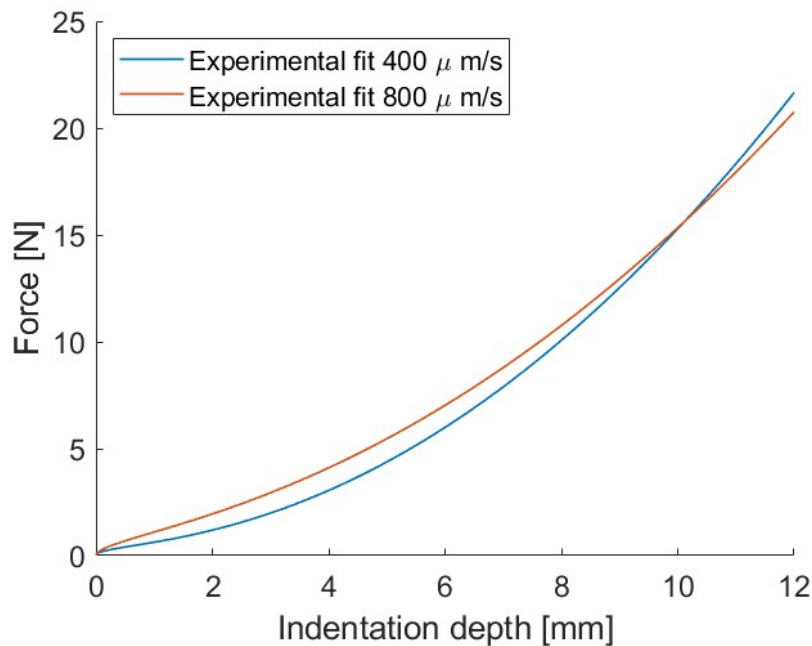


Figure 5.3.1: Average fits of test results from indentation velocity 400 and 800  $\mu\text{m/s}$  extended to an indentation depth of 12 mm

as seen in Figure 4.3.4. These voids could be the reason for the unexpected material behavior. In Figure 5.3.2 the experimental fits without the data from the second test at an indentation velocity of 800  $\mu\text{m/s}$  and new simulation results are compared and in Figure 5.3.3 the new viscosities used in the simulations are compared. The new test and simulation results fit better together, as the tail end of the simulated fit does not split of the test results at a rate of 800  $\mu\text{m/s}$  anymore. Furthermore, the indentation force of low indentation velocities does not overtake the indentation force of higher indentation velocities anymore. On another note, the viscosities of the simulations are lower for higher indentation velocities. From this we can assume that the material displays shear thinning behavior. This is in line with the research done by Stanley and Mallon [44], who found that UD thermoplastic composites display shear thinning behavior in the transverse direction.

Voids in a specimen apparently influence the test results enough to skew the test averages, as the elastic component seemed to decrease at high void contents. This was the conclusion of research done by Huang and Talreja [45] as well, which stated that transverse elasticity modulus, and therefore the shear modulus, reduces when void content increases. Furthermore, the fact that one outlying test result can skew the results means that more tests per indentation velocity need to be done. Not only for a more diverse average and to reduce the influence unfit specimens have, but also to see if test 2 at a rate 800  $\mu\text{m/s}$  actually is an outlier.

The indentation tests together with the simulations give a reasonable approximation to the viscosity of the material, but the indentation test is not designed to measure elasticity in the material. To fully understand the elastic behavior of the material, and thus have better approximations for the shear modulus, stress relaxation tests need to be done. One possibility could be a test method where strain should be applied to a specimen at a constant rate to increase the indentation force. Then, the strain should be held constant. If the indentation force returns to zero after a prolonged time, the composite is purely viscous. If not, an elastic component is present. Developing a method to characterize the elastic response in the material could further help to understand the viscoelastic behavior of compos-

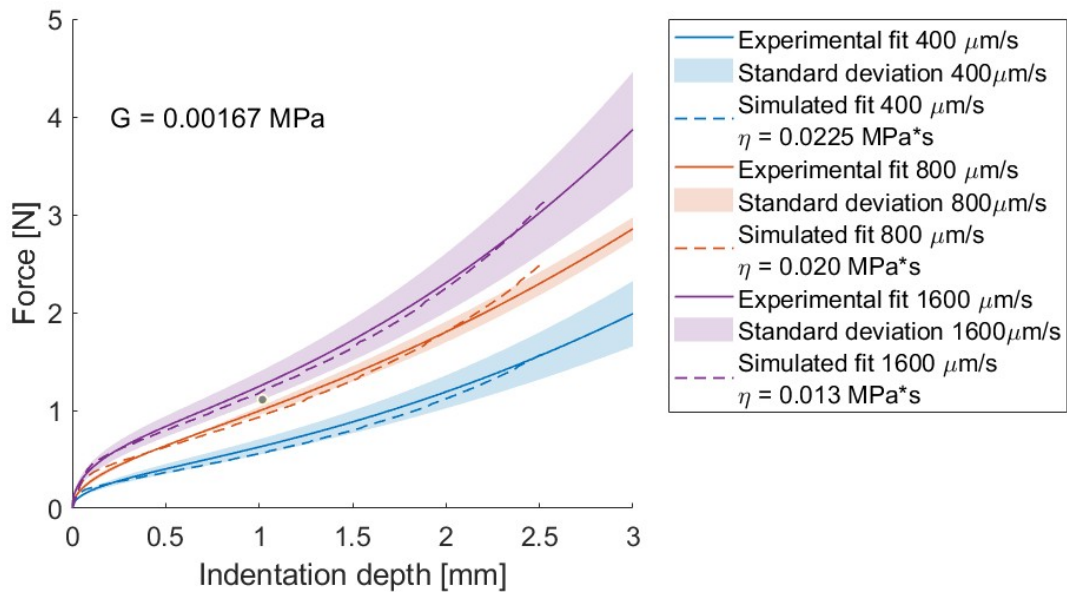


Figure 5.3.2: Comparison between the average forces and simulations of all composite data sets, where the second test of data set 5 is left out

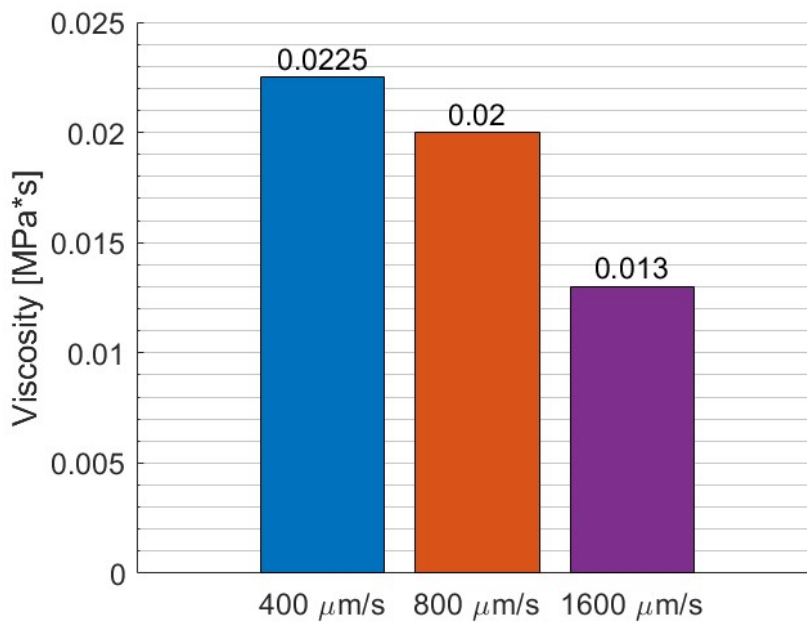


Figure 5.3.3: Comparison between the viscosity parameter used in the new UD composite indentation simulations.

ite, which in turn helps to understand the shear behavior of composites in transverse direction.

## 5.4 Specimen deformation

From the result seen in Figure 4.2.1 and Figure 4.2.6 it appears that the thickness of the specimen significantly increased during the heating process. This was confirmed for the UD composite specimens in Section 4.3.1. This increase in specimen thickness means that the point of contact between indenter and specimen and the indentation depth of the specimen can not be easily controlled. Because of this, it is difficult to have consistent start and end points to the tests, which can cause inaccurate results. Furthermore, due to the increase in thickness the specimen thickness of the tests and simulations will not match. Some increase in the specimen dimensions is expected due to thermal expansion. Although the coefficient of thermal expansion (CTE) of LMPAEEK is not published by Victrex, the linear CTE above  $T_g$  of comparable PEEK materials is between  $10 * 10^{-6}$  and  $150 * 10^{-6} K^{-1}$  [46]. If the maximum value is applied to the examined specimen, a thermal expansion of 0.41 mm is expected, which is less than the measured increase. One possibility for the increase in height is that moisture trapped inside the specimen evaporates and expands when heated. However, this seems unlikely due to the extensive drying of the plies during the preparation of the specimen and the extra drying step done just before testing. Furthermore, Rotink [47] found that a more extensive drying method for UD composites with a laminate made of 64 plies does not change the observed material expansion.

another possibility for the deformation of the material is that residual stresses were created inside the composite during press consolidation and the subsequent cooling of the UD composite. Parleviet et. al. [48] summarized residual stress formation during thermoplastic composite forming. On a micro-mechanical scale the mismatch in thermal expansion between the fibers and the matrix could have caused compressive and tensile stresses in the material, while a gradient in the temperature or cooling rate could lead to stresses in a 'global' scale, if composite material on the outside of the laminate cools down faster than material in the middle of the laminate.

Other deformations after the specimen was indented were considered to check if the boundary conditions used for the simulations were maintained. From Figure 4.3.2a it can be concluded that although the movement is minimal, the bottom of the specimen is not pinned like it was assumed in the simulation. An improvement on the test method would be to tape the bottom down with kapton tape, to prevent it from moving. Another tested boundary condition was the incompressibility of the material. The change in area seen in Figure 4.3.2b indicates a possibility that the material is compressible, even though the material in the simulations is assumed to be incompressible. However the decrease in surface area is about 0.5% of the total and therefore practically zero. This conclusion has been drawn under the assumption that the specimen did not deform lengthwise, as this could not be measured when the material was in melt.

To prevent problems with deforming specimen and high void content in following research, a different approach to preparing the specimen material should be taken. Using autoclave processing [49] reduces void content, and a slow cooling rate might reduce the temperature gradient inside the composite laminate and reduce residual stresses introduced on a global level.

## Chapter 6

# Conclusion

This research aimed to provide more insight on the characterization of mechanical behavior of materials in melt, in particular the transverse mechanical behavior of thermoplastic UD composites. To this end, indentation methods were used. Therefore, a test method, based on existing indentation tests and various material models, to measure the force needed to indent material at different velocities was developed. The test method lowers a spherical indenter for isotropic materials and a cylindrical indenter for UD composites at a constant velocity to indent a specimen, while the force needed to indent the specimen is measured. This is done in a rheometer at processing temperatures in a nitrogen-rich environment to prevent thermal degradation. The measured force can be used to characterize the flow behavior of the material.

Testing was conducted with neat LMPAEK resin to see if the indentation method was comparable to conventional methods. While the test results could not accurately describe material characteristics, the simulated results could.

The results of C/LMPAEK tests showed rate dependent behavior, which could be approximated with a Kelvin model. Different viscosity parameters were needed for the simulations to fit on the tests results for tests done at different indentation rates, where the increase in viscosity did not linearly correlate with the increase in indentation velocity, which indicated shear thinning behavior in the material.

A secondary goal of this research was to see if it was possible to do these tests in a rheometer, specifically the TA HR 20, as using this machine is more convenient than the laborious test set-ups previous research needed. It was found that the axial force sensitivity and resolution for low viscosity materials were too low to obtain accurate force measurements. Furthermore, the highest possible linear sampling frequency that does not repeat data points can not collect enough data for small indentations at high velocities. Using the fast sampling setting can provide a faster sampling frequency. However, the data point collected decrease logarithmically over time and it decreases the force sensitivity even further. Therefore, the fast sampling setting can only be used for high viscosity materials at very short test times.

## Chapter 7

# Recommendations

The results of the low amount of tests gave ambiguous results. If the tests were to be repeated or further build upon, it is recommended that more than 3 tests per data set will be done. This way outliers can easily be identified and a more accurate average and standard deviation can be calculated.

According to the simulations, the small dimensions of the specimen were affecting the results. Having specimen with larger dimensions might give results closer to theoretical values. However, this is limited by the size of the rheometer oven. the rheometer itself poses a problem as well as it is not that accurate. Using a different machine that has either a bigger oven, or a more sensitive force sensor can solve one of these problems.

For now the results gained from tests done on isotropic materials with a spherical indenter were not conclusive. Redoing these tests with LMPAEEK at lower temperatures, and thus higher viscosities, can result in better results. Otherwise, other high viscosity materials could be used to validate the method.

Further research to the elasticity of C/LMPAEEK in melt needs to be done to better characterize the material during indentation. A stress relaxation test method using indentation methods can be proposed to this end.

# Bibliography

- [1] Sebastiaan Haanappel. "Forming of UD fibre reinforced thermoplastics". In: (2013).
- [2] Dennis Brands. "Forming simulations for unidirectional thermoplastic composites: Improving in-plane shear characterization and modeling". English. PhD Thesis - Research UT, graduation UT. Netherlands: University of Twente, Jan. 2025. ISBN: 978-90-365-6350-5. DOI: 10 . 3990 / 1 . 9789036563512.
- [3] SP Haanappel and Remko Akkerman. "Shear characterisation of uni-directional fibre reinforced thermoplastic melts by means of torsion". In: *Composites Part A: Applied science and manufacturing* 56 (2014), pp. 8–26.
- [4] P Harrison, T Haylock, and AC Long. "Measurement of the transverse and longitudinal viscosities of continuous fibre reinforced composites". In: *Proc. 8th ESAFORM Conference*. Citeseer. 2005, pp. 1015–1018.
- [5] SF Shuler and SG Advani. "Transverse squeeze flow of concentrated aligned fibers in viscous fluids". In: *Journal of Non-Newtonian Fluid Mechanics* 65.1 (1996), pp. 47–74.
- [6] JA Barnes and FN Cogswell. "Transverse flow processes in continuous fibre-reinforced thermoplastic composites". In: *Composites* 20.1 (1989), pp. 38–42.
- [7] GB McGuinness and CM ÓBrádaigh. "Characterisation of thermoplastic composite melts in rhombus-shear: the picture-frame experiment". In: *Composites Part A: Applied Science and Manufacturing* 29.1-2 (1998), pp. 115–132.
- [8] RW Roberts and RS Jones. "Rheological characterization of continuous fibre composites in oscillatory shear flow". In: *Composites Manufacturing* 6.3-4 (1995), pp. 161–167.
- [9] AB Wheeler and RS Jones. "A characterization of anisotropic shear flow in continuous fibre composite materials". In: *Composites Manufacturing* 2.3-4 (1991), pp. 192–196.
- [10] JA Goshawk and RS Jones. "Structure reorganization during the rheological characterization of continuous fibre-reinforced composites in plane shear". In: *Composites Part A: Applied Science and Manufacturing* 27.4 (1996), pp. 279–286.
- [11] Christopher W Macosko. *Rheology: Principles, Measurements, and Applications*. VCH, 1994.
- [12] Faith A Morrison et al. *Understanding rheology*. Vol. 1. 3.1. Oxford university press New York, 2001, pp. 225–250.
- [13] Fridtjov Irgens. *Rheology and non-newtonian fluids*. Vol. 1. Springer, 2014.
- [14] Rheosense. *Viscosity of Newtonian and non-Newtonian Fluids*. 2024. URL: <https://www.rheosense.com/applications/viscosity/newtonian-non-newtonian>.
- [15] T. Osswald and N. Rudolph. "Polymer rheology". In: *Carl Hanser, München* (2015).
- [16] The efficient engineer. *An Introduction to Stress and Strain*. 2025. URL: <https://efficientengineer.com/stress-and-strain/>.

- 
- [17] Eiji Tanaka and Theo Eijden. "Biomechanical Behavior of the Temporomandibular Joint Disc". In: *Critical reviews in oral biology and medicine : an official publication of the American Association of Oral Biologists* 14 (Feb. 2003), pp. 138–50. DOI: 10.1177/154411130301400207.
- [18] Atul Bhattad. "Review on viscosity measurement: devices, methods and models". In: *Journal of Thermal Analysis and Calorimetry* 148.14 (2023), pp. 6527–6543.
- [19] tec-science. *Experimental determination of viscosity (viscometer)*. 2020. URL: <https://www.tec-science.com/mechanics/gases-and-liquids/experimental-determination-of-viscosity/>.
- [20] JD Ferry. *Viscoelastic Properties of Polymers*. Wiley, 1980.
- [21] Anton Paar. *basics of rheology*. 2025. URL: <https://wiki.anton-paar.com/en/basics-of-rheology/#oscillation-tests-and-viscoelasticity>.
- [22] WP Cox and EH Merz. "Correlation of dynamic and steady flow viscosities". In: *Journal of Polymer Science* 28.118 (1958), pp. 619–622.
- [23] SG Advani, SF Shuler, et al. "Rheology of long fiber-reinforced composites in sheetforming". In: *Composite materials series*. Vol. 11. Elsevier, 1997, pp. 323–369.
- [24] M V Brusckhe and SG Advani. "Flow of generalized Newtonian fluids across a periodic array of cylinders". In: *Journal of Rheology* 37.3 (1993), pp. 479–498.
- [25] R Balasubramanyam, RS Jones, and AB Wheeler. "Modelling transverse flows of reinforced thermoplastic materials". In: *Composites* 20.1 (1989), pp. 33–37.
- [26] Ingrid Zacharias Martins et al. "Janka hardness of hardwood species evaluated by the nondestructive sclerometric method". In: *Materials and Structures* 55.9 (2022), p. 227.
- [27] Medway Campus and Chatham Maritime. "Understanding the IRHD and Shore Methods used in Rubber Hardness Testing" by R. Morgans\* BSc, S. Lackovic 2 BSc PhD, P. Cobbold 2 1. University of Greenwich School of Engineering". In: (1999).
- [28] Smooth-on. *Durometer Shore hardness scale*. 2025. URL: <https://www.smooth-on.com/page/durometer-shore-hardness-scale/>.
- [29] Nilgün Becenen, Bülent Eker, and Mumin Sahin. "Mechanical properties of plastic matrix composite materials used in tractor bonnets". In: *Journal of reinforced plastics and composites* 29.24 (2010), pp. 3637–3644.
- [30] Didier Chicot et al. "Comparison of instrumented Knoop and Vickers hardness measurements on various soft materials and hard ceramics". In: *Journal of the European Ceramic Society* 27.4 (2007), pp. 1905–1911.
- [31] Thomas Koch and Sabine Seidler. "Correlations between indentation hardness and yield stress in thermoplastic polymers". In: *Strain* 45.1 (2009), pp. 26–33.
- [32] William D Callister Jr and David G Rethwisch. *Callister's materials science and engineering*. John Wiley & Sons, 2015, pp. 214–237.
- [33] Valentin L Popov, Markus Heß, and Emanuel Willert. *Handbook of contact mechanics: exact solutions of axisymmetric contact problems*. Springer Nature, 2019.
- [34] Heinrich Hertz. "Ueber die Berührung fester elastischer Körper." In: (1882).
- [35] Anton Van Beek. "Advanced engineering design Lifetime performance and reliability". In: (2015), pp. 102–115.
- [36] Victrex. *Enhanced Processing, Stronger Parts, and Faster Production with LMPAEK™ Polymers*. 2025. URL: <https://www.victrex.com/en/lmpaek>.
-

- 
- [37] John Grasmeyer. *LMPAEK™ Explained and why it's suited to composites and additive manufacturing*. 2021. URL: <https://www.victrex.com/en/blog/2021/lmpaek>.
- [38] Toray Cetex TC1225 LMPAEK. v7.1. Toray. June 2023.
- [39] TA Instruments. *HR 20*. 2025. URL: <https://www.tainstruments.com/hr-20/>.
- [40] Han Huetink. "On the simulation of thermo-mechanical forming processes". English. PhD Thesis - Research UT, graduation UT. Netherlands: University of Twente, June 1986. DOI: 10.3990/1.6068695.
- [41] Remko Akkerman. "Euler-Lagrange simulations of nonisothermal viscoelastic flows". Undefined. PhD Thesis - Research UT, graduation UT. Netherlands: University of Twente, Dec. 1993. ISBN: 90-9006764-7.
- [42] Hans Christiaan Stoker. *Developments of the Arbitrary Lagrangian-Eulerian Method in non-linear Solid Mechanics*. Undefined. PhD Thesis - Research UT, graduation UT. Netherlands, Feb. 1999.
- [43] DiekA development group. *DiekA Users Manual*. University of Twente.
- [44] WF Stanley and PJ Mallon. "Intraply shear characterisation of a fibre reinforced thermoplastic composite". In: *Composites Part A: Applied Science and Manufacturing* 37.6 (2006), pp. 939–948.
- [45] Hansong Huang and Ramesh Talreja. "Effects of void geometry on elastic properties of unidirectional fiber reinforced composites". In: *Composites Science and Technology* 65.13 (2005), pp. 1964–1981.
- [46] *Victrex PEEK properties guid*. Victrex. Sept. 2016.
- [47] Gijs Rotink. *Characterizing transverse flow of unidirectional thermoplastic composite in melt using the squeeze flow test*. Undefined. Netherlands, Dec. 2023.
- [48] Patricia P Parlevliet, Harald EN Bersee, and Adriaan Beukers. "Residual stresses in thermoplastic composites—A study of the literature—Part I: Formation of residual stresses". In: *Composites Part A: Applied Science and Manufacturing* 37.11 (2006), pp. 1847–1857.
- [49] FYC Boey and SW Lye. "Void reduction in autoclave processing of thermoset composites: Part 1: High pressure effects on void reduction". In: *Composites* 23.4 (1992), pp. 261–265.
- [50] TA Instruments. *DSC 250*. 2025. URL: <https://www.tainstruments.com/dsc-250/>.

## **Appendix A**

# **Indentation viscosity measurements protocol**

This section contains a thorough step by step protocol on how to conduct the indentation tests with the rheometer. Included is specimen preparation, indentation tool preparation, rheometer usage, and the actual testing.

# UNIVERSITY OF TWENTE

## Test Protocol Indentation Experiments

---

*Authors:*

TIJN KOOPMAN

*Date:*

APRIL 3, 2025

# Contents

<b>1</b>	<b>Introduction</b>	<b>1</b>
<b>2</b>	<b>General overview of the testing method</b>	<b>2</b>
<b>3</b>	<b>Test preparation</b>	<b>3</b>
3.1	Specimen preparation . . . . .	3
3.2	Fixture preparation . . . . .	4
<b>4</b>	<b>Rheometer testing</b>	<b>6</b>
4.1	Starting up the rheometer . . . . .	6
4.2	Preparation before the experiment . . . . .	7
4.3	Conducting the experiment . . . . .	8
4.4	Shutting down the rheometer . . . . .	10

## 1 Introduction

To better understand the manufacturability and reshapability of Thermoplastic composites, their deformation and flow behavior need to be investigated. One key parameter to explore is the viscosity of the composite and its thermoplastic matrix in melt. This protocol is a guide to perform the material characterization of unidirectional thermoplastic composites and its matrix material through the proceedings of a number of steps.

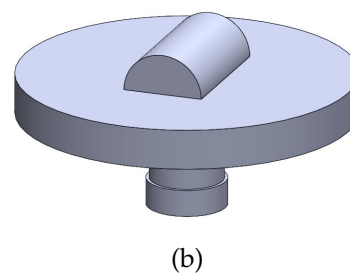
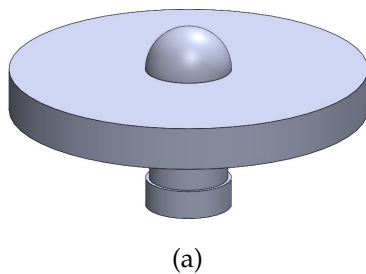
Experiments are conducted with the TA rheometer H20 present in the lab at the University of Twente. With the indentation tests, axial force is needed to indent tests specimen. The indentation force measured over the indentation depth is used to characterize the material.

Before this test protocol is used, an introduction to the rheometer by a lab technician of the University of Twente should be done.

## 2 General overview of the testing method

Viscosity is defined as the resistance to flow. In this testing method the viscosity will be tested by pressing a special shaped indenter in a prepared specimen that is brought in melt. The measured indentation force combined with the indentation depth and velocity will give an approximation to the characterized viscosity of the material tested.

A TA H20 rheometer is used to conduct the tests. A standard plate bottom fixture is used to place the test specimen on. A specialized indentation top fixture for either a polymer material Figure 2.1a test or a UD composite Figure 2.1b test is used to indent into the material. When both fixtures are mounted on the rheometer the specimen is placed inside the environmental chamber to heat up above melting point. When the specimen is at the desired temperature, the top fixture lowers at a constant velocity to the desired depth. When that depth is reached, the test ends and the measured force data can be collected to determine the viscosity characteristics.



### 3 Test preparation

Two important preparations are needed before conducting the indentation tests: preparation of the specimen and preparation of the top fixture. It is important to note that the preparation of the matrix material specimen are slightly different than that of the UD composite specimen.

#### 3.1 Specimen preparation

Specimen are made of 150 by 150 by 6 mm plates of material. The matrix specimen should be cut into 16 by 16 mm squares and the UD composite specimen should be cut into 16 by 10 mm rectangles.

##### **matrix material specimen**

1. Ensure the following is present:
  - Diamond saw (available at the University of Twente)
  - Caliper
  - Test material
  - Cleaning paper
  - Oven
  - Aluminum foil
  - Box cutter
  - Cutting board
  - Ruler
  - Marker
2. Set the guard of the diamond saw to a distance of 16 mm from the right side of the saw blade with help of the caliper.
3. Cut squares of the plate with the necessary precautionary preparations needed for the diamond saw.
4. Clean the diamond saw machine with the cleaning paper.
5. Dry the specimen in an oven at 125° preferably overnight.
6. Cut two squares of aluminum foil of approximately 60 by 60 mm with the box cutter and the ruler.
7. Fold the squares of aluminum foil over the bottom and the sides of the specimen, leaving the top exposed.
8. Cut the excess amount of aluminum foil away with the box cutter. Be careful not to tear the aluminum foil at any other face of the specimen.
9. Mark the underside of the specimen with the marker
10. Clean up



### UD composite material specimen

1. Ensure the following is present:
  - Diamond saw (available at the University of Twente)
  - Caliper
  - Test material
  - Cleaning paper
  - Oven
2. Set the guard of the diamond saw to a distance of 16 mm from the right side of the saw blade with help of the caliper.
3. Cut a strip from the material plate in fiber direction of the plate with the necessary precautionary preparations needed for the diamond saw.
4. Set the guard of the diamond saw to a distance of 10 mm from the right side of the saw blade with help of the caliper.
5. Cut the strip transverse to the fiber direction with the necessary precautionary preparations needed for the diamond saw.
6. Clean the diamond saw machine with the cleaning paper.
7. Dry the specimen in an oven at 125° preferably overnight.
8. mark the underside of the specimen with the marker
9. Clean up

### 3.2 Fixture preparation

The top fixture should be prepared in such a way that the molten specimen will not stick to it after the tests.

1. Ensure the following is present:
  - Top fixture (for matrix material choose the spherical indentation tool, for UD composite material choose the cylindrical indentation tool, see Figure ??)
  - Nitrile gloves
  - Cleaning paper
  - Release agent
  - Fume hood
  - Box cutter
  - cutting board
  - Polyimide foil
2. Put a layer of cleaning paper under the fume hood and put on nitrile gloves as protection.
3. pour a few drops of release agent on another wad of cleaning paper and rub it over every surface of the top fixture.
4. Place the top fixture on the layer of cleaning paper to air dry for a few seconds.
5. Cut a 25 by 25 mm square of polyimide foil with the box cutter.
6. Clean up

## 4 Rheometer testing

### 4.1 Starting up the rheometer

1. Turn on the PC and monitor. Log-in using username 'iaflab' and password 'I@Flab2013' (both without ' ').
2. Turn on the air flow by turning the red handle 90 degrees to the left (in-line with the tube). The handle is located 1m to the left of the reometer desk.



3. Power on the rheometer using the button at the front of the device.



4. Select the trios shortcut on the PC, open it and when the rheometer is fully booted, connect the rheometer to the PC via the pop-up window (not the offline one).

## 4.2 Preparation before the experiment

1. Open the oven of the rheometer. Screw the protective cap from the rotor pin, using the knob at the top of the device.



2. Look for the black boxes located on the bottom shelf of the desk. Look for the box containing the top shaft and the bottom fixture. Once you have found them, take them out of the box.



3. Obtain a new (or clean recycled) bottom plate fixture from the second desk drawer and place in the bottom plate fixture. Gently tighten the plate using the small screws with a hex key.
4. Take the previously prepared indentation tool fixture and place in the top shaft. Gently tighten the indenter using the small screws with a hex key.

5. Gently install the shaft to the rheometer using the knob at the top of the device.
6. Install the bottom plate fixture, mind the alignment of the pin. Also connect the serial connector.
7. Check if the hardware needs to be calibrated in the calibration menu. If all items check out green, no need to run a calibration.



8. zero the gap on the rheometer.



9. lock the rotational movement of the rheometer with the lock button on the front of the rheometer.



### 4.3 Conducting the experiment

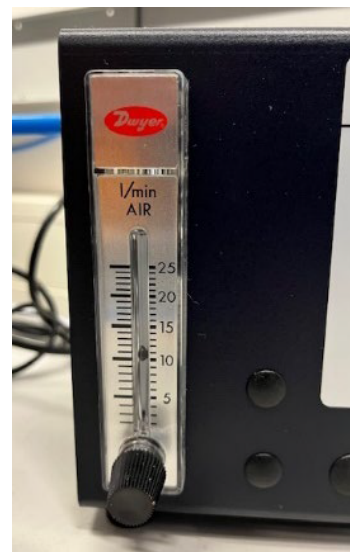
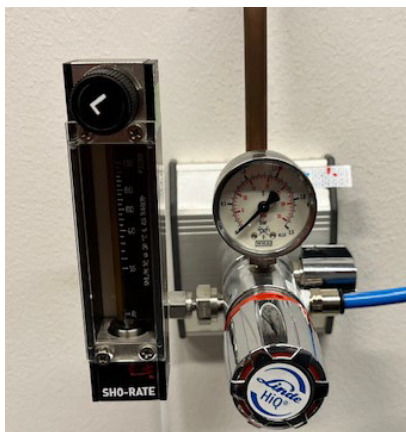
NOTE: be sure to have an USB stick to retrieve the data from the PC after the test is done.

1. Under "Sample": fill in the relevant information and choose the relevant file path.
2. Under "Geometry": set the gap to the desired height according to Table 1 or Table 2 and the loading gap to a setting where you can comfortably yet accurately place the specimen e.g. 15000  $\mu\text{m}$ .
3. At "Gap": select loading geometry.
4. Under "Procedure": select "Other", "Axial", and use the following settings
  - Temperature: 365

- Soak Time: 0
  - Duration: see Table 1 or Table 2
  - Motor direction: Compression
  - Constant linear rate: see Table 1 or Table 2
  - Angular velocity: 0
  - Sampling: Linear for polymer material, Fast sampling for composite material
  - Initial time between samples (if applicable): 0,25
5. place the polyimide foil and the test specimen in the middle of the bottom fixture plate.  
IMPORTANT: For the UD composite material, make sure to align the cylindrical indentation tool such that the flat side of the cylinder is facing the same way as the broad side of the specimen. this ensures that the transverse behavior of the specimen is being measured.



6. Close the oven. Go to Environmental and set point to 365 °C. Check box purge gas only. Open the N2 valve located 3 meters to the left of the rheometer desk (above another desk). Check the manometer on the rheometer desk, set the N2 flow to 10 l/min.



7. While the rheometer is heating up select "go to geometry gap"



8. When the oven is heated to the correct temperature, wait for 5 minutes to heat the specimen fully through. After 5 minutes, press zero axial force and then start.



9. When the rheometer has completed the program, set the environment to idle, open the oven to cool down the specimen, and shut of the N2 gas.
10. If any microscopy research needs to be done to the specimen, wait until it is completely cooled down, manually raise the rheometer with the buttons on the front and carefully take out the specimen. Otherwise, the sample can be discarded.



11. export the data to an Excel file and retrieve it from the PC using a USB stick.
12. repeat step 1 to 9 if another specimen needs to be tested.

#### 4.4 Shutting down the rheometer

1. remove the rod from the rheometer by unscrewing the knob at the top of the device and remove the bottom fixture by pressing the release button on the device and lifting it up gently.
2. close the trios software, shut down the PC and the monitor. Press the power button on the rheometer to shut it down as well.
3. Remove the top indenter fixture and the bottom plate fixture from the rod and the bottom fixture by loosening the bolts using a hex key and store all parts in their proper place.
4. Clean up



Table 1: Matrix indentation

Constant linear rate [ $\mu\text{m}/\text{s}$ ]	Gap [ $\mu\text{m}$ ]	Duration [s]
400	9000	10
800	13000	10
1600	21000.	10

Table 2: UD composite indentation

Constant linear rate [ $\mu\text{m}/\text{s}$ ]	Gap [ $\mu\text{m}$ ]	Duration [s]
400	10500	10
800	12100	7
1600	14500	5

## Appendix B

# Differential Scanning Calorimetry

To see if any degradation took place during the making and testing of the specimen, differential scanning calorimetry (DSC) tests were done. A DSC measures the heat flow into or out of a material as it is heated or cooled, helping to determine its thermal properties and degradation. A TA Instruments DSC 250 [50] was used for this purpose. This was done by heating small samples weighing between 5 and 10 milligrams that were chipped off a larger sample piece. These samples were placed in a cup, and weighed to gain the information needed for the DSC to operate. A lid was then pressed on the cup and the cup was placed in the loading tray of the DSC. The DSC then ran a program of heating from 25 °C to 340 °C at a rate of 20°C per minute, where it stayed for one minute. During this isothermal moment, the sample could fully melt and cover the bottom of the cup. The DSC then cooled down to 25 °C at 20 °C per minute and stayed at that temperature for one minute. The temperature profile can be seen in Figure B.0.1. The heating, dwell, and cooling phases were repeated once for more accurate results, thanks to better material to cup contact once the material was molten. Afterward, the DSC discarded the sample. This procedure was executed to accurately find the melting temperature of the LMPAEK and the C/LMPAEK, and to determine if any degradation took place in the material during testing: drying in the oven, being pressed, and being tested in the rheometer.

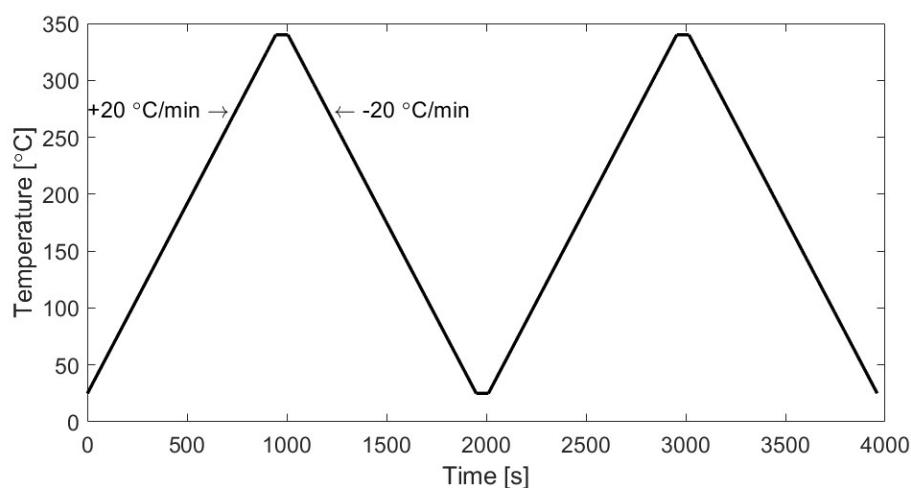


Figure B.0.1: The temperature profile used for the DSC tests

The results of all DSC tests are shown in Figure B.0.2, Figure B.0.3, Figure B.0.4, Figure B.0.5, and Figure B.0.6. The results are normalized over the weight of the samples for fair comparison. Each sample has a line with a negative and positive heat flow over temperature. The lines of negative heat flow represent the material heating up whereas the lines of positive heat flow represent the material

cooling down. As the results of the DSC are very similar for all stages of material processing and testing it can be assumed that no significant degradation is taking place.

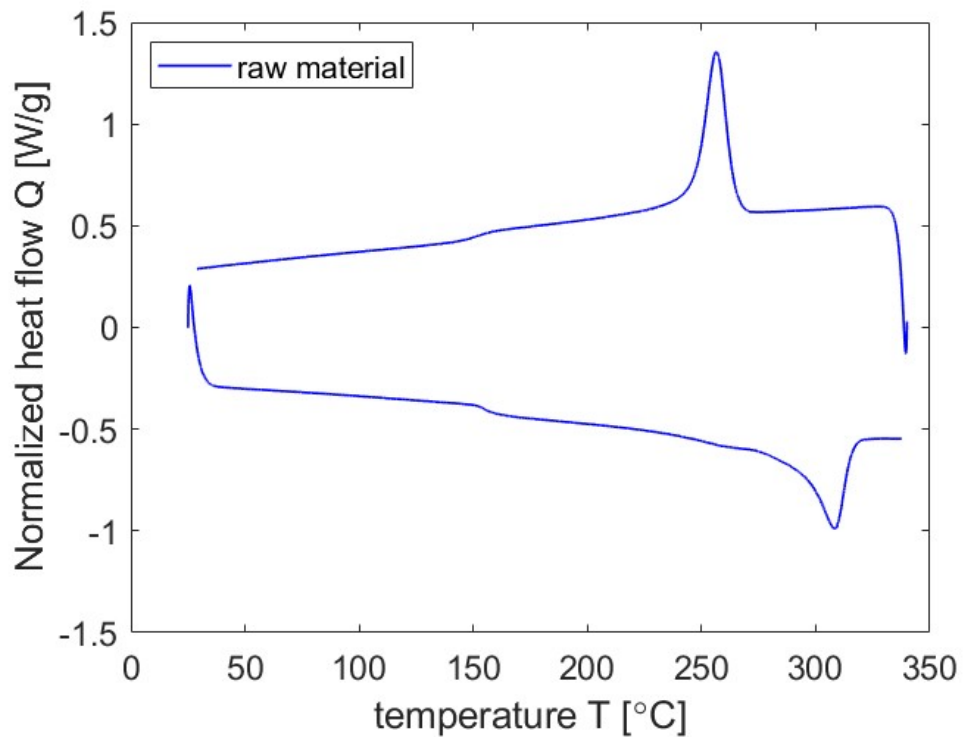


Figure B.0.2: Heat flow normalized with sample weight over a temperature range of 25 to 340 °C, for the raw material

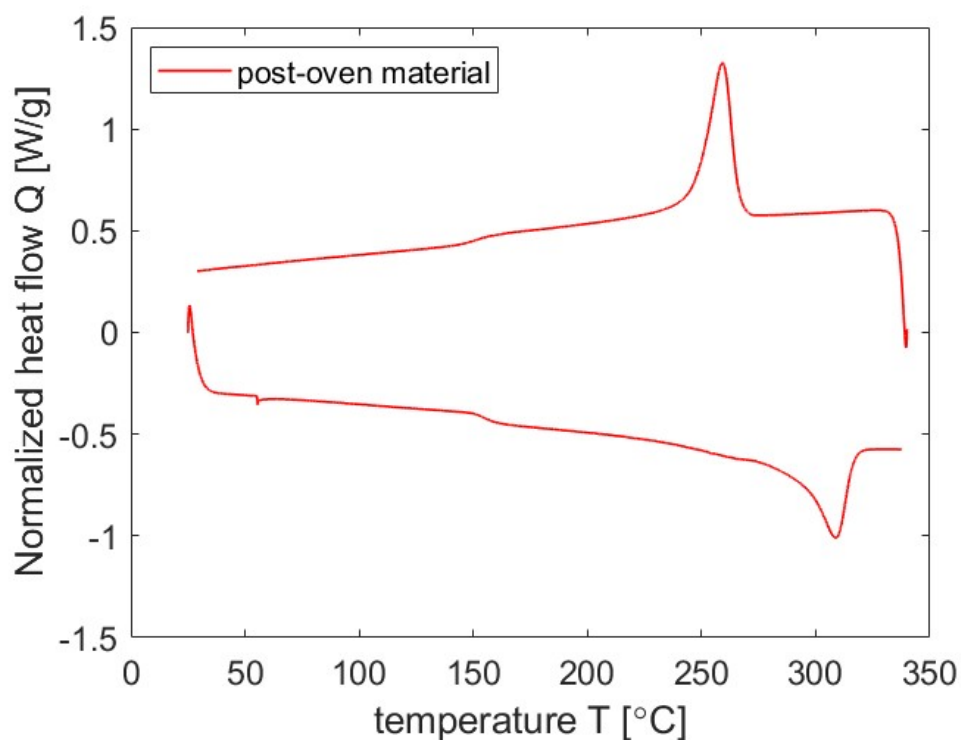


Figure B.0.3: Heat flow normalized with sample weight over a temperature range of 25 to 340 °C, for the material after oven drying it

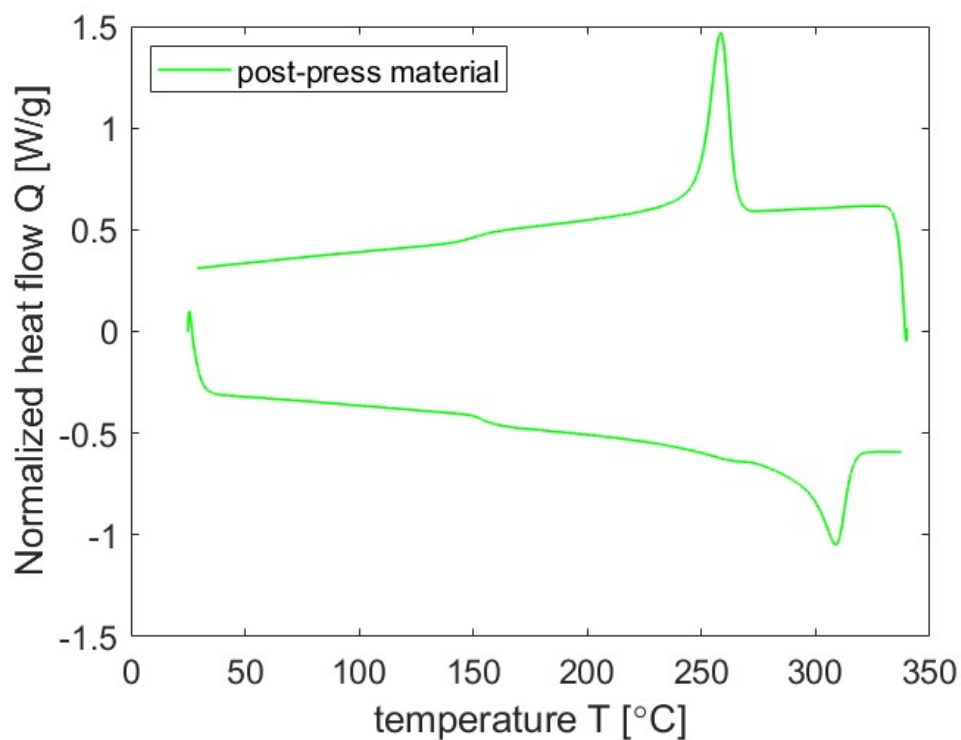


Figure B.0.4: Heat flow normalized with sample weight over a temperature range of 25 to 340 °C, for the material after pressing it

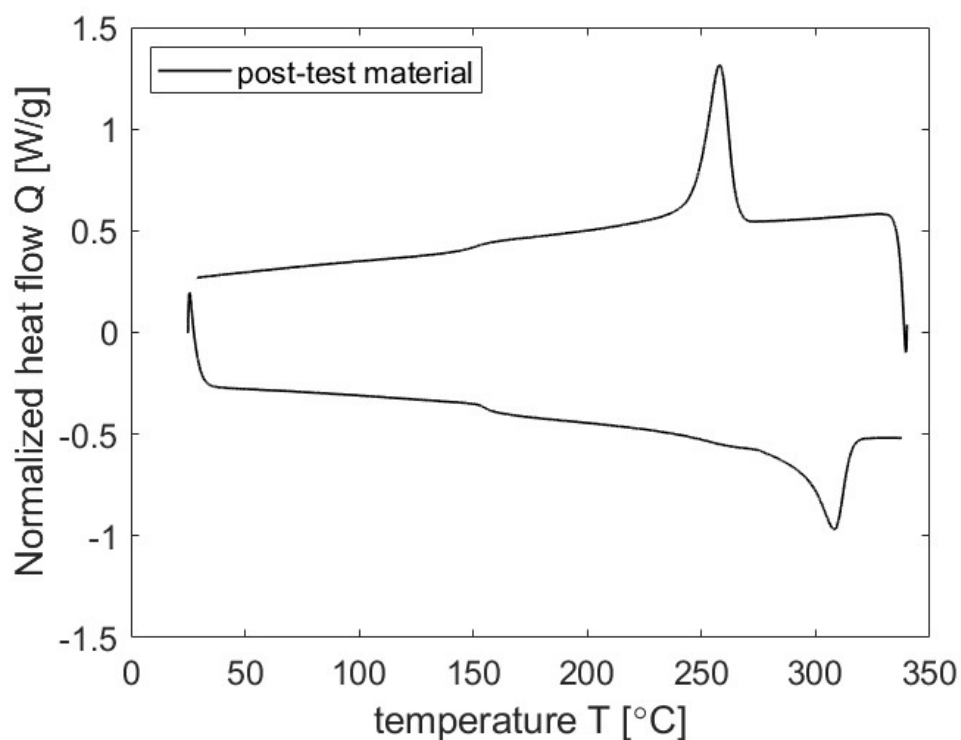


Figure B.0.5: Heat flow normalized with sample weight over a temperature range of 25 to 340 °C, for the material after it has been tested

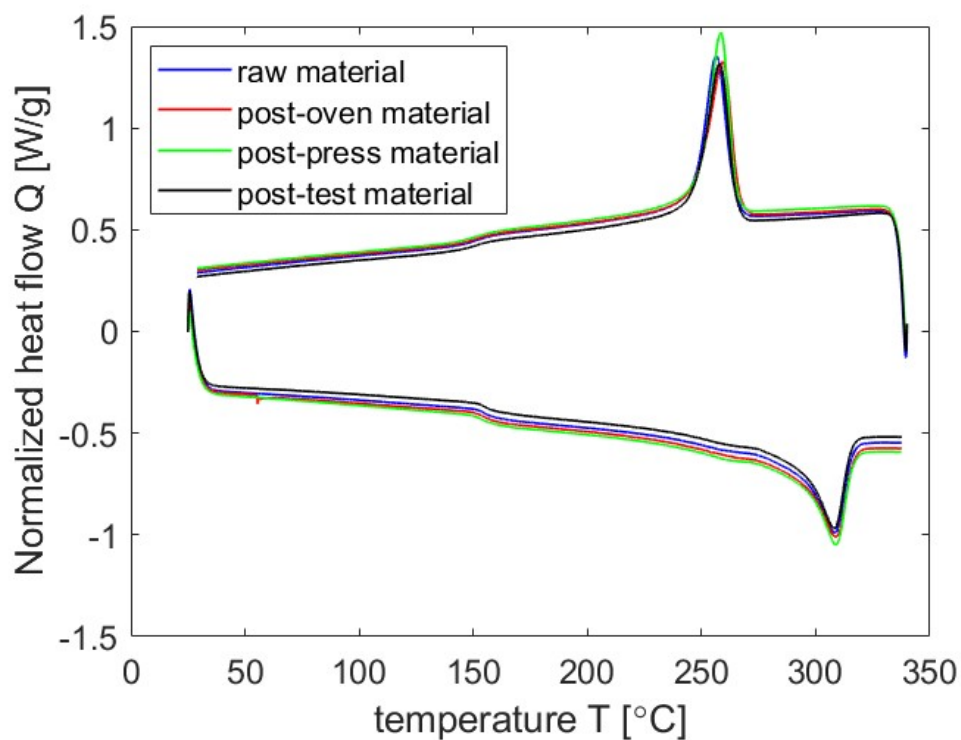


Figure B.0.6: Heat flow normalized with sample weight over a temperature range of 25 to 340 °C, combined

# Appendix C

## Simulation files

In this section, the content from Section 3.6 will be explained in more detail. First, a detailed overview on how the specimen models and the indentation tool were constructed in the simulation input files is given. Then, property parameters used in the plane strain simulations that were not touched upon in Section 3.6 will be explained. At last, the input files used for all simulations will be shown.

### C.1 Construction of the simulated specimen

In Figure C.1.1 a schematic overview on how the specimen model and indentation tool are constructed can be seen. 4 nodes (1, 2, 3, 4) are created and define the radius and height of the material, where node 4 is at  $x = 0$  and  $y = 0$ . The nodes are connected by lines (1, 2, 3, 4). Constraints were placed upon node 1 and 2, to not move at all and upon line 4 to only be able to move in  $y$  direction. Then, the area created by the lines was filled with elements, where the elements are smaller close to node 4 and increase in size closer to line 1 and 2. Next, the contact elements are made by making 4 more nodes (13, 14, 23, 24) where nodes 13 and 14, and nodes 23 and 24 were connected respectively to make lines 13 and 14. Node 24 is the bottom of a spherical indenter. Nodes 3 and 13, and 4 and 14 are connected respectively, making them move simultaneously when a force is acting upon them. Between line 13 and 14 one row of contact elements is created. Lines 13 and 14 are programmed in such a way that they can not move through each other and therefore when line 14 moves downwards, line 13 does so as well. The last node created is node 5, which dictates how lines 23 and 24 moves, by imposing a displacement in  $y$  direction.

### C.2 Property parameters

For the plane strain model a few properties were not touched upon for ease of use of the simulations. These were the elasticity modulus  $E$ , the Poisson's ratio  $\nu$  [–], and the viscosity fraction  $\psi_v$ . The shear modulus  $G$  given for the simulations is can not be filled in in the input file, but is calculated with  $E$  and  $\nu$  according to:

$$G = \frac{E}{2 \cdot (1 + \nu)} \quad (\text{C.2.1})$$

Similarly, the bulkmodulus  $C_b$  can be calculated with:

$$C_b = \frac{E}{3 \cdot (1 - 2 \cdot \nu)} \quad (\text{C.2.2})$$

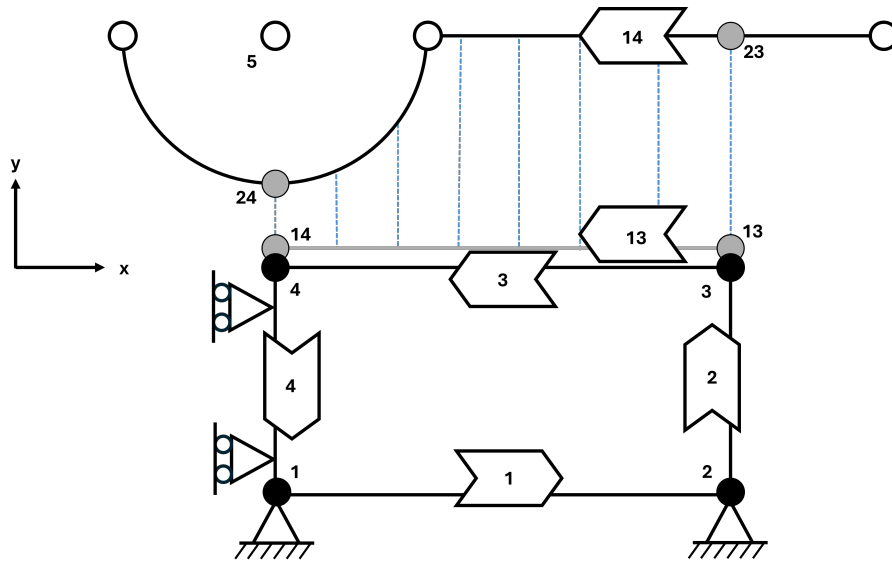


Figure C.1.1: Schematic overview of the nodes, lines and boundary conditions that construct the specimen model and the indentation tool.

$E$  was changed over the iterative simulation process to find the best approximated fit on the test results. For  $\nu$  a value of 0.4999 instead of 0.5 was chosen to describe the material as close to incompressible as possible while still having a defined solution for Equation C.2.2. In Section 3.6, a sufficiently high bulkmodulus was given for simplicity sake.

The viscosity fraction dictates how much the viscosity and elastic components contribute to the equation. The elastic fraction is calculated with  $\psi_e = 1 - \psi_v$ . The viscosity fraction was set to 0.5, which signifies that the viscous and elastic components contributed equally.

### C.3 Input files

Placing all files in the appendix would be too much. One example of an input file will be given and information on the commands used in the input file can be found in the user manual [43]. If other input files are requested, please contact: [t.h.koopman@student.utwente.nl](mailto:t.h.koopman@student.utwente.nl)

```
*START

*IMAGE

*NODES
MESHGEN
POLES
  1  0.  -5.6
  2  8.  -5.6
  3  8.   0.
  4  0.   0.
 13  8.   0.
 14  0.   0.
 23  8.   3.
```

24 0. 3.  
EOG

## CURVES

## LINE

1	1	2	40	8.	101
2	2	3	20	0.25	201
3	3	4	40	0.125	301
4	4	1	20	4.	401
13	13	14	40	0.125	701
14	23	24	40	0.125	801

EOT

EOG

## REGI

1	4	40	20	1001
	1	2	3	4
2	2	40	1	2101
	14	-13		

EOG

EOD

## \*TOOLNODES

5

EOG

EOD

## \*BWOP

## \*ELEMENTS

## AXI4

1 1

## MESHGEN

1 800 1

EOT

EOG

## AXC4

2 1

## MESHGEN

2 40 1001

EOT

EOG

EOD

## \*CONNECT

## NODE

13 3 0

```
14 4 0
23 5 0
24 5 0
2 1 2
```

EOG

GEDOF

```
19 401 1 1 1 0 1 2
```

EOG

CURVENOD

```
13 3 0
```

EOG

CURVETN

```
1 1 2
```

```
14 5 2
```

EOG

EOD

\*SUPPRESS

```
1 1
```

```
1 2
```

```
4 1
```

```
5 1
```

EOG

EOD

\*MATERIAL

VISC

CROSS

2.00E+02

```
0.000438 1.79 0.615
```

EOG

LINEAR

VISC 5.

```
0.002 10000 0.01 0. 0. 0.
```

EOG

EOD

\*NECO

```
0 0
```

\*MODB

\*TIME

```
1.0E-9
```

\*CONTOUR

1

5 2

CIRCLE

0. 3. 3. -3.1415 0.

LINE

3. 3. 12. 3.

EOG

EOD

\*PRESCRIBED

5 2 -0.001

EOG

EOD

\*UPDATED

\*MAXITER

20

0.02 0.0

\*OUTPUT

ELGROUP

1 2

NODAL

5 6 21

TOTSTRESS

PRESSURE

FORCES

TOOL

DISPLACEMENT

PARTTR

INCRDIS

GV

FOLLOW

REAC

5 2 5 2

EOT

EOG

EOD

\*SURFACE contact + ALE curves/region

MANPRIOR

OPT10

0 0 0

```
23 3 1 1 0 1
24 4 1 1 2 1
EOT
CURVEOPT
14 3 1 0 0 0 0 0 2
EOT
EOG
CURVE
WEIGHT
SPLINE
3 1 1. 4. 0.5 0
EOS
EOT
EOG
REGION
TFM
1 5
EOT
EOG
EOD
```

```
*POST
*STEP
*NOPOST

*MAXITER
10
0.02 0.0
```

```
*POFU
DISPL
5 2
-0.25
-0.5
-0.75
-1.0
-1.25
-1.5
-1.75
-2.0
EOG
EOD
```

```
*TIME
0.01
```

```
*PRESCRIBED  
  5 2 -0.004  
EOG  
EOD
```

```
*AUTO  
10000  2.  10.
```

```
*STEP 9999
```

```
*POST  
*STEP
```

```
*STOP
```

## Appendix D

# Error assessment of the rheometer

An analysis on the inherent noise of the rheometer was done. The rheometer was programmed to lower at a linear rate of  $1 \mu\text{m}/\text{s}$  for 30 minutes to see if any forces were measured when no indentation took place. The force over time can be seen in Figure D.0.1 and the important values extracted from this test can be seen in Table D.0.1. This noise influence the matrix material tests as the noise forces are on the same order of magnitude as the measured indentation forces. Similarly, obtaining more data samples with the fast sampling setting was not viable, as this setting produced even more noise as seen in Figure D.0.2. The fast sampling setting seemed to generate more noise than already exists in the rheometer. For this reason this setting could not be used for the indentation of the matrix material.

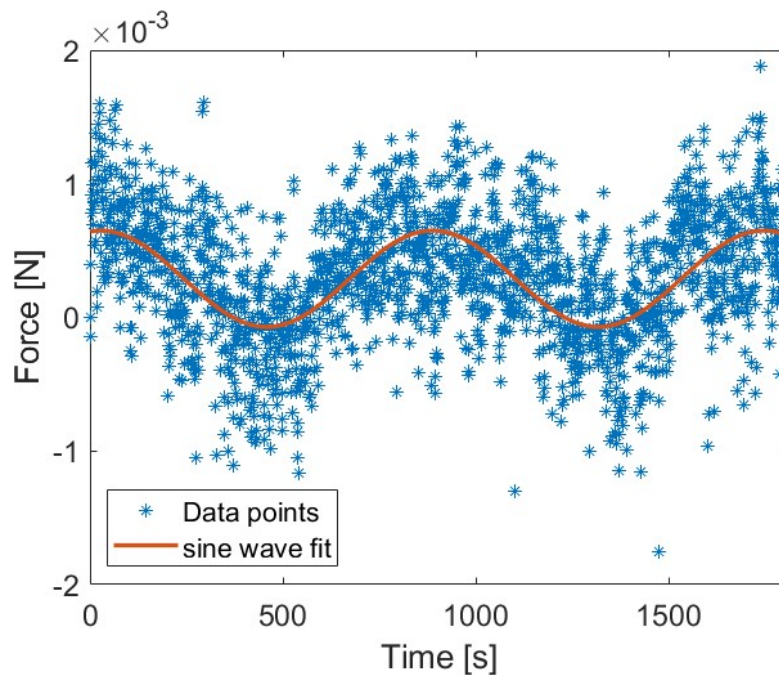


Figure D.0.1: Force over time of the rheometer for a 30 minutes period where no indentation takes place.

Table D.0.1: Values measured on the rheometer without indentation

Maximum force	Minimum force	standard deviation	amplitude	period
1.9 mN	-1.7 mN	0.42 mN	3.6 mN	14 minutes

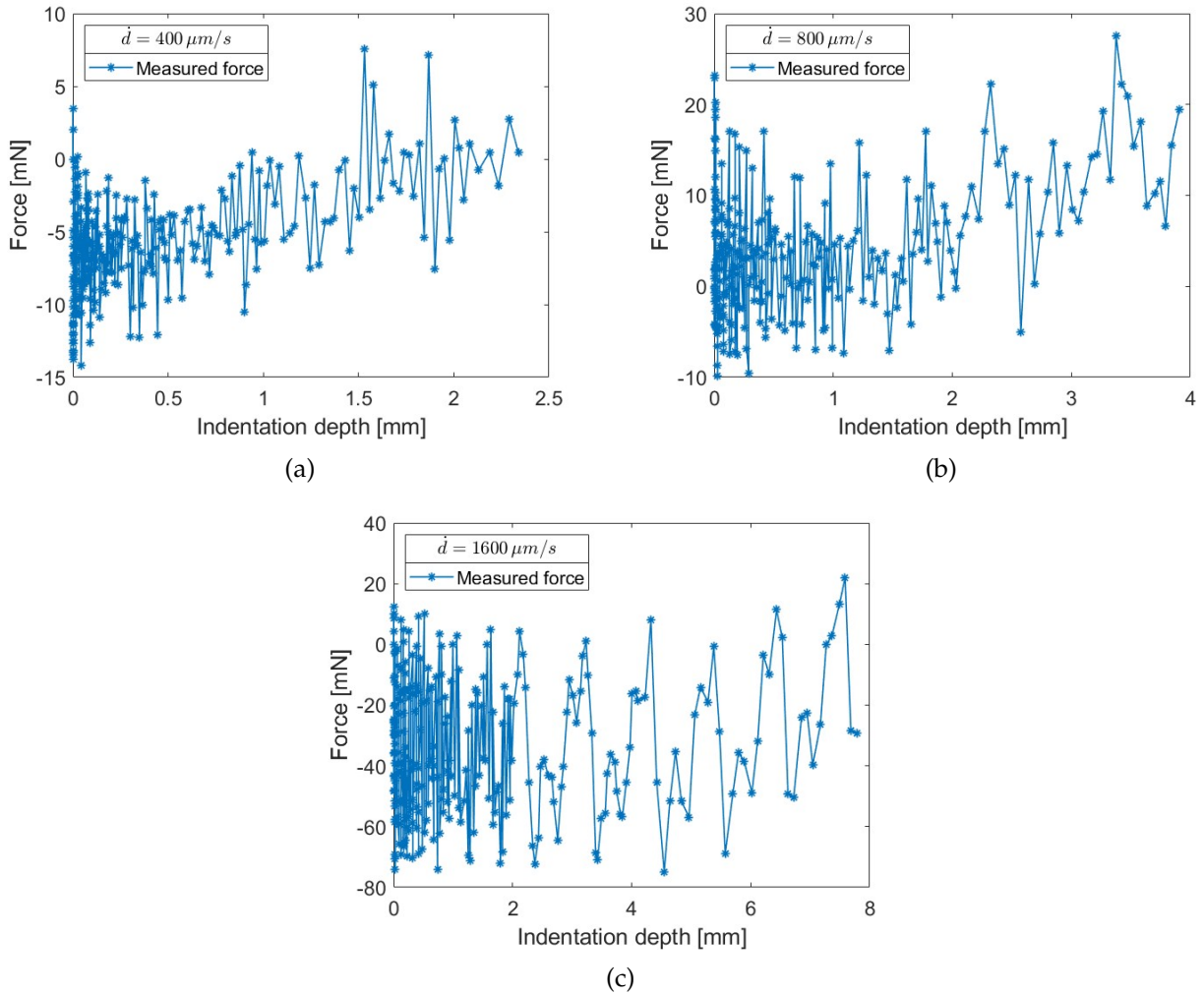


Figure D.0.2

Table D.0.2: Maximum, minimum, and difference in maximum and minimum forces measured during the fast sampling tests of the matrix material.

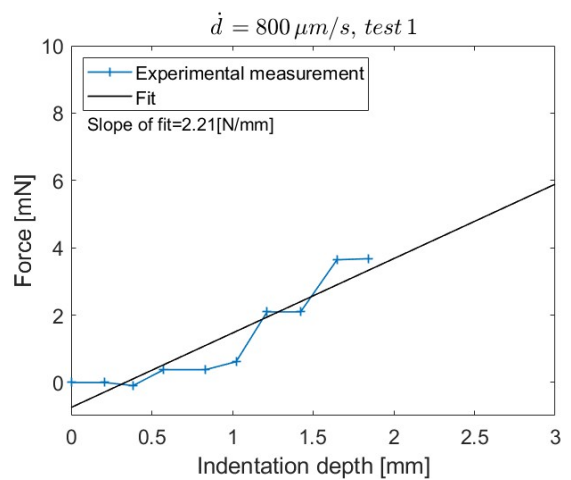
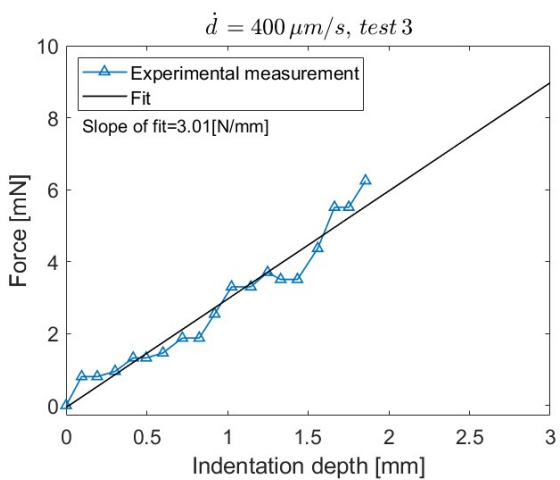
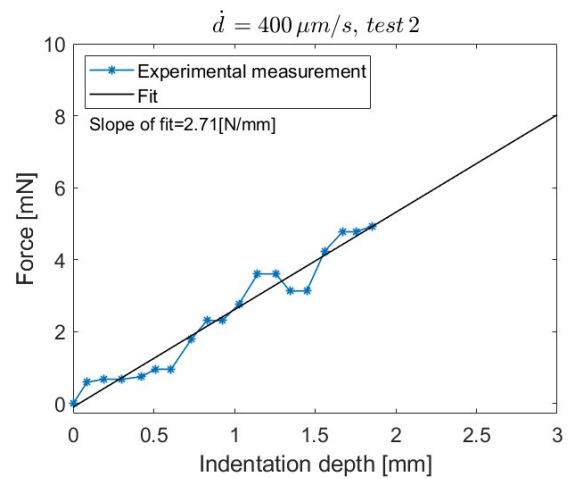
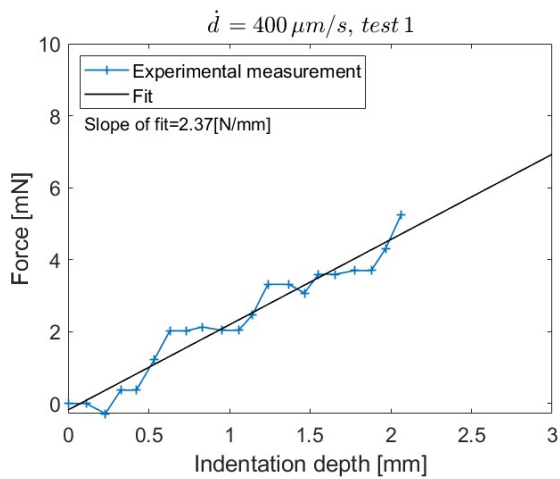
	$\dot{d} = 400 \mu\text{m/s}$	$\dot{d} = 800 \mu\text{m/s}$	$\dot{d} = 1600 \mu\text{m/s}$
Maximum force [mN]	7.57	27.54	22.03
Minimum force [mN]	-14.17	-9.88	-74.96
Difference [mN]	21.75	37.42	96.99

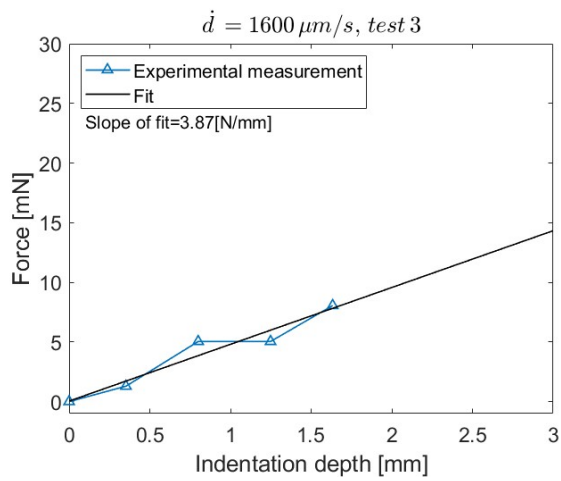
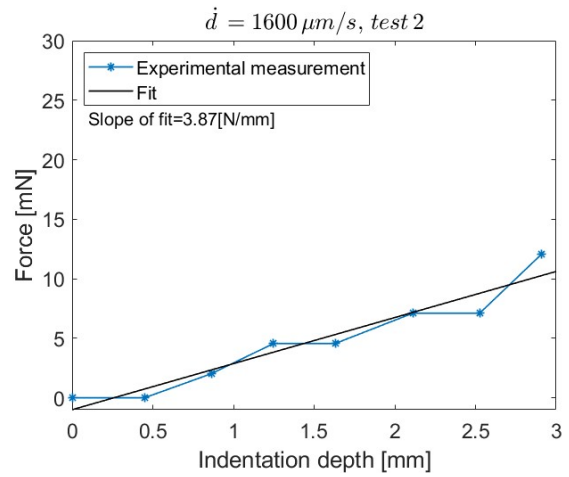
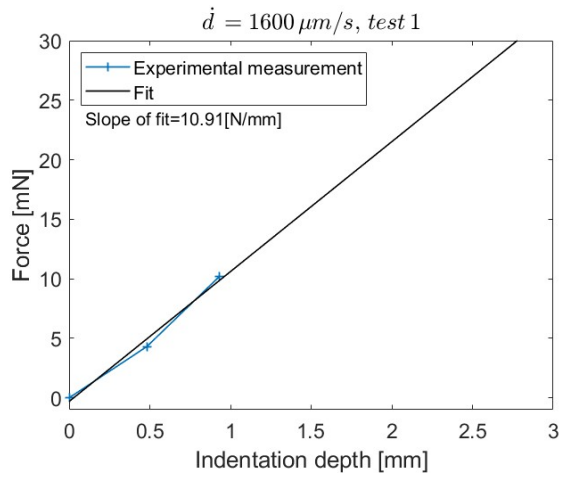
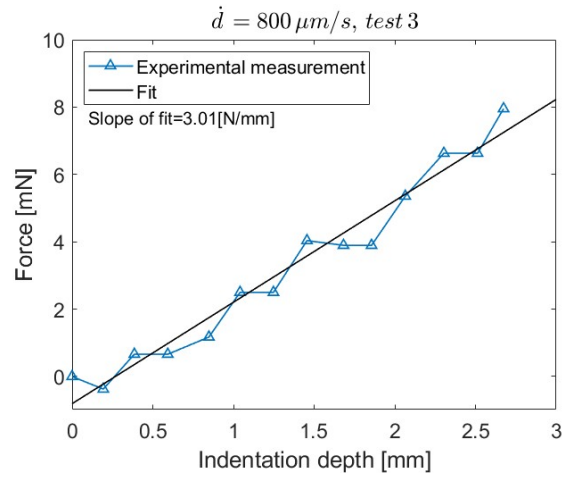
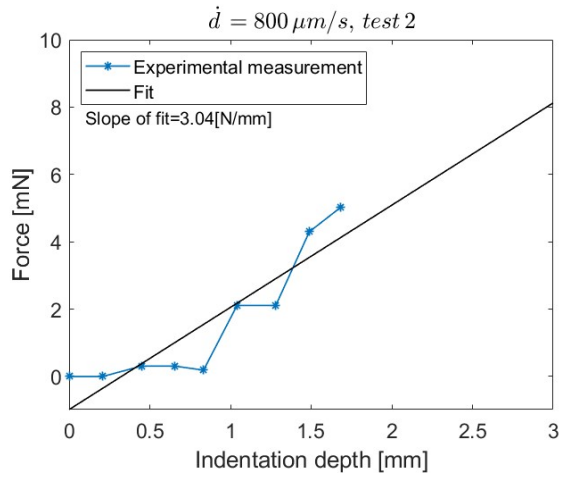
# Appendix E

## Test results

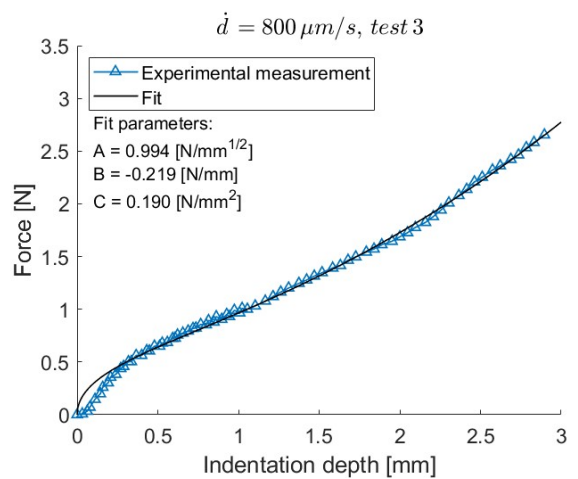
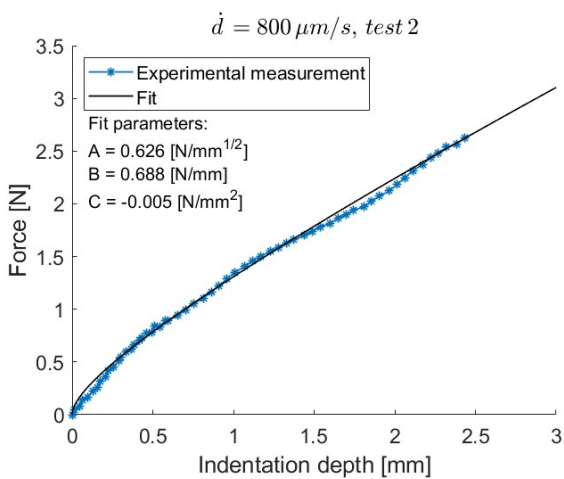
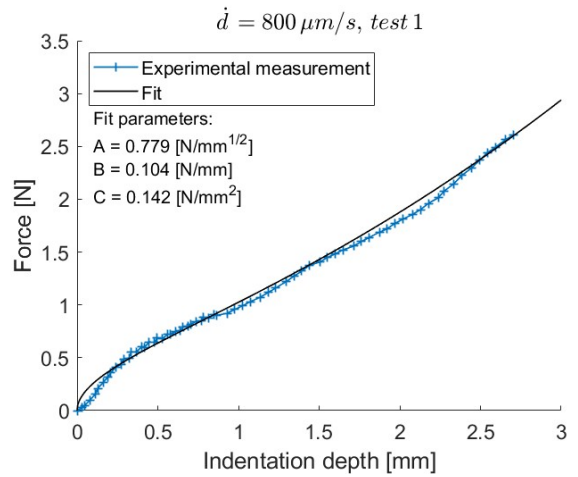
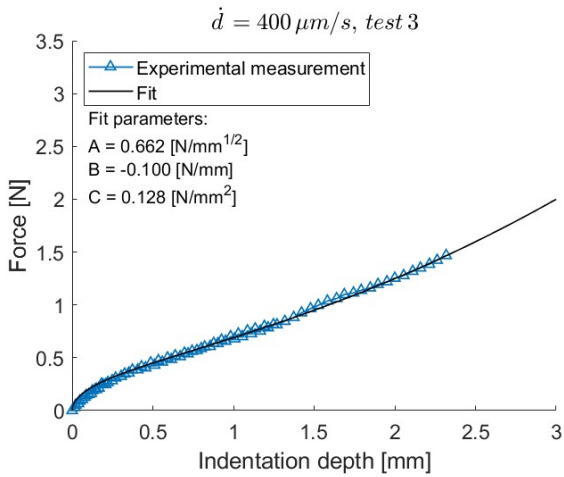
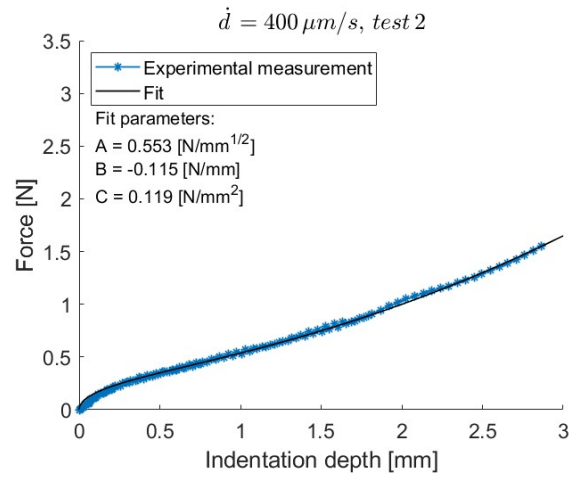
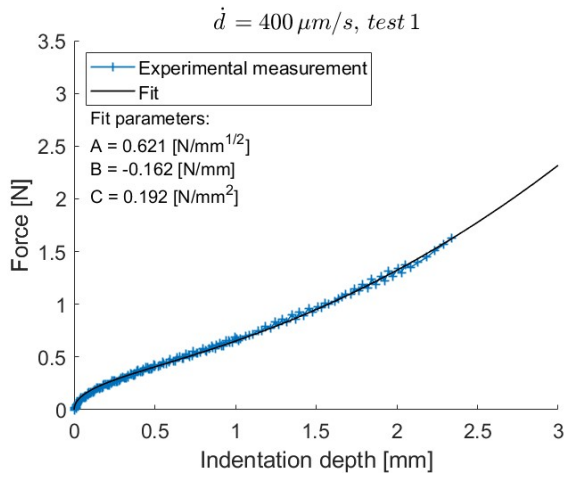
In this appendix all test results from the indentation tests are presented per test. For the matrix material the slopes of the linear fits are given and for the UD composite material the fit parameters are given.

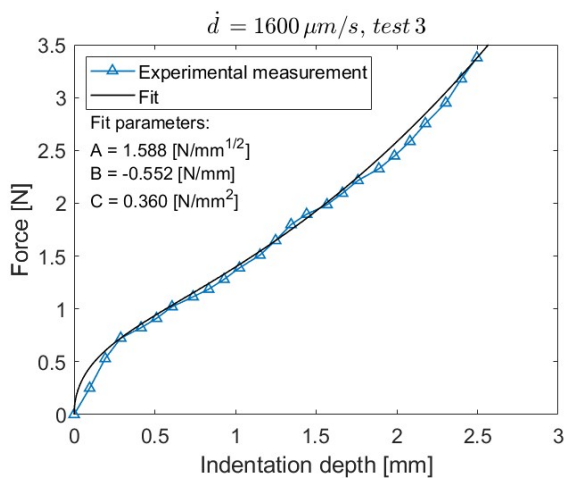
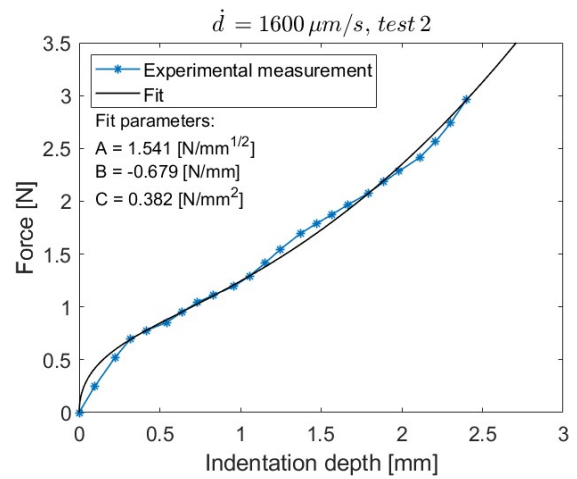
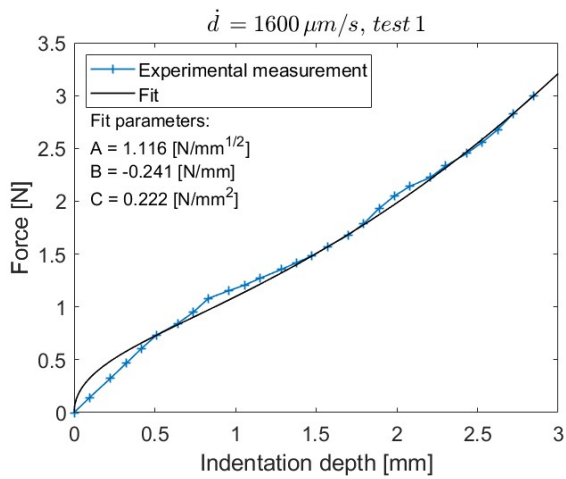
### E.1 Matrix indentation test results





## E.2 UD composite indentation test results





# Tijn Koopman

## Masters\_Thesis\_Indentation\_of\_composites (3).pdf

 University of Twente

---

### Document Details

Submission ID

trn:oid::6294:276543155

Submission Date

Apr 6, 2025, 8:44 PM GMT+2

Download Date

Apr 6, 2025, 10:23 PM GMT+2

File Name

Masters\_Thesis\_Indentation\_of\_composites (3).pdf

File Size

19.3 MB

74 Pages

20,027 Words

100,130 Characters

# 10% Overall Similarity

The combined total of all matches, including overlapping sources, for each database.

## Filtered from the Report

- ▶ Bibliography
- ▶ Quoted Text
- ▶ Cited Text
- ▶ Small Matches (less than 8 words)

## Match Groups

- 145** Not Cited or Quoted 10%  
Matches with neither in-text citation nor quotation marks
- 0** Missing Quotations 0%  
Matches that are still very similar to source material
- 0** Missing Citation 0%  
Matches that have quotation marks, but no in-text citation
- 0** Cited and Quoted 0%  
Matches with in-text citation present, but no quotation marks

## Top Sources

- 7% Internet sources
- 6% Publications
- 1% Submitted works (Student Papers)

## Integrity Flags

### 1 Integrity Flag for Review

- Replaced Characters**  
9 suspect characters on 6 pages  
Letters are swapped with similar characters from another alphabet.

Our system's algorithms look deeply at a document for any inconsistencies that would set it apart from a normal submission. If we notice something strange, we flag it for you to review.

A Flag is not necessarily an indicator of a problem. However, we'd recommend you focus your attention there for further review.